NASA TECHNICAL NOTE

NASA TN D-4246

c.1

LOAN COPY: RETURN TO
AFWL (WLIL-2)
KIRTLAND AFB, N MEX

TECH LIBRARY KAFB, NM
0130841

NASA TN D-4246

MIDCOURSE-GUIDANCE PROCEDURE WITH SINGLE POSITION FIX OBTAINED FROM ONBOARD OPTICAL MEASUREMENTS

by Harold A. Hamer, Katherine G. Johnson, and W. Thomas Blackshear

Langley Research Center
Langley Station, Hampton, Va.

RECEIVED
11 DEC 1967
Technical Library
Air Force Weapons Laboratory

NATIONAL AERONAUTICS AND SPACE ADMINISTRATION • WASHINGTON, D. C. • DECEMBER 1967

TECH LIBRARY KAFB, NM
0130841

NASA TN D-4246

MIDCOURSE-GUIDANCE PROCEDURE WITH SINGLE POSITION FIX OBTAINED FROM ONBOARD OPTICAL MEASUREMENTS

By Harold A. Hamer, Katherine G. Johnson,
and W. Thomas Blackshear

Langley Research Center
Langley Station, Hampton, Va.

NATIONAL AERONAUTICS AND SPACE ADMINISTRATION

For sale by the Clearinghouse for Federal Scientific and Technical Information
Springfield, Virginia 22151 – CFSTI price $3.00

TABLE OF CONTENTS

MIDCOURSE-GUIDANCE PROCEDURE WITH SINGLE POSITION FIX OBTAINED FROM ONBOARD OPTICAL MEASUREMENTS

By Harold A. Hamer, Katherine G. Johnson,
and W. Thomas Blackshear
Langley Research Center

SUMMARY

A manual procedure is developed for midcourse-guidance application. The procedure requires only limited onboard calculations and leads to guidance predictions sufficiently accurate for emergency or backup operations. Although high accuracy cannot be obtained by manual methods as compared with automatic methods, the accuracy of the present method is shown to be adequate to the point where a terminal guidance system could take over with relatively simple equipment. The method is applied to Earth-Moon trajectories and is studied in detail for an example lunar mission.

Basically, the determination of only one position fix is required rather than the determination of a large number of position fixes as is usually required in any manual or automatic procedure. This condition is made possible by use of precalculated data which linearly relate deviations from the nominal trajectory at the time of the position fix to those farther along the trajectory. This procedure is especially important for lunar missions where time is limited for making measurements and calculations prior to the first midcourse maneuver. The effects on aim-point accuracy of measurement errors, maneuver errors, star selection, and linear approximation are discussed.

INTRODUCTION

The navigation and guidance operations in manned space missions will normally be accomplished by elaborate statistical procedures (such as those described in refs. 1 and 2), which require extensive use of automatic computing equipment to process large quantities of onboard and/or Earth-based measurements. A procedure of this kind is necessary in order to obtain the accuracy requirements dictated by manned space flight. In case of malfunction or failure of this complex system, it would be highly desirable to have a backup procedure wherein the astronaut could, from several onboard measurements, manually guide his spacecraft by the use of relatively simple guidance calculations. (Hereafter in this report, navigation and guidance are referred to merely as guidance.)

A method that could be applied to a manual guidance procedure is developed herein. The method is based on a fixed-time-of-arrival condition; that is, the spacecraft is guided to a certain point on a nominal or reference trajectory. Although the method is developed for Earth-Moon trajectories, it could serve for interplanetary trajectories. The method pertains to midcourse guidance – that is, guiding the spacecraft in a translunar trajectory from a point relatively near the Earth to a point near the Moon. As would any manual method involving such large distances, the present method exhibits relatively large errors at the aim point (inaccuracies of several hundred kilometers for present-day instrument angular measurements) and would normally be intended only as an emergency procedure to get the spacecraft back near the right course. Additional refinement of the trajectory, which may be necessary farther along the trajectory, could be achieved by manual terminal guidance methods such as those described in references 3 to 5. As an example, for a manned circumlunar mission in which the spacecraft is to circumnavigate the Moon and return directly to Earth, the present method could serve to correct the translunar Earth-Moon trajectory and a terminal method could be used to insure a reasonable perilune at the Moon and a safe perigee (or corridor) for Earth reentry.

The method developed herein is based on a linear perturbation procedure, which makes use of the so-called transition matrix, and permits much of the computation to be handled by preflight calculations. The method is developed from one that makes use of a knowledge of vehicle position at two discrete times along the trajectory to calculate the velocity and hence to determine the magnitude and direction of the velocity correction required for the midcourse maneuver. Although repeated range measurements may be required for increased accuracy, the method basically employs a single position fix relating to a preselected time. The position fix is obtained from onboard optical angular measurements between certain combinations of stars, the Earth, and the Moon. The off-nominal vehicle-position deviations at different times can be linearly related; therefore, measurements are not required for a position fix at the second time. Hence, this position fix can be empirically determined in terms of the first one and most of the error associated with guidance from measurements at two discrete points can be eliminated.

The accuracy characteristics of the method are thoroughly discussed; results of a Monte Carlo analysis of measurement errors and the effects of star selection are included. Also discussed are effects on guidance accuracy due to the linear approximation made in using transition-matrix theory. The range measurement is the most critical from the standpoint of accuracy in any type of guidance system; therefore, the various means for manually determining range are examined, along with their relative errors.

In this report the term "manual" infers that guidance measurements are made onboard the space vehicle and that all necessary guidance calculations are performed without resort to an automatic computing machine with built-in programs and procedures.

However, it is not meant to preclude the use of a simple machine to perform desk-type calculations; in fact, such a machine would be the minimum capability required in any manual guidance calculation.

SYMBOLS

A	angle formed at vehicle by line of sight to Earth center and line of sight to Moon center
a	constant of ellipse (appendix B); semimajor axis (appendix C)
$\Delta A, \Delta B, \Delta C, \Delta\theta$	difference between actual value and nominal value of A, B, C, and θ, respectively (for example, $\Delta A = A_a - A_n$)
B	angle formed at Earth center by line to vehicle and line to Moon center
b	constant of ellipse (appendix B)
b_∞	perpendicular distance between asymptote of hyperbolic lunar approach trajectory and center of Moon
C	angle formed at Moon center by line to vehicle and line to Earth center
c	distance between center of ellipse and center of circle (appendix B)
D,E,F	off-nominal position component in direction of star 1, star 2, and star 3, respectively (D in figs. 7 and 8 is component in direction of specific stars named)
$\delta D, \delta E, \delta F$	difference between values of D, E, and F, respectively, at T_{pf} and T_1 $\left(\text{for example, } \delta D = D_{T_1} - D_{T_{pf}}\right)$
DC,RA	angle of declination and of right ascension, respectively
$[d],[e],[f],[g],[h]$	3×3 matrices in guidance equations
f_f	focus factor
$[G]$	orthogonal rotation matrix $\left(\text{eigenvectors of } [\Sigma\epsilon_r]\right)$

$\bar{h}$ vector perpendicular to instantaneous Earth-Moon-vehicle plane (fig. 31)

$\bar{i},\bar{j},\bar{k}$ unit vector along X-, Y-, and Z-axis, respectively

K_1,K_2,K_3 constants in equations (9) and (10)

l,m,n direction cosine of line of sight to star with respect to X-, Y-, and Z-axis, respectively

$[P]$ transformation matrix

$p_{11}p_{12}p_{13}$
$p_{21}p_{22}p_{23}$ elements of $[P]$
$p_{31}p_{32}p_{33}$

q constant in equations (18) and (19)

r range or distance, $\left(x^2 + y^2 + z^2\right)^{1/2}$

Δr incremental range or distance, $r_a - r_n$

s position deviation from nominal trajectory, $\left(\Delta x^2 + \Delta y^2 + \Delta z^2\right)^{1/2}$

s' position deviation from trajectory resulting from midcourse maneuver performed with no execution errors

T time from injection

T_{pf} time of position fix

T_1 time of first midcourse guidance maneuver

T_f time of second or final (aim-point) maneuver

u velocity deviation from nominal trajectory, $\left(\Delta\dot{x}^2 + \Delta\dot{y}^2 + \Delta\dot{z}^2\right)^{1/2}$

u' velocity deviation from trajectory resulting from midcourse maneuver performed with no execution errors

V velocity

ΔV first-midcourse-maneuver velocity correction

ΔV_f final- or second-midcourse-maneuver velocity correction

$\delta V, \delta\theta', \delta\phi'$ random errors in equation (A2)

X,Y,Z rectangular right-hand axis system in which X-axis is in the direction of Aries, XY-plane is parallel to Earth equatorial plane, and Z-axis is in the direction of celestial north pole

x,y,z position coordinates in X, Y, Z system

$\Delta x, \Delta y, \Delta z$ off-nominal position component in direction of X-, Y-, and Z-axis, respectively – for example, $\Delta x = x_a - x_n$ (the notation $\{\overline{\Delta x}\}$ represents the vector $\begin{Bmatrix}\Delta x\\ \Delta y\\ \Delta z\end{Bmatrix}$)

$\dot{x},\dot{y},\dot{z}$ velocity coordinates in X, Y, Z system

$\Delta\dot{x}, \Delta\dot{y}, \Delta\dot{z}$ off-nominal velocity component in direction of X-, Y-, and Z-axis, respectively – for example, $\Delta\dot{x} = \dot{x}_a - \dot{x}_n$ (the notation $\{\overline{\Delta\dot{x}}\}$ represents the vector $\begin{Bmatrix}\Delta\dot{x}\\ \Delta\dot{y}\\ \Delta\dot{z}\end{Bmatrix}$)

$\delta\dot{x}, \delta\dot{y}, \delta\dot{z}$ velocity error at injection (appendix A)

X',Y',Z' vehicle-centered normal axes of error ellipsoid

x',y',z' position coordinates in X', Y', Z' system

X'',Y'',Z'' rectangular right-hand axis system (appendix B)

x'',y'',z'' position coordinates in X'', Y'', Z'' system

X''',Y''',Z''' rectangular right-hand axis system (appendix B)

x''',y''',z''' position coordinates in X''', Y''', Z''' system

X_r,Y_r,Z_r rotating rectangular right-hand axis system in which X_r-axis lies along Earth-Moon line, X_rY_r-plane is in Earth-Moon plane, and Z_r-axis is in northerly direction

x_r,y_r,z_r position coordinates in X_r, Y_r, Z_r system

α,γ half-cone angles for star-to-body measurements (appendix B)

β angle (or supplement) formed by lines of sight to two stars (appendix B)

δ angle formed at vehicle by line of sight to star and its projection in the instantaneous Earth-Moon-vehicle plane

ϵ eccentricity of orbit (appendix C)

ζ,λ in-plane and out-of-plane pointing direction error, respectively, of midcourse-velocity guidance vector

θ angle formed at vehicle by line of sight to star and line of sight to body center (referred to as star-to-body angle); true anomaly (appendix C)

θ_I,θ_{II} angular measurements used for determining θ (fig. 15)

θ_∞ angle defined in figure 38

θ',ϕ' orientation angles (appendix A)

Θ angle formed at vehicle by line to Earth and projection of line to star in the instantaneous Earth-Moon-vehicle plane

μ product of universal gravitational constant and mass of Moon (appendix C)

$[\Sigma\epsilon_r]$ covariance matrix of position errors in X, Y, Z system

$[\Sigma\epsilon_{r'}]$ covariance matrix of position errors in X', Y', Z' system

σ standard-deviation value or 1-sigma error

$[\Phi],[\phi]$ state-transition matrices

$[\Phi_1],[\Phi_2],[\Phi_3],[\Phi_4]$ 3×3 submatrices in state-transition matrix for transitioning from T_1 to T_f

$[\phi_1],[\phi_2],[\phi_3],[\phi_4]$ 3×3 submatrices in state-transition matrix for transitioning from T_1 to T_{pf}

Subscripts:

A angle formed at vehicle by line of sight to Earth center and line of sight to Moon center

a actual or measured (assuming no error) value

B angle formed at Earth center by line to vehicle and line to Moon center

calc calculated from equation (14)

D,E,F off-nominal position component in direction of star 1, star 2, and star 3, respectively

em Earth center to Moon center

ev Earth center to vehicle

n nominal value

p perilune

r range measurement

s position deviation; sphere of influence (appendix C)

T_{pf}	at time of position fix
T_1	at time of first midcourse maneuver
T_f	at time of second or final maneuver
u	velocity deviation
V	injection velocity
v	first-midcourse-maneuver velocity
ve	vehicle to Earth center
vm	vehicle to Moon center
x,y,z	position component in direction of X-, Y-, and Z-axis, respectively
x',y',z'	position component in direction of X'-, Y'-, and Z'-axis, respectively
$\dot{x},\dot{y},\dot{z}$	velocity component in direction of X-, Y-, and Z-axis, respectively
$\theta_1,\theta_2,\theta_3$	measurement of angle formed at vehicle by line of sight to star 1, star 2, and star 3, respectively, and line of sight to body center
θ',ϕ'	orientation angles
1,2,3	star 1, star 2, and star 3, respectively

Notation:

$[\ ]$	square matrix
$[\ ]^T$	transpose of square matrix
$[\ ]^{-1}$	inverse of square matrix
$\{\ \}$	column matrix

$[\ ]$ row matrix

$|\ |$ absolute value

A bar over a symbol indicates a vector.

BASIC METHOD

Synopsis

In general, any guidance correction is determined from information on the vehicle velocity. In the simplest method, velocity can be determined from vehicle-position measurements at two discrete times along the trajectory. Such a method, however, would be unacceptable because small errors in the position measurements would produce excessive error in the velocity determination and, hence, in the guidance calculation.

In an attempt to circumvent this deficiency, the characteristics of a large number of perturbed trajectories were analyzed with regard to the position deviations from a nominal trajectory. It was found, for a wide range of perturbed trajectories, that the deviations in the directions of certain stars were linearly related over a given time interval. Use of these stars for the guidance equations permits the position at the second time to be predicted on the basis of the initial position measurement and eliminates much of the effect of measurement error.

The procedure for calculating the midcourse-maneuver velocity correction is developed from standard guidance equations. These equations incorporate three star-to-body measurements along with a range measurement. The range measurement also normally includes one or two star-to-body measurements, with limits as to the location of the stars. Various criteria are developed herein for preselecting (before the mission) suitable stars for the range measurement and for the guidance equations.

General Considerations

Transition matrices.- The present method is based on a linear perturbation procedure using the so-called state-transition matrix. This matrix can be used to relate the deviations in the state of the trajectory at one time to those at some other time. For example,

$$\begin{Bmatrix} \Delta x \\ \Delta y \\ \Delta z \\ \Delta \dot{x} \\ \Delta \dot{y} \\ \Delta \dot{z} \end{Bmatrix}_{T_1} = [\Phi] \begin{Bmatrix} \Delta x \\ \Delta y \\ \Delta z \\ \Delta \dot{x} \\ \Delta \dot{y} \\ \Delta \dot{z} \end{Bmatrix}_{T_{pf}}$$

where the state-transition matrix $[\Phi]$ maps the position and velocity deviations (from the nominal values) at time T_{pf} to those at time T_1. The state-transition matrix

$$[\Phi] = \begin{bmatrix} \frac{\partial x_{T_1}}{\partial x_{T_{pf}}} & \frac{\partial x_{T_1}}{\partial y_{T_{pf}}} & \frac{\partial x_{T_1}}{\partial z_{T_{pf}}} & \frac{\partial x_{T_1}}{\partial \dot{x}_{T_{pf}}} & \frac{\partial x_{T_1}}{\partial \dot{y}_{T_{pf}}} & \frac{\partial x_{T_1}}{\partial \dot{z}_{T_{pf}}} \\ \frac{\partial y_{T_1}}{\partial x_{T_{pf}}} & \frac{\partial y_{T_1}}{\partial y_{T_{pf}}} & \frac{\partial y_{T_1}}{\partial z_{T_{pf}}} & \frac{\partial y_{T_1}}{\partial \dot{x}_{T_{pf}}} & \frac{\partial y_{T_1}}{\partial \dot{y}_{T_{pf}}} & \frac{\partial y_{T_1}}{\partial \dot{z}_{T_{pf}}} \\ \frac{\partial z_{T_1}}{\partial x_{T_{pf}}} & \frac{\partial z_{T_1}}{\partial y_{T_{pf}}} & \frac{\partial z_{T_1}}{\partial z_{T_{pf}}} & \frac{\partial z_{T_1}}{\partial \dot{x}_{T_{pf}}} & \frac{\partial z_{T_1}}{\partial \dot{y}_{T_{pf}}} & \frac{\partial z_{T_1}}{\partial \dot{z}_{T_{pf}}} \\ \frac{\partial \dot{x}_{T_1}}{\partial x_{T_{pf}}} & \frac{\partial \dot{x}_{T_1}}{\partial y_{T_{pf}}} & \frac{\partial \dot{x}_{T_1}}{\partial z_{T_{pf}}} & \frac{\partial \dot{x}_{T_1}}{\partial \dot{x}_{T_{pf}}} & \frac{\partial \dot{x}_{T_1}}{\partial \dot{y}_{T_{pf}}} & \frac{\partial \dot{x}_{T_1}}{\partial \dot{z}_{T_{pf}}} \\ \frac{\partial \dot{y}_{T_1}}{\partial x_{T_{pf}}} & \frac{\partial \dot{y}_{T_1}}{\partial y_{T_{pf}}} & \frac{\partial \dot{y}_{T_1}}{\partial z_{T_{pf}}} & \frac{\partial \dot{y}_{T_1}}{\partial \dot{x}_{T_{pf}}} & \frac{\partial \dot{y}_{T_1}}{\partial \dot{y}_{T_{pf}}} & \frac{\partial \dot{y}_{T_1}}{\partial \dot{z}_{T_{pf}}} \\ \frac{\partial \dot{z}_{T_1}}{\partial x_{T_{pf}}} & \frac{\partial \dot{z}_{T_1}}{\partial y_{T_{pf}}} & \frac{\partial \dot{z}_{T_1}}{\partial z_{T_{pf}}} & \frac{\partial \dot{z}_{T_1}}{\partial \dot{x}_{T_{pf}}} & \frac{\partial \dot{z}_{T_1}}{\partial \dot{y}_{T_{pf}}} & \frac{\partial \dot{z}_{T_1}}{\partial \dot{z}_{T_{pf}}} \end{bmatrix}$$

is strictly applicable only when the equations of vehicle motion are linear. Because of the actual nonlinearity of these equations, this procedure is limited to perturbed trajectories that are reasonably close to the nominal. The transition matrix can be computed by several methods (see, for example, refs. 6 and 7) and there exist a number of computer programs (for example, orbit-determination programs) which have the capability of generating this matrix for any time interval along a trajectory.

Measurement of position.- As in any onboard guidance system, the guidance calculations are based on measurements of the position of the spacecraft at given times along

the trajectory. These measurements are used to determine the spacecraft velocity which, in turn, is used to derive the velocity correction required for a midcourse maneuver. The combinations of onboard optical measurements chosen for the present method are illustrated in figure 1.

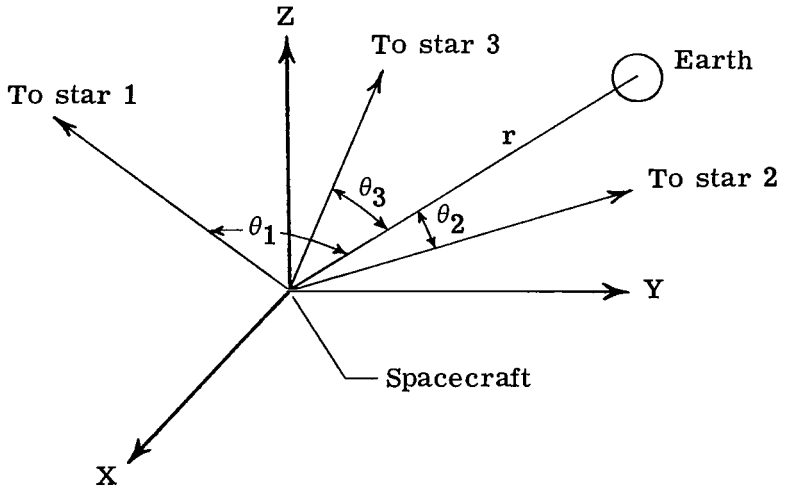

Figure 1.- Required measurements for position fix.

Of the many combinations of possible onboard measurements that will give a position fix (ref. 8), the method using three star-to-Earth angular measurements together with a range measurement (see fig. 1) is the most applicable to manual position fixing. (See ref. 9 for a study of this method as applied to a manual procedure.) Because the measurements are made onboard, the range is necessarily determined from angular measurements, as is discussed in a subsequent section.

From the aforementioned measurements, the set of equations (for a vehicle-centered coordinate system) which leads to the solution of the position vector of the Earth for a given time is

$$\begin{Bmatrix} x \\ y \\ z \end{Bmatrix} = \begin{bmatrix} l_1 m_1 n_1 \\ l_2 m_2 n_2 \\ l_3 m_3 n_3 \end{bmatrix}^{-1} \begin{Bmatrix} r \cos \theta_1 \\ r \cos \theta_2 \\ r \cos \theta_3 \end{Bmatrix}$$

or, for the position deviation of the vehicle off the nominal trajectory,

$$\begin{Bmatrix} x_a - x_n \\ y_a - y_n \\ z_a - z_n \end{Bmatrix} = \begin{bmatrix} l_1 m_1 n_1 \\ l_2 m_2 n_2 \\ l_3 m_3 n_3 \end{bmatrix}^{-1} \begin{Bmatrix} r_a \cos \theta_{1,a} - r_n \cos \theta_{1,n} \\ r_a \cos \theta_{2,a} - r_n \cos \theta_{2,n} \\ r_a \cos \theta_{3,a} - r_n \cos \theta_{3,n} \end{Bmatrix}$$

By letting

$$\begin{Bmatrix} r_a \cos \theta_{1,a} - r_n \cos \theta_{1,n} \\ r_a \cos \theta_{2,a} - r_n \cos \theta_{2,n} \\ r_a \cos \theta_{3,a} - r_n \cos \theta_{3,n} \end{Bmatrix} = \begin{Bmatrix} D \\ E \\ F \end{Bmatrix} \tag{1}$$

the set of equations may be written as

$$\begin{Bmatrix} \Delta x \\ \Delta y \\ \Delta z \end{Bmatrix} = \begin{bmatrix} l_1 m_1 n_1 \\ l_2 m_2 n_2 \\ l_3 m_3 n_3 \end{bmatrix}^{-1} \begin{Bmatrix} D \\ E \\ F \end{Bmatrix} \tag{2}$$

where l, m, and n are the known direction cosines of the respective stars and D, E, and F are the position-deviation components in the direction of the stars as illustrated in figure 2.

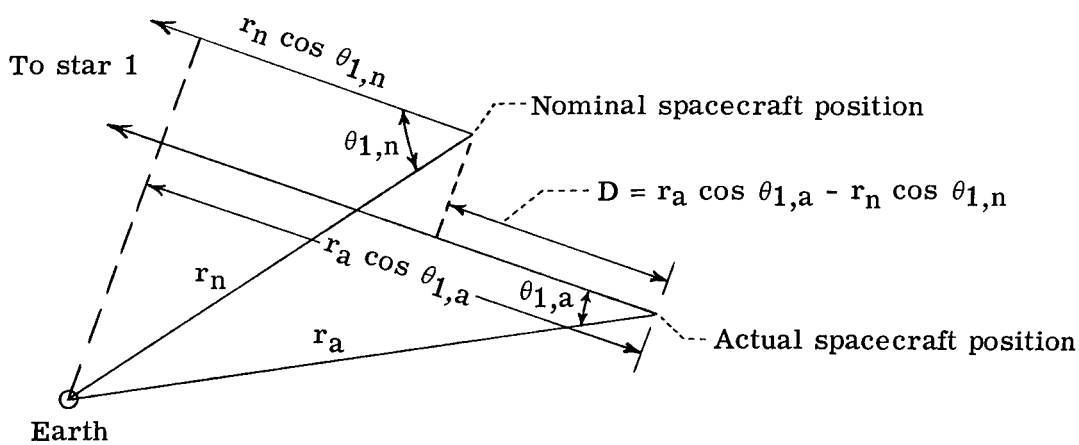

Figure 2.- Example of variables involved in determining off-nominal position components.

Development of Guidance Procedure

The present method is composed of two guidance maneuvers: (1) the primary maneuver, which is executed shortly after Earth injection, and (2) the one made at the

aim point, necessitated by the first maneuver. The aim point is defined as that point on the nominal trajectory to which the first midcourse maneuver attempts to correct. In this report, aim points at two different times are investigated: one at perilune and one at a point near the lunar sphere of influence. The purpose of investigating the different aim points is explained in a subsequent section.

First-midcourse-maneuver guidance equations.- The equations for the first midcourse maneuver are developed according to figure 3.

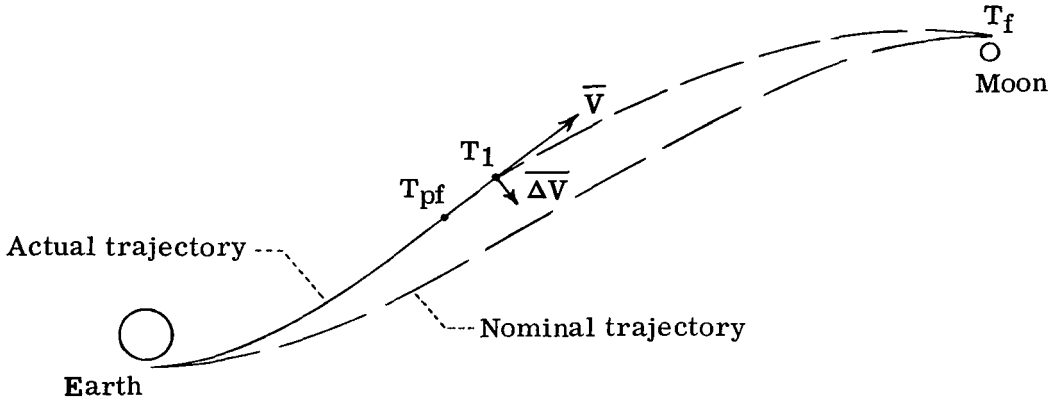

Figure 3.- Schematic sketch of guidance procedure.

The deviations from the nominal trajectory at the final (aim-point) time T_f after a midcourse guidance correction (see ref. 6, for example) are

$$\begin{Bmatrix} \overline{\Delta x}_{T_f} \\ \overline{\Delta \dot{x}}_{T_f} \end{Bmatrix} = \begin{bmatrix} [\Phi_1] & [\Phi_2] \\ [\Phi_3] & [\Phi_4] \end{bmatrix} \begin{Bmatrix} \overline{\Delta x}_{T_1} \\ \overline{\Delta \dot{x}}_{T_1}' \end{Bmatrix} \tag{3}$$

where the transition matrix is the mapping matrix from T_1 to the final time T_f and the prime denotes the velocity deviation immediately after the instantaneous (practically) guidance maneuver. For a fixed-time-of-arrival guidance law, the objective is to arrive at the aim point on the nominal trajectory, without regard for the final velocity deviation $\left\{\overline{\Delta \dot{x}}_{T_f}\right\}$. Hence

$$[\Phi_1]\left\{\overline{\Delta x}_{T_1}\right\} + [\Phi_2]\left\{\overline{\Delta \dot{x}}_{T_1}'\right\} = \{0\}$$

Then

$$\left\{\overline{\Delta\dot{x}}_{T_1}{}'\right\} = -\left[\Phi_2\right]^{-1}\left[\Phi_1\right]\left\{\overline{\Delta x}_{T_1}\right\} \tag{4}$$

or from equation (2)

$$\left\{\overline{\Delta\dot{x}}_{T_1}{}'\right\} = -\left[\Phi_2\right]^{-1}\left[\Phi_1\right]\begin{bmatrix} l_1m_1n_1 \\ l_2m_2n_2 \\ l_3m_3n_3 \end{bmatrix}^{-1}\begin{Bmatrix} D \\ E \\ F \end{Bmatrix}_{T_1}$$

$$= -\left[d\right]\begin{Bmatrix} D \\ E \\ F \end{Bmatrix}_{T_1} \tag{5}$$

Next, the velocity deviation immediately before the instantaneous guidance maneuver $\left\{\overline{\Delta\dot{x}}_{T_1}\right\}$ is obtained from

$$\begin{Bmatrix} \overline{\Delta x}_{T_{pf}} \\ \overline{\Delta\dot{x}}_{T_{pf}} \end{Bmatrix} = \begin{bmatrix} \left[\phi_1\right] & \left[\phi_2\right] \\ \left[\phi_3\right] & \left[\phi_4\right] \end{bmatrix}\begin{Bmatrix} \overline{\Delta x}_{T_1} \\ \overline{\Delta\dot{x}}_{T_1} \end{Bmatrix}$$

where the transition matrix is the mapping matrix from T_1 to T_{pf}. Then,

$$\left[\phi_1\right]\left\{\overline{\Delta x}_{T_1}\right\} + \left[\phi_2\right]\left\{\overline{\Delta\dot{x}}_{T_1}\right\} = \left\{\overline{\Delta x}_{T_{pf}}\right\}$$

or, by solving for $\left\{\overline{\Delta\dot{x}}_{T_1}\right\}$,

$$\left\{\overline{\Delta\dot{x}}_{T_1}\right\} = \left[\phi_2\right]^{-1}\left\{\overline{\Delta x}_{T_{pf}}\right\} - \left[\phi_2\right]^{-1}\left[\phi_1\right]\left\{\overline{\Delta x}_{T_1}\right\}$$

From equation (2)

$$\left\{\overline{\Delta\dot{x}}_{T_1}\right\} = \left[\phi_2\right]^{-1}\begin{bmatrix} l_1m_1n_1 \\ l_2m_2n_2 \\ l_3m_3n_3 \end{bmatrix}^{-1}\begin{Bmatrix} D \\ E \\ F \end{Bmatrix}_{T_{pf}} - \left[\phi_2\right]^{-1}\left[\phi_1\right]\begin{bmatrix} l_1m_1n_1 \\ l_2m_2n_2 \\ l_3m_3n_3 \end{bmatrix}^{-1}\begin{Bmatrix} D \\ E \\ F \end{Bmatrix}_{T_1}$$

$$= \left[e\right]\begin{Bmatrix} D \\ E \\ F \end{Bmatrix}_{T_{pf}} - \left[f\right]\begin{Bmatrix} D \\ E \\ F \end{Bmatrix}_{T_1} \tag{6}$$

Therefore, the required first-midcourse-maneuver velocity-correction vector $\overline{\Delta V}$, obtained by subtracting equation (5) from equation (6), is

$$\overline{\Delta V} = \left[e\right]\begin{Bmatrix} D \\ E \\ F \end{Bmatrix}_{T_{pf}} + \left(\left[d\right] - \left[f\right]\right)\begin{Bmatrix} D \\ E \\ F \end{Bmatrix}_{T_1}$$

$$= \left[e\right]\begin{Bmatrix} D \\ E \\ F \end{Bmatrix}_{T_{pf}} + \left[g\right]\begin{Bmatrix} D \\ E \\ F \end{Bmatrix}_{T_1} \tag{7}$$

where $\left[e\right]$ and $\left[g\right]$ are 3×3 matrices which can be precalculated from a knowledge of the transition matrices and the direction cosines of the pertinent stars. Since the measurements D, E, and F pertain to a vehicle reference system, the correction vector $\overline{\Delta V}$ is added to the vehicle velocity vector.

Second-midcourse-maneuver guidance equations.- In deriving the equations for the first midcourse maneuver, the corrected trajectory is designed to pass through the aim point; no attempt is made to control the velocity vector at this point. Hence, the second midcourse maneuver merely corrects the velocity error introduced at the aim point by the derivation of the first midcourse velocity. If the nominal perilune is the aim point, the second-midcourse-maneuver velocity correction could be readily combined with the lunar deboost maneuver, if this type of mission were contemplated.

From equation (3), then, the required second-midcourse-maneuver velocity-correction vector is

$$\overline{\Delta V}_f = \left\{\overline{\Delta\dot{x}}_{T_f}\right\} = \left[\Phi_3\right]\left\{\overline{\Delta x}_{T_1}\right\} + \left[\Phi_4\right]\left\{\overline{\Delta\dot{x}}_{T_1}'\right\}$$

or, from equation (4),

$$\overline{\Delta V_f} = \left[\Phi_3\right]\left\{\overline{\Delta x}_{T_1}\right\} - \left[\Phi_4\right]\left[\Phi_2\right]^{-1}\left[\Phi_1\right]\left\{\overline{\Delta x}_{T_1}\right\}$$

and, from equation (2),

$$\overline{\Delta V_f} = \left(\left[\Phi_3\right] - \left[\Phi_4\right]\left[\Phi_2\right]^{-1}\left[\Phi_1\right]\right)\begin{bmatrix} l_1 m_1 n_1 \\ l_2 m_2 n_2 \\ l_3 m_3 n_3 \end{bmatrix}^{-1}\begin{Bmatrix} D \\ E \\ F \end{Bmatrix}_{T_1}$$

By use of the inversion property of the transition matrix (ref. 6) which is

$$\left[\Phi\right]^{-1} = \begin{bmatrix} \left[\Phi_4\right]^T & -\left[\Phi_2\right]^T \\ -\left[\Phi_3\right]^T & \left[\Phi_1\right]^T \end{bmatrix}$$

it can be shown that the expression for $\overline{\Delta V_f}$ reduces to

$$\overline{\Delta V_f} = -\left[\Phi_2^{-1}\right]^T\begin{bmatrix} l_1 m_1 n_1 \\ l_2 m_2 n_2 \\ l_3 m_3 n_3 \end{bmatrix}^{-1}\begin{Bmatrix} D \\ E \\ F \end{Bmatrix}_{T_1}$$

$$= \left[h\right]\begin{Bmatrix} D \\ E \\ F \end{Bmatrix}_{T_1} \tag{8}$$

where $\left[h\right]$ is a 3×3 matrix that can be precalculated. As in the case for the first midcourse maneuver, the correction vector $\overline{\Delta V_f}$ is added to the vehicle velocity vector.

Method of Determining Position at T_1

General considerations.- As shown by equation (6), the first-midcourse-maneuver velocity-correction vector $\overline{\Delta V}$ is determined from a knowledge of spacecraft position at two times. For this type of method, which uses no statistical procedure to reduce a large number of position measurements in determining the guidance velocity, extreme measurement accuracy is necessary. For example, if a measurement is made at each time, the position-determination errors are equally as likely to be opposite in sign (direction). Even if the position-determination errors are small at the two times, a

large error could be introduced (as illustrated in fig. 4) in the calculation of the velocity vector of the actual trajectory and thus a large error could result at the aim point.

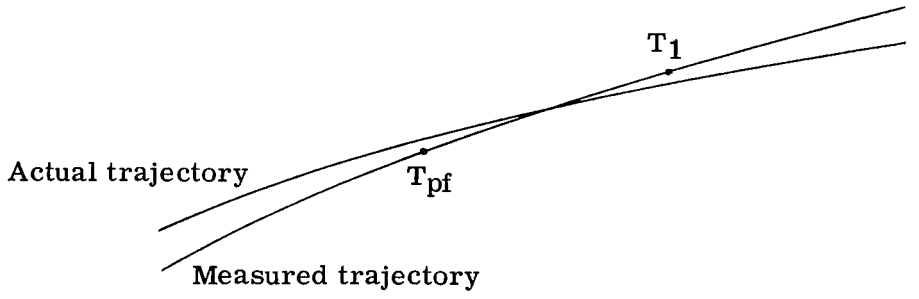

Figure 4.- Sketch showing position-determination errors that are in opposite directions at T_{pf} and T_1.

Greater accuracy in determining the velocity vector of the actual trajectory could be achieved if the position-determination errors at both times were in the same direction and also of the same magnitude, as illustrated in figure 5.

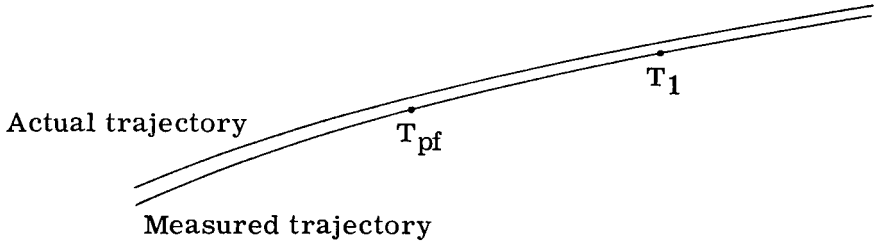

Figure 5.- Sketch showing position-determination errors that are in the same direction at T_{pf} and T_1.

Empirical procedure.- In order to essentially satisfy the conditions illustrated in figure 5, a procedure is herein developed whereby the position at time T_1 is not measured but is predicted from the position at T_{pf}. This prediction is possible since, for a number of perturbed trajectories, a change in deviation in the direction of a particular star over the interval T_{pf} to T_1 is a linear function of the deviation at time T_{pf}.

Shown in table I is a comparison of results obtained by the present method and by the method involving separate measurements at T_{pf} and T_1. Values shown were determined from a Monte Carlo error analysis (presented in a subsequent section) and correspond to 1-sigma measurement errors of 10 kilometers in the range and 10 arc-seconds in the star-to-body angles.

TABLE I.- COMPARISON OF ACCURACIES OF PRESENT METHOD AND METHOD INVOLVING POSITION MEASUREMENTS AT TWO TIMES

Method	Position error σ_s at T_f = 56 hr, km	Velocity error σ_u at T_f = 56 hr, m/sec
Present	162	1.2
Two-position fix	2535	17.5

The characteristics of the nominal trajectory used throughout this report are given in table II. This typical 3-day translunar trajectory is presented in figure 6 in the rotating-axis system which shows the relative positions of the Earth, Moon, and vehicle at any given time.

TABLE II.- CHARACTERISTICS OF NOMINAL TRAJECTORY

Injection position:	
x, km	-2104.8415
y, km	5395.4303
z, km	2874.9062
Injection velocity:	
$\dot{x}$, km/sec	-10.519851
$\dot{y}$, km/sec	-2.6309587
$\dot{z}$, km/sec	-2.0283715
Coordinate system	Cartesian equatorial of date
Injection date	March 18, 1968
Injection Greenwich mean time, hr:min:sec	22:27:15
Julian date	2439934.43559025
Perilune distance, km	3403.62
Perilune velocity (selenocentric), km/sec	1.98051
Approximate time to perilune	70 hr, 37 min
Approximate time to lunar sphere of influence	56 hr

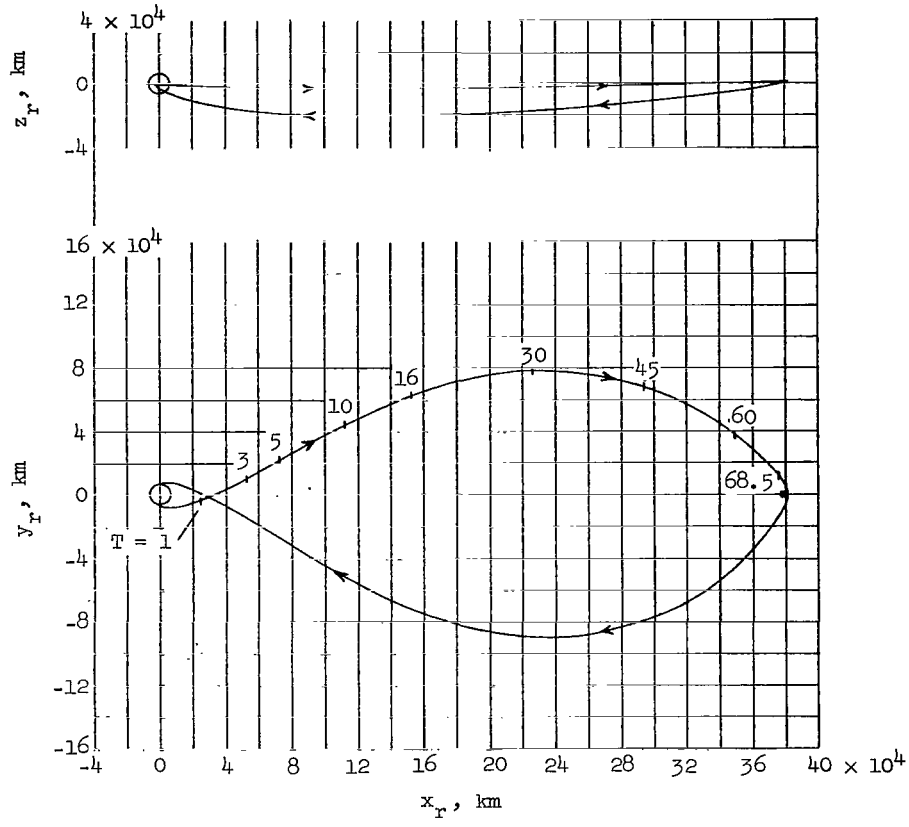

Figure 6.- Nominal trajectory in a rotating-axis system. (T denotes hours from injection.)

For the present procedure, a number of perturbed trajectories (see table III) are generated from which values of D are calculated at times T_{pf} and T_1. (In the guidance equations, D, E, and F represent different stars.) The values of D can be calculated from equation (1) or from the equation

$$D = l(x_a - x_n) + m(y_a - y_n) + n(z_a - z_n)$$

where l, m, and n are the direction cosines of the particular star and x, y, and z are vehicle-centered coordinates. Plots of δD as a function of D for given stars are obtained (for example, see figs. 7 and 8). For a given star the variation of δD with D provides the relationship

$$D_{T_{pf}} + \frac{\delta D}{D_{T_{pf}}} D_{T_{pf}} = D_{T_1}$$

or

$$K_1 D_{T_{pf}} = D_{T_1}$$

TABLE III.- PERTURBED TRAJECTORIES USED IN STUDY

Perturbed-trajectory no.	Injection-position perturbations, km			Injection-velocity perturbations, m/sec			Δr (at T_{pf} = 9.5 hr), km	Off-nominal conditions at aim point for perfect measurements and perfect guidance maneuver at first midcourse when –			
								T_f = 56 hr		T_f = 70 hr, 37 min (nominal perilune)	
	Δx	Δy	Δz	Δẋ	Δẏ	Δż		s, km	u, m/sec	s, km	u, m/sec
1	-5						135.87	3.263	0.015		
2	-10						271.85	5.925	.051	11.387	1.285
3		-5					-342.54	2.668	.021		
4		-10					-686.23	15.661	.100	45.028	10.676
5			5				182.60	3.218	.026		
6			10				365.09	6.020	.052	10.178	1.828
7	2.9	2.9	2.9				225.31	3.394	.027	7.501	1.544
8				9.15			-840.68	13.550	.094	40.700	9.589
9				-9.15			836.58	16.512	.071		
10				4.57			-419.37	5.045	.041	13.804	3.005
11					9.15		-207.24	2.413	0.015	6.821	1.696
12						-10	175.67	3.364	.024		
13						10	-175.00	1.156	.008	3.418	.843
14						-5	87.75	1.587	.011		
15						5	-87.58	6.124	.034		
16					-7	-7	281.58	2.574	.025	7.991	1.715
17					7	7	-281.29	1.557	.012		
18					-7	7	36.38	.372	.003		
19					7	-7	-35.55	2.025	.014		
20				5.27	5.27	5.27	-696.20	13.539	.084	39.100	9.621
21				4.57	5.27	5.27	-631.79	11.729	0.073		
22					9.15	5.27	-299.68	2.476	.018		
23		-6		6			-963.57	17.568	.116	52.050	12.483
24	-5			-10			1049.16	22.760	.188	23.800	5.691
25	5			10			-1055.57	21.661	.147		
26	-10			-10			1184.33	26.002	.211	29.669	7.922
27	10			10			-1192.06	29.210	.197		
28		-5				-10	-166.44	3.100	.027		
29		-10				-10	-509.71	14.412	.096	39.704	9.070
30		10				10	507.40	9.625	.082		
31			-5	10			-1102.85	22.291	0.143		
32			5	-10			1095.55	23.855	.198	24.974	5.840
33			-10	10			-1286.84	27.882	.177	82.143	20.390
34			10	-10			1276.88	31.989	.262		
35			-5		10		-409.47	6.661	.041		
36			-10		10		-592.59	12.935	.078	36.697	9.009
37			10		-10		591.47	10.507	.088		
38		-5		10			-1263.70	27.648	.175		
39		-10		10			-1609.62	42.745	.266	123.298	31.174
40		10		-10			1591.37	48.743	.367		

Values of constants K_1, K_2, and K_3 for three suitable stars are then used to determine off-nominal position components D, E, and F at time T_1 for any given perturbed trajectory. This method insures that the position-determination errors are about the same at times T_1 and T_{pf}. Substituting the constants into guidance equations (7) and (8) yields

$$\overline{\Delta V} = [e]\begin{Bmatrix} D \\ E \\ F \end{Bmatrix}_{T_{pf}} + [g]\begin{Bmatrix} K_1 D \\ K_2 E \\ K_3 F \end{Bmatrix}_{T_{pf}} \tag{9}$$

$$\overline{\Delta V_f} = [h]\begin{Bmatrix} K_1 D \\ K_2 E \\ K_3 F \end{Bmatrix}_{T_{pf}} \tag{10}$$

Star Selection

This section deals with the problem of selecting stars for obtaining linear plots of δD as a function of D. Range-measurement accuracy also depends on the selection of stars, as discussed in a subsequent section.

Geometry considerations.- The overall guidance accuracy of the present procedure depends on the three preselected stars used for the position measurement at time T_{pf}. Suitable stars give good linear plots of δD as a function of D and yield a minimum amount of scatter. Scatter is equivalent to position error, and the less scatter, the less chance of introducing error in calculating the guidance velocity.

Figures 7(a) to 7(f) are for suitable stars; stars considered in figures 7(g) and 7(h) are unsuitable. Figures 7(b), 7(e), and 7(f) are for fictitious stars and illustrate the linearity characteristics of stars in the particular directions indicated.

Experience has shown that the greatest degree of linearity is obtained when the star yields maximum values of both D and δD. This fact leads to consideration of probable errors in the injection conditions and the resulting error ellipsoid at T_{pf}. The major axis of this error ellipsoid is the most probable locus of deviations from the

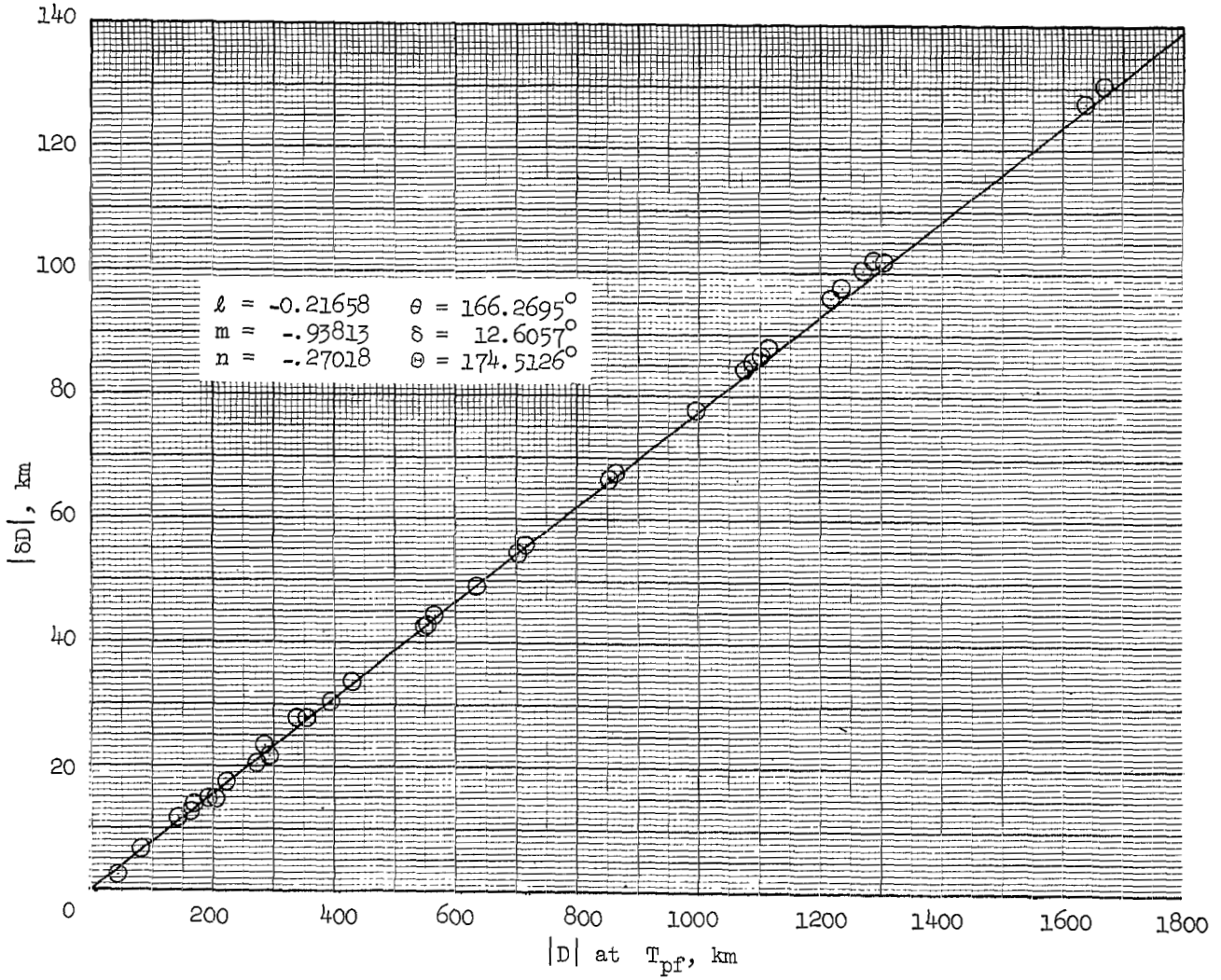

(a) Rasalhague.

Figure 7.- Change in off-nominal position component in the direction of the various indicated stars plotted for different perturbed trajectories. Data apply to nominal trajectory described in table II. (Signs of D and δD are the same except for data plotted below the zero-line.)

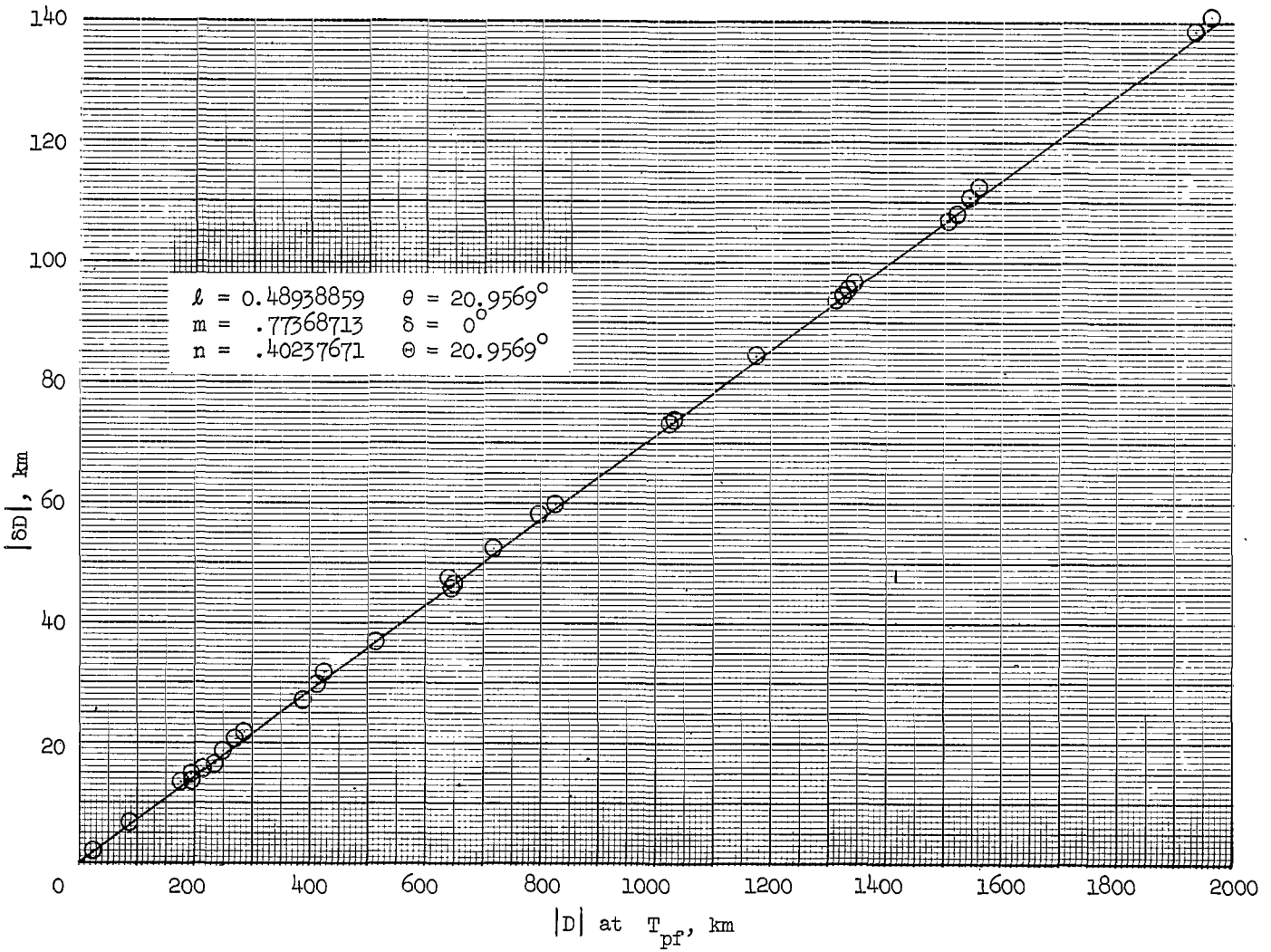

(b) Fictitious star in direction of Earth-Moon line.

Figure 7.- Continued.

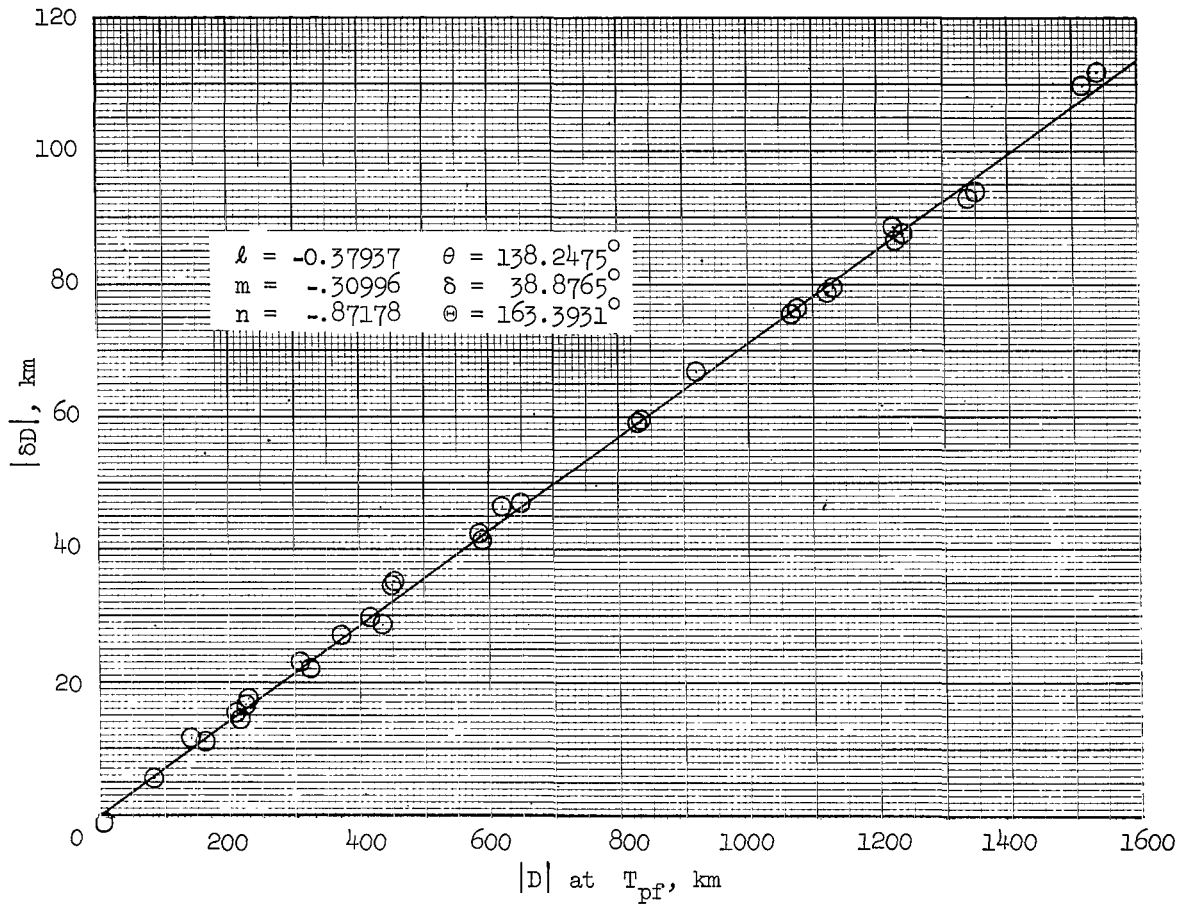

(c) Rigil Kentaurus.

Figure 7.- Continued.

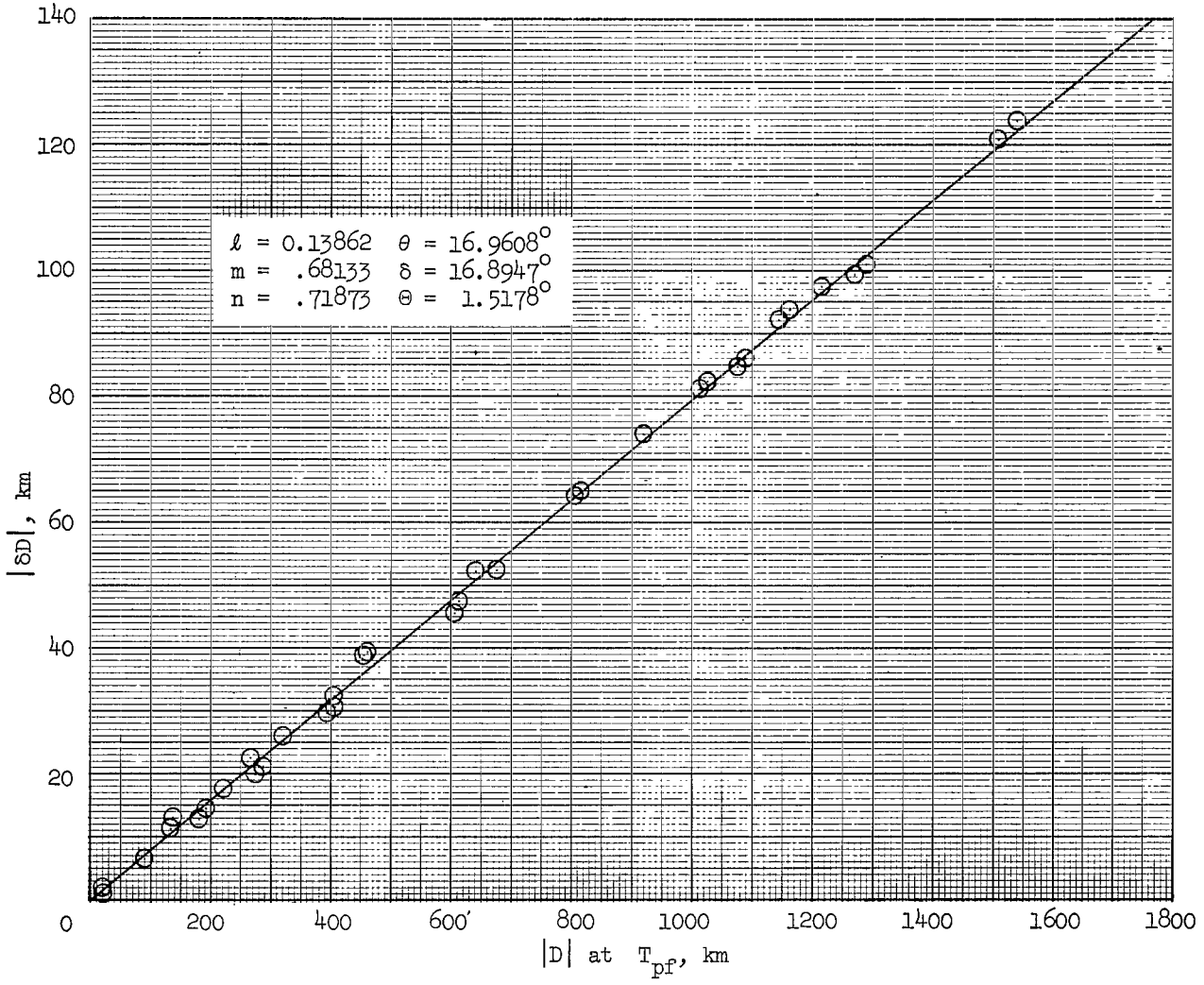

(d) Capella.

Figure 7.- Continued.

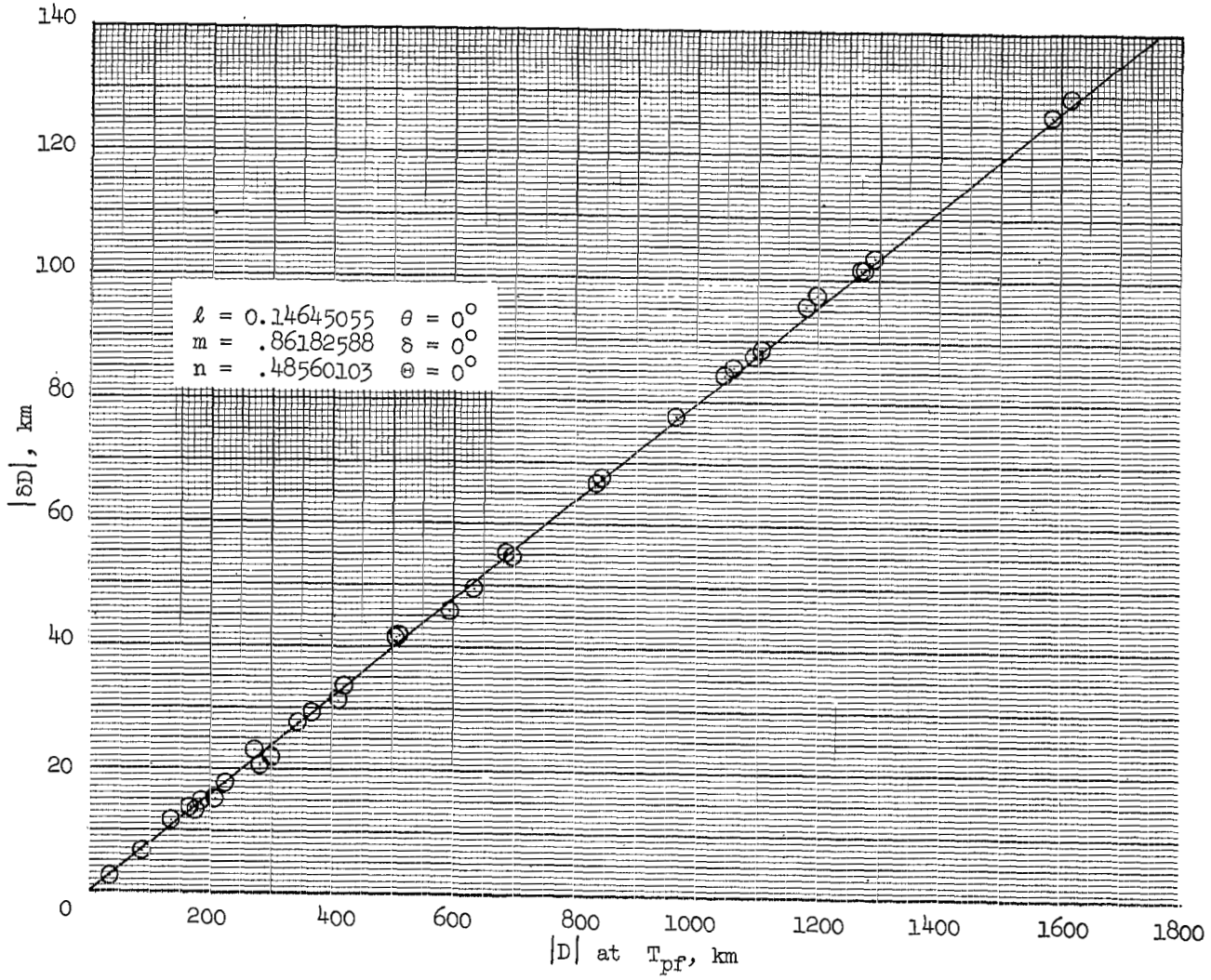

(e) Fictitious star in direction of vehicle-Earth line.

Figure 7.- Continued.

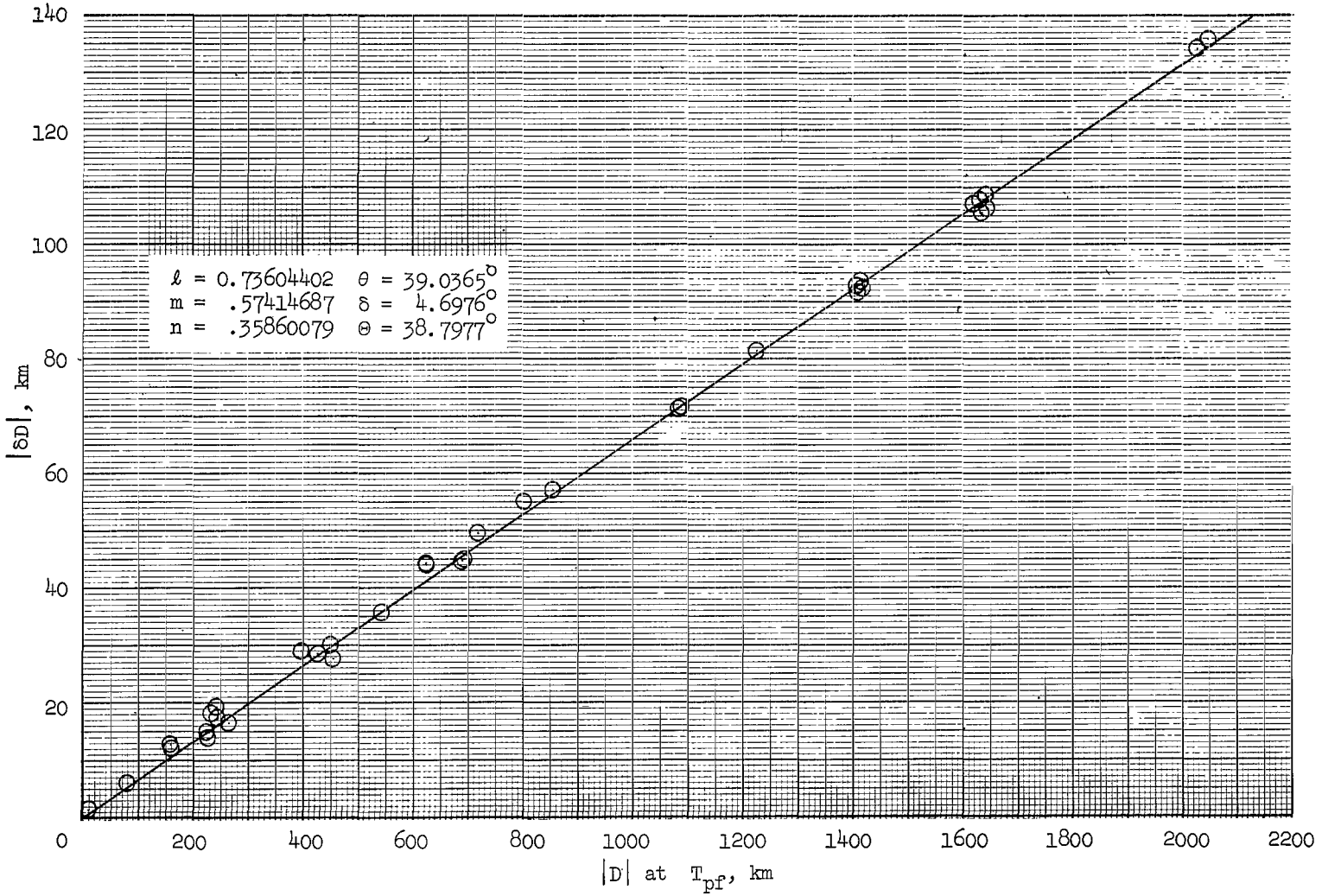

(f) Fictitious star in direction of major axis of error ellipsoid.

Figure 7.- Continued.

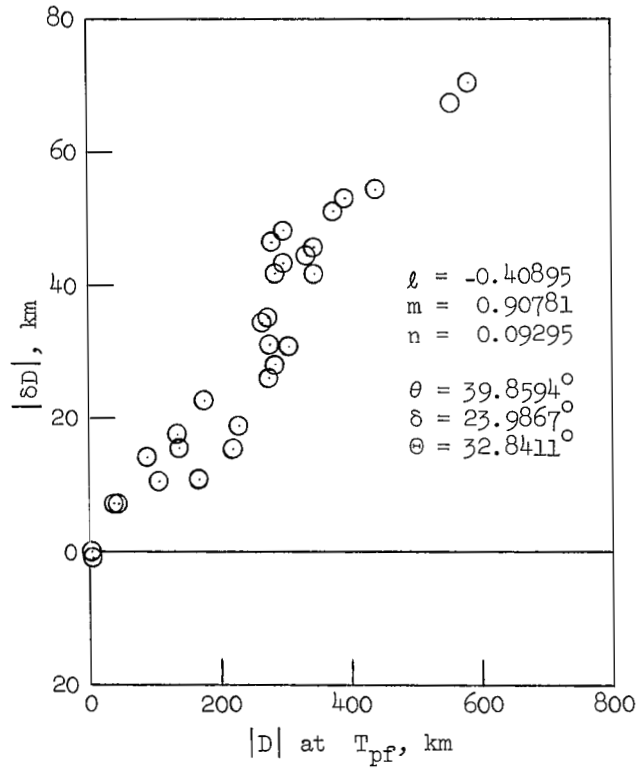

(g) Procyon.

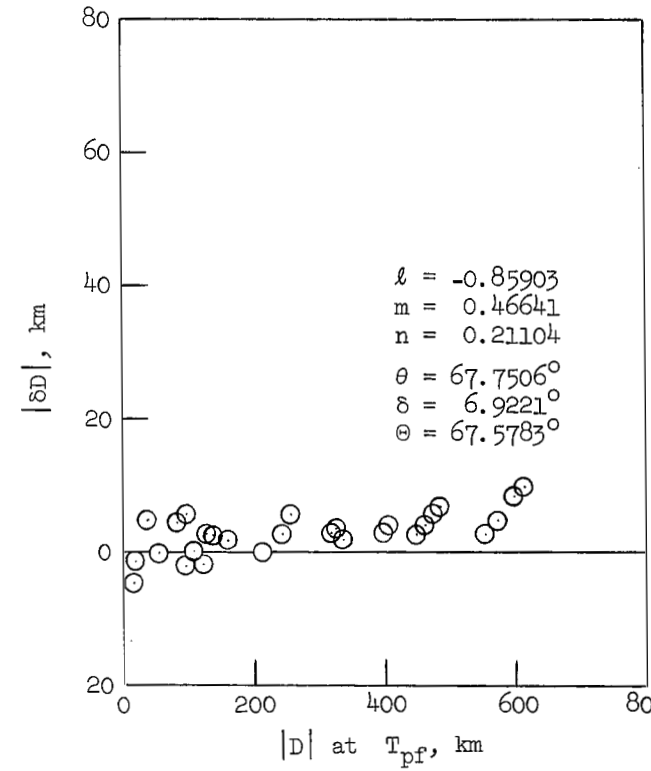

(h) Regulus.

Figure 7.- Concluded.

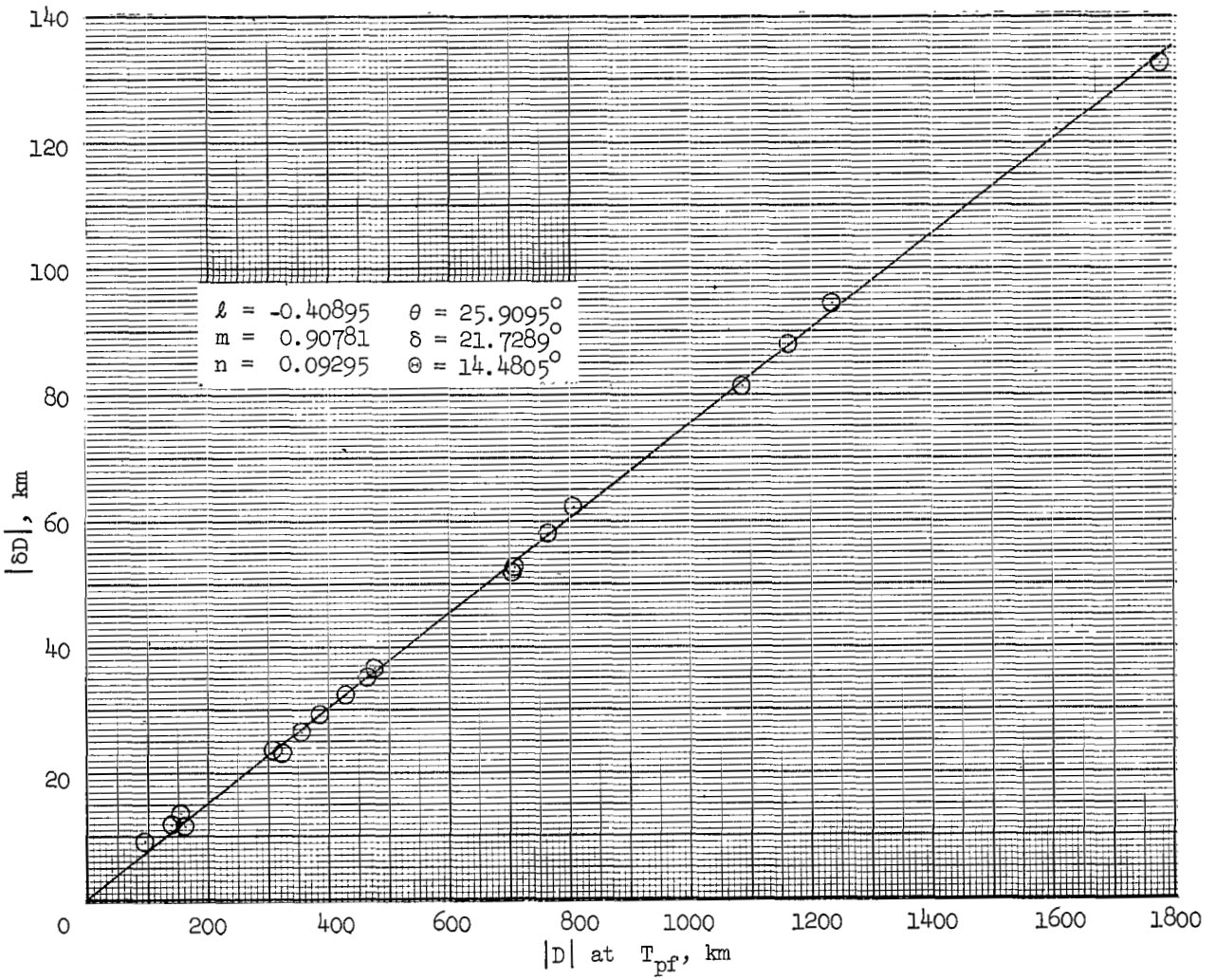

Figure 8.- Change in off-nominal position component in the direction of the star Procyon plotted for different perturbed trajectories. Data apply to nominal 68-hour translunar trajectory (injection date: May 15, 1968). (Signs of D and δD are the same.)

nominal trajectory at time T_{pf}. As illustrated in figure 9, maximum values of D will most likely be measured if the chosen star falls on or near this major axis. Maximum values for δD are obtained by measuring stars in the direction of the velocity vector (or along the range vector $\bar{r}_{ve}$ which lies close to the velocity vector in the midcourse portion of the trajectory). As shown by figure 9, the nominal and perturbed trajectories are approximately parallel; hence, measuring stars perpendicular to the trajectory (velocity vector) gives no indication of a change in D between T_{pf} and T_1.

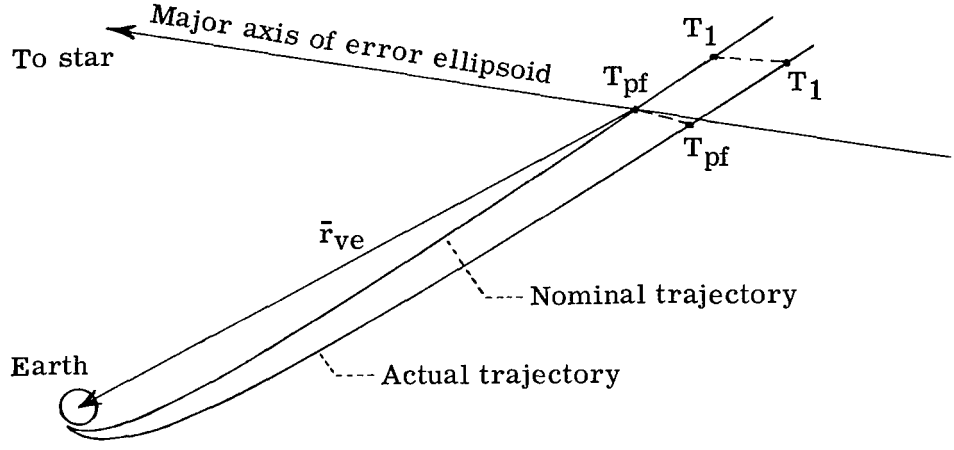

Figure 9.- Sketch showing geometry for star selection. (All lines shown lie near the Earth-Moon plane.)

It appears, then, that for the present guidance method, stars should be selected in the general region of the cone whose apex is formed by the error-ellipsoid major axis and the range vector $\bar{r}_{ve}$ (see fig. 10).

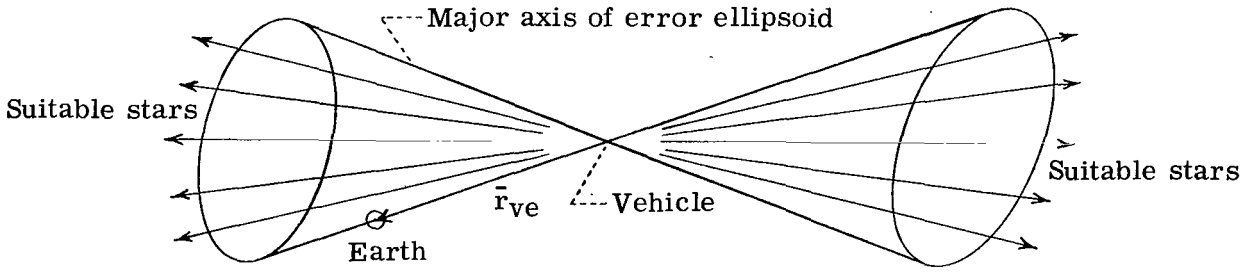

Figure 10.- Region of stars suitable for guidance measurements.

The most suitable stars would lie in the middle of this region since use of these stars is the best compromise for obtaining large values of both D and δD.

By referring to the data in figures 7 and 8 along with the angles listed in these figures for the respective stars, the differences between the plots can be readily explained. The stars cited in figures 7(a) to 7(f) all lie within the region described in figure 10 and can be considered suitable. For figure 7(e) with the star in the direction of the vehicle-Earth line, the actual measurement, of course, would have to be to a star in the opposite direction. A star in the direction of the Earth-Moon line (fig. 7(b)) is shown to be about the most suitable since this star is almost directly between $\bar{r}_{ve}$ and the major axis of the error ellipsoid. Rigil Kentaurus (fig. 7(c)) lies between these two lines also, but is inclined about 39^{o} to the Earth-Moon-vehicle plane. The stars Rasalhague (fig. 7(a)) and Capella (fig. 7(d)) are in the general direction of the vehicle-Earth line. Regulus (fig. 7(h)) is nearly perpendicular to both the major axis of the error ellipsoid and the range vector $\bar{r}_{ve}$ (see fig. 11); hence, the values of both D and δD are small and Regulus could not be used for the present nominal trajectory (table II).

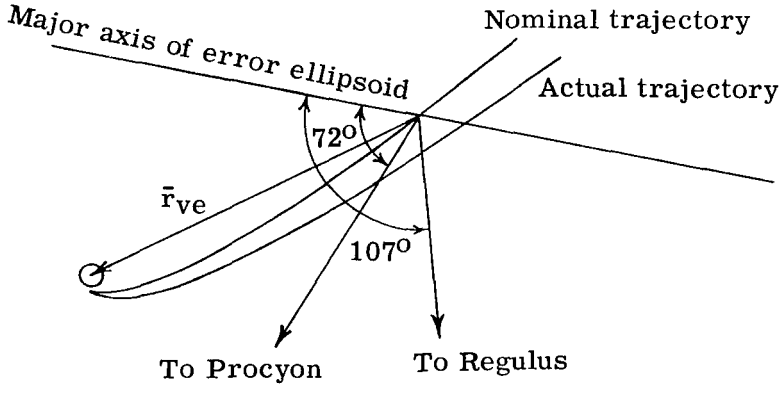

Figure 11.- Projection of lines in the Earth-Moon-vehicle plane.

Procyon (fig. 7(g)) is nearly perpendicular to the major axis of the error ellipsoid; hence, the values of D are small and Procyon could not be used for the present nominal trajectory. The spatial direction of the major axis, however, is dependent upon the particular nominal trajectory (injection date, injection velocity, etc.) and, as is shown in figure 8, Procyon would be a highly desirable star for the nominal 68-hour translunar trajectory in reference 10.

Calculation of major axis of error ellipsoid.- As indicated in the previous discussion, a knowledge of the direction of the major axis of the position-error ellipsoid is important since it serves to define a limit on the star-to-Earth angle measurements. The position-error ellipsoid at T_{pf} can be determined from

$$\left[\Sigma\epsilon_{r'}\right] = \left[G\right]\left[\Sigma\epsilon_{r}\right]\left[G\right]^{T} \tag{11}$$

where $\left[\Sigma\epsilon_{r'}\right]$ is a diagonal matrix whose elements are $\sigma_{x'}^2$, $\sigma_{y'}^2$, and $\sigma_{z'}^2$, the variances in the values of x', y', and z', respectively (for example, see ref. 11). These variances are a measure of the three normal axes of the error ellipsoid and are easily calculated, as they are the eigenvalues of $\left[\Sigma\epsilon_{r}\right]$, the covariance matrix of position errors $\left(\text{at } T_{pf}\right)$ in the X, Y, Z system. The matrix $\left[G\right]$ is the rotational transformation matrix such that

$$\begin{Bmatrix} x' \\ y' \\ z' \end{Bmatrix}_{T_{pf}} = \left[G\right] \begin{Bmatrix} x \\ y \\ z \end{Bmatrix}_{T_{pf}} \tag{12}$$

This matrix is also easily calculated; the normalized eigenvectors of the matrix $\left[\Sigma\epsilon_{r}\right]$ form the rows of $\left[G\right]$ which are the direction cosines (with respect to the X-, Y-, and Z-axes) of the three normal axes of the error ellipsoid. Hence, the major axis of the ellipsoid is determined by the largest eigenvalue, and the direction cosines of the major axis are determined by the corresponding row (eigenvectors) of the matrix $\left[G\right]$.

Actually the error ellipsoid is six dimensional, if the velocity errors are considered also. However, the position-error characteristics of this ellipsoid, as determined from equations (11) and (12) used with six-dimensional matrices, are almost exactly the same as those determined from the 3×3 position-error covariance matrix.

The position-error ellipsoid for the nominal trajectory in the present paper (table II) was determined at $T_{pf} = 9.5$ hours and the results for various injection errors are shown in table IV. The program in reference 7, which uses equations similar to equation (11), was employed to obtain the covariance matrix of position errors at $T_{pf} = 9.5$ hours by mapping forward the covariance matrix of injection errors. Because the injection errors are dependent upon the type of vehicle used, arbitrary injection-error values had to be assumed. Given in the first column of table IV are the various types of assumed errors, some of which are defined in appendix A. Except for those types defined in appendix A, the 1-sigma values of the magnitude of the position and velocity errors were assumed to be 10 kilometers and 10 m/sec, respectively. The elements of the

TABLE IV.- ERROR-ELLIPSOID MAGNITUDE AND DIRECTION AT T_{pf} FOR VARIOUS INJECTION ERRORS

Types of errors assumed at injection	Elements of diagonal covariance matrix of injection errors						1-sigma values for ellipsoid of trajectory-state deviations			Direction cosines of major axis of error ellipsoid			Angle* between major axis and $\bar{r}_{ve}$, deg
	σ_x^2, km^2	σ_y^2, km^2	σ_z^2, km^2	$\sigma_{\dot{x}}^2$, $(km/sec)^2$	$\sigma_{\dot{y}}^2$, $(km/sec)^2$	$\sigma_{\dot{z}}^2$, $(km/sec)^2$	Major axis, km	Mean axis, km	Minor axis, km	l	m	n	
Spherical position; spherical velocity	33.33	33.33	33.33	0.00003333	0.00003333	0.00003333	930.19	124.09	96.69	0.73604402	0.57414687	0.35860079	39.037
Spherical position; no velocity	33.33	33.33	33.33	0	0	0	615.05	92.67	78.20	0.74941316	0.56076837	0.35202090	40.184
No position; spherical velocity	0	0	0	0.00003333	0.00003333	0.00003333	698.58	95.04	27.72	-0.72545294	-0.58438199	-0.36361478	38.145
No position; velocity in direction of velocity vector	0	0	0	0.00009094	0.00000566	0.00000339	1132.54	37.99	9.28	0.74264802	0.56867225	0.35367463	39.592
Spherical position; velocity in direction of velocity vector	33.33	33.33	33.33	0.00009094	0.00000566	0.00000339	1288.76	93.20	87.05	0.74417814	0.56689993	0.35330345	39.725
No position; velocity according to appendix A	0	0	0	0.00009948	0.00009355	0.00009653	1205.79	159.96	46.99	-0.72634358	-0.58352027	-0.36322046	38.220
Spherical position; velocity according to appendix A	33.33	33.33	33.33	0.00009948	0.00009355	0.00009653	1353.47	179.02	103.91	0.73118129	0.57887490	0.36094007	38.625
Position and velocity according to appendix A	87.738	94.827	106.236	0.00009948	0.00009355	0.00009653	1593.09	206.28	169.83	-0.73465308	-0.57402232	-0.36163959	38.930
Position according to appendix A; no velocity	87.738	94.827	106.236	0	0	0	1041.41	163.26	128.08	0.74557412	0.56113183	0.35951393	39.882

*Either angle or supplement of angle given, whichever is smaller.

resulting covariance matrix (assumed to be diagonal) of the injection errors are also shown in this table.

It is important to note that for the nominal trajectory, the value of T_{pf}, and the injection-error covariance matrices used in this report, table IV shows the direction of the major axis of the error ellipsoid to be essentially unaffected by the choice of injection errors. The angle between the major axis and the range vector $\bar{r}_{ve}$ (see fig. 10) is approximately 39^{o}.

RANGE DETERMINATION

The accuracy of the range measurement is the predominant factor affecting the accuracy of the position fix (see ref. 9) and hence the accuracy of the guidance method. Because of the importance of this measurement, the various aspects of the onboard optical (manual) determination of range are discussed in this section.

Methods of Optically Measuring Range

The two basic methods of determining range to the Earth center from onboard optical measurements are: (1) the method involving measurement of the angular diameter of the Earth, and (2) the method involving measurement of two or more angles between certain combinations of stars, the Earth, and the Moon. Large errors are inherent in angular diameter measurements, so the former method would ordinarily not be considered.

The latter method has many alternatives, although basically it involves using the sine law to solve the triangle shown in figure 12 for the magnitude of $\bar{r}_{ve}$.

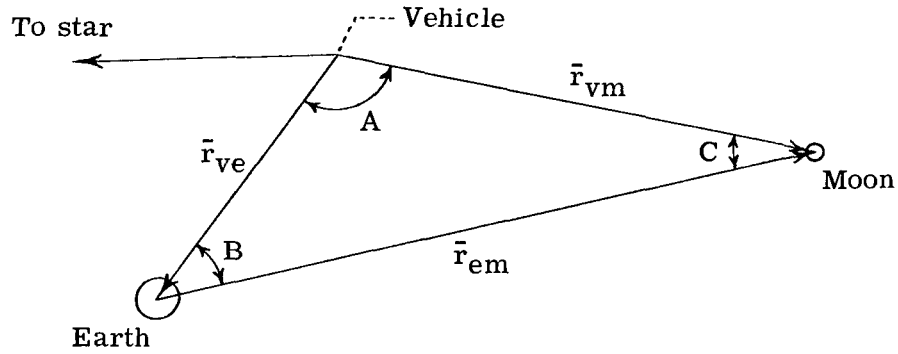

Figure 12.- Variables involved in determining range from vehicle to Earth center.

For any given time, $\bar{r}_{em}$ is known; the angle A can be measured directly. In order to solve for $|\bar{r}_{ve}|$ then, only the angle C remains to be determined. Once the required angular measurements have been made, the sine-law equation

$$r_{ve} = \frac{\sin C}{\sin A} r_{em} \tag{13}$$

could be solved directly. This procedure involves use of trigonometric tables and use of a large number of significant figures, although calculations show that five-place trigonometric functions provide range-determination accuracy within ±4 kilometers. If a desk calculating machine is available, these requirements present no problem as to calculation time or calculation accuracy.

Another way of determining range, which lends itself more readily to manual calculations, pertains to the perturbation procedure (ref. 9) about a nominal trajectory. For this procedure the difference in range from the nominal value is

$$\Delta r_{ve} = -\frac{r_{vm}}{\sin A} \Delta A + r_{em}(\cos B \cot A - \sin B)\Delta B \tag{14}$$

or in terms of the angle C

$$\Delta r_{ve} = -r_{ve}(\cot A)\Delta A + r_{ve}(\cot C)\Delta C \tag{15}$$

All values in equations (14) and (15) are based on the nominal trajectory and ΔA, ΔB, and ΔC are the measured deviations from the respective nominal angles.

Measurement of Angles B and C

The solution for range r_{ve} by the method involving the measurement of two or more angles requires that either B or C be determined. There are essentially three ways by which angle B (or C) can be determined from onboard measurements: (1) by measuring the declination and right ascension of the Earth (or Moon), (2) by measuring one star-to-body angle, and (3) by measuring two star-to-body angles. The first method has some disadvantages in that the measurements must be referenced to a stable platform. Also, a fair amount of calculation is involved in computing the angle. First, the direction of the Earth (for determining B) is determined from

$$\left.\begin{aligned} \frac{x_{ve}}{r_{ve}} &= \cos DC \cos RA \\ \frac{y_{ve}}{r_{ve}} &= \cos DC \sin RA \\ \frac{z_{ve}}{r_{ve}} &= \sin DC \end{aligned}\right\} \tag{16}$$

where DC and RA are the angles of declination and right ascension, respectively. Then, from the dot product of the vehicle-Earth vector and the Earth-Moon vector, the following equation is obtained:

$$\cos B = -\left(\frac{x_{em} \cos DC \cos RA + y_{em} \cos DC \sin RA + z_{em} \sin DC}{r_{em}}\right) \tag{17}$$

The calculations in equations (16) and (17) could be performed before the mission and presented in a form such as that shown in figure 13. (Fig. 13 is discussed subsequently in connection with the two-star method.)

If the one-star method were used, $|\Delta B|$ would be approximately equal to $|\Delta\theta|$ for a star near the Earth-Moon-vehicle plane (see fig. 12) and equation (14) could be written as

$$\Delta r_{ve} = -\frac{r_{vm}}{\sin A} \Delta A + q r_{em}(\cos B \cot A - \sin B)\Delta\theta \tag{18}$$

where θ is the angle between the line of sight to the star and the line of sight to the Earth center. Likewise, equation (15) could be written as

$$\Delta r_{ve} = -r_{ve}(\cot A)\Delta A + q r_{ve}(\cot C)\Delta\theta \tag{19}$$

where θ is the angle between the line of sight to the star and the line of sight to the Moon center. The term q in these equations is either ± 1, depending on the location of the star (see ref. 9). The one-star method, however, is highly restrictive because of accuracy considerations. For reasonable accuracy the star must be in or very close to the nominal Earth-Moon-vehicle plane, as is shown subsequently.

In using the two-star method, the angle B (or C) can be measured directly, as shown in appendix B. The calculations are quite extensive, but can be done before the flight and presented in the form shown in figure 13 for use in the perturbation procedure given by equations (14) and (15). (The data could be plotted in terms of the total angle C

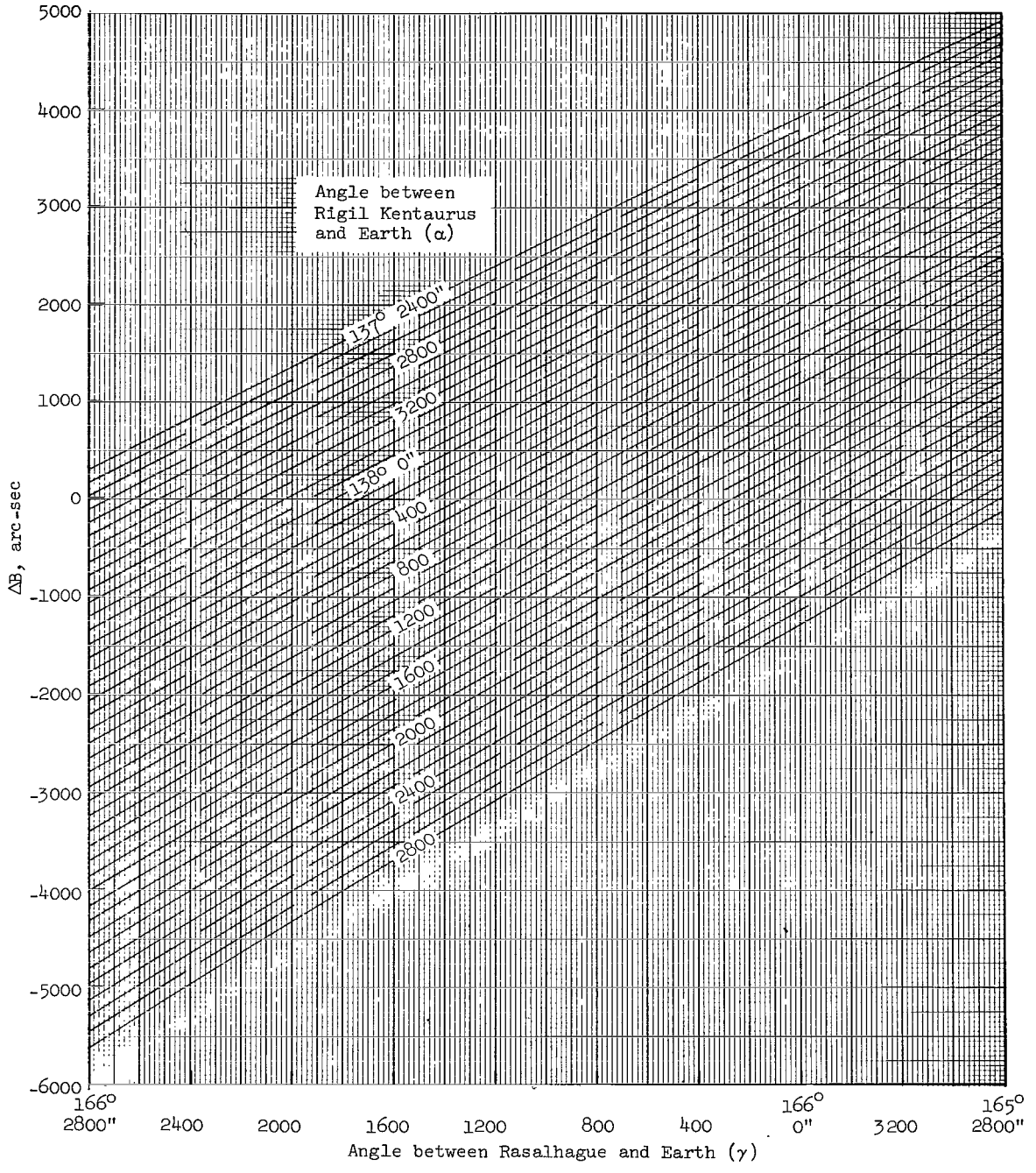

Figure 13.- Difference in angle B from nominal value, as obtained from two onboard star-to-Earth measurements at T_{pf} = 9.5 hours. (Data apply to nominal trajectory in table II and can be used to determine range by the perturbation method.)

for direct use in eq. (13)). Although the stars are not required to be in a particular plane, they are limited (because of the method used to solve the cone equations) by the requirement

$$(\beta + \gamma) < 90^{o}$$

Thus, the angle (or supplement) between the lines to the two stars must be less than $(90^{o} - \gamma)$. This limitation is not very severe since the same star-to-body angles used for the range measurement would ordinarily be used for two of the three position-component measurements (D, E, and F). As shown in table V and figure 10, the suitable stars for position measurement are necessarily limited to a small region.

TABLE V.- ANGLES[a] BETWEEN VARIOUS COMBINATIONS OF SUITABLE STARS

Star / Star	Fictitious (Moon-Earth line)	Capella	Rigil Kentaurus	Rasalhague
Fictitious (vehicle-Earth line)	20.957°	16.961°	41.653°	13.731°
Fictitious (Moon-Earth line)		27.850°	39.081°	19.859°
Capella	27.850°		27.073°	30.301°
Rigil Kentaurus	39.081°	27.073°		52.520°

[a]Either angle or supplement of angle, whichever is smaller.

Accuracy of Range-Measurement Methods

A summary of the relative accuracy characteristics is given in figure 14 for the various methods of onboard optical range measurement. The standard deviation of range error $\sigma_{r_{ve}}$ was calculated from equations (14) and (15). For example,

$$\left(\sigma_{r_{ve}}\right)^2 = \left(\frac{r_{vm}}{\sin A}\,\sigma_A\right)^2 + \left[r_{em}(\cos B \cot A - \sin B)\sigma_B\right]^2 \tag{20}$$

where the angular measurements A and B are considered to have random uncorrelated errors, each with a standard deviation of 10 arc-seconds (for the one-star measurement method). For the method using the two-star measurements, the standard deviation for each of the star measurements was assumed to be 10 arc-seconds. Using these values in connection with figure 13 gives an overall 1-sigma error for the angle B of

$$\sigma_B = \sqrt{(14)^2 + (14)^2} = 19.8 \text{ arc-seconds}$$

The two stars used in figure 13 were Rasalhague and Rigil Kentaurus; however, the accuracy shown is representative of any two stars. The reading error is not included since it would be relatively small and have little overall effect on the value of σ_B. It should be stated that, in reference to equation (20), error in the angle A has a comparatively small effect on the standard deviation of range error $\sigma_{r_{ve}}$, especially in the two-star measurement method. In fact, for this method, σ_A could be doubled without significantly changing the value of $\sigma_{r_{ve}}$.

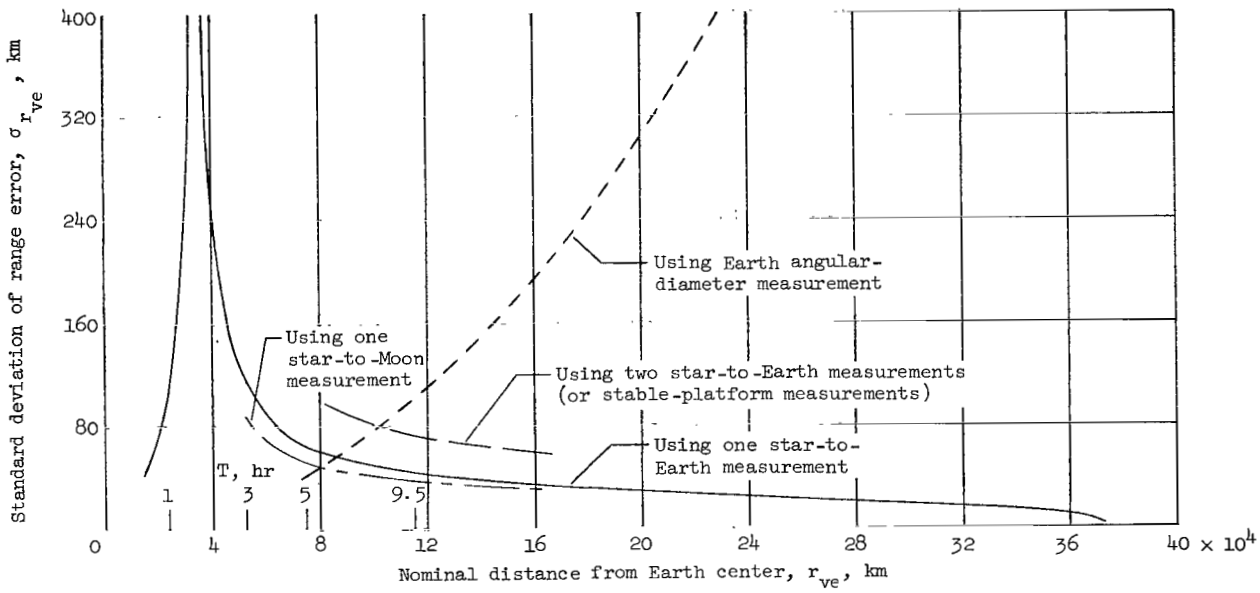

Figure 14.- Accuracy characteristics of various range-measurement methods. 1-sigma angular-measurement error is 10 arc-seconds. (Methods involving star-to-body measurements also include angular measurement between Earth and Moon.)

In figure 14 the curve for the angular-diameter measurement method shows this method to be accurate only near the Earth. The other three curves in the figure apply to the determination of range by either equation (13) or by the perturbation method (eq. (14) or (15)). In the perturbation method an additional error, which is predictable under certain conditions, is caused by out-of-plane effects and is discussed in the next section. The rapid rise indicated near the Earth for these curves is caused by the close proximity of the vehicle to the Earth-Moon line as explained in reference 9. The important items to note from figure 14 are (1) that the range-determination error (at first midcourse) is somewhat lower for star-to-Moon measurements than for star-to-Earth

measurements and (2) that the error is almost twice as large for two-star measurements (or stable-platform measurements) as for one-star measurements.

The star-to-body angle would be most likely determined from measurements such as those shown in figure 15.

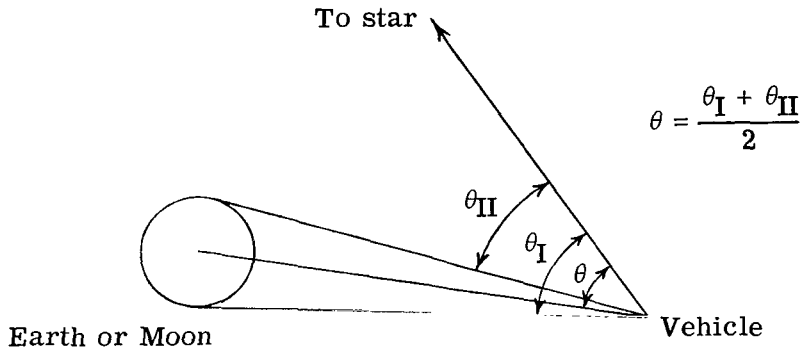

Figure 15.- Measurements for determining θ.

Under the assumption that the Moon is more nearly spherical than the Earth, error due to oblateness effects would be much smaller if the Moon were used as the body.

Out-of-Plane Effects on Range Measurement

As previously stated, the perturbation method of measuring range has an inherent error due to out-of-plane effects. This error is caused by the fact that for any perturbed trajectory the vehicle will not lie in the nominal Earth-Moon-vehicle plane at T_{pf}. For the two-star measurement method, as well as for the one-star measurement method in which the star is in or very near the nominal plane, this error is essentially predictable as shown in figure 16. The plots in figure 16 were obtained from the data presented in table VI. (For calculations involving stars much out of the nominal Earth-Moon-vehicle plane, an additional factor is required in the last term of eqs. (18) and (19) as shown in reference 9. This factor has been included in the calculations for table VI but is important only for the out-of-plane star Alpheratz ($\delta = 28.391^{o}$).) In figure 16 the ordinate is the difference between the true value of Δr_{ve} and the value calculated from equation (14). Values of $\Delta r_{ve} - \Delta r_{ve,calc}$ are shown in table VI for various stars, most of which are fictitious, to show how the error is affected by star location.

The empirical curves in figure 16 can be used to correct the range measurement. The scatter in figure 16(b) is less than that in figure 16(a), the implication being that the use of a star in the direction of the Moon-Earth line (or the two-star method)

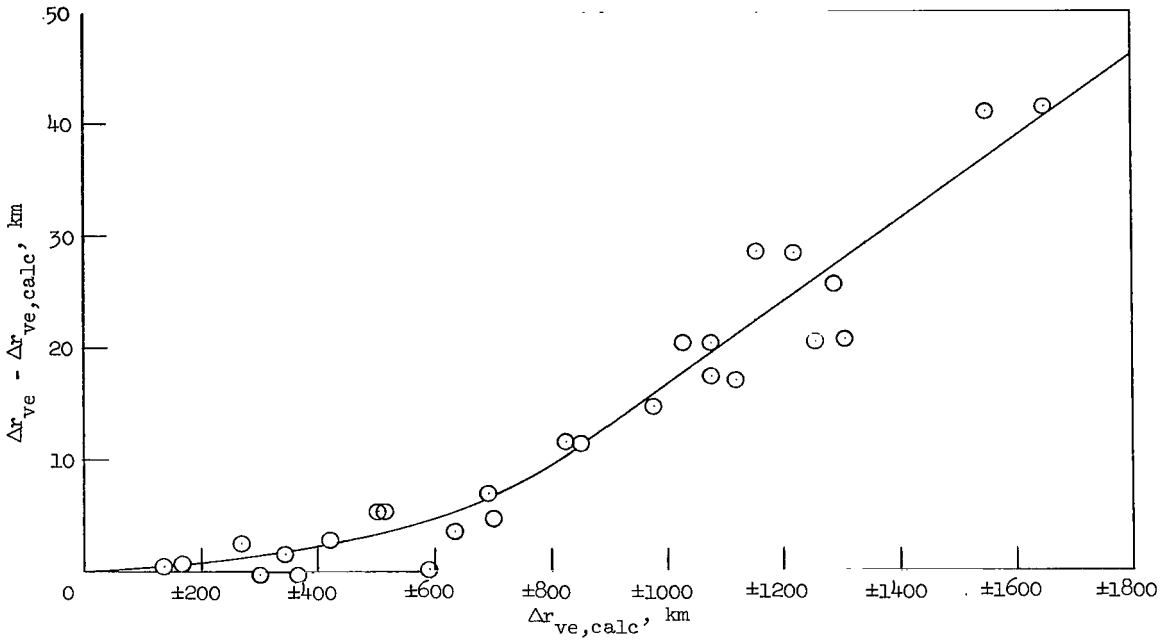

(a) Star in Earth-Moon-vehicle plane; $\theta = 90^0$.

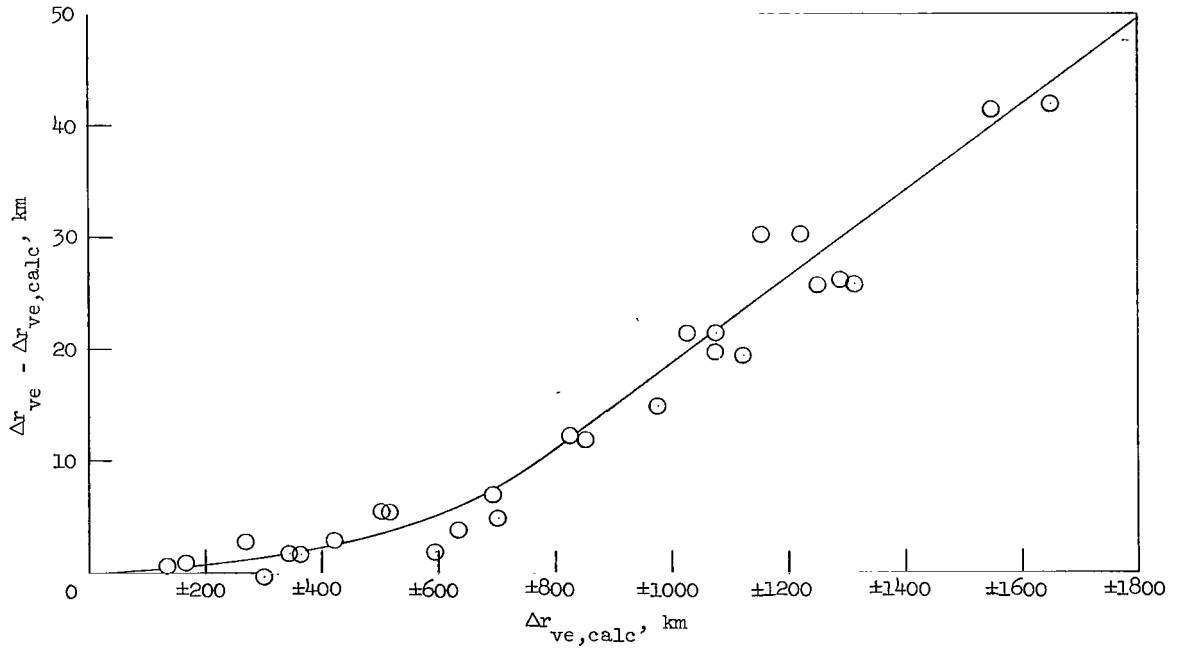

(b) Star in Earth-Moon-vehicle plane in direction of Moon-Earth line (or two-star method).

Figure 16.- Out-of-plane effects on range measurement by perturbation method.

TABLE VI.- ERRORS IN RANGE DETERMINATION BY PERTURBATION METHOD

[No measurement error]

Perturbed-trajectory no. / Condition	Δr_{ve}, km	$\Delta r_{ve} - \Delta r_{ve,calc}$, km, for –								
		Star in nominal Earth-Moon-vehicle plane; $\theta = 90^o$, $\delta = 0^o$	Star in nominal Earth-Moon-vehicle plane; $\theta = 64.242^o$, $\delta = 0^o$	Star in direction of Earth-Moon line; $\theta = 20.957^o$, $\delta = 0^o$ (*)	Star 10 arc-min out of Earth-Moon-vehicle plane; $\theta = 64.2419^o$, $\delta = 0.1667^o$	Star 20 arc-min out of Earth-Moon-vehicle plane; $\theta = 64.2422^o$, $\delta = 0.3333^o$	Star 1.0^o out of Earth-Moon-vehicle plane; $\theta = 64.246^o$, $\delta = 1.0^o$	Star in direction of major axis of error ellipsoid; $\theta = 39.036^o$, $\delta = 4.698^o$	Regulus; $\theta = 67.751^o$, $\delta = 6.922^o$	Alpheratz; $\theta = 67.523^o$, $\delta = 28.391^o$
1	135.87	0.43	0.43	0.55	-0.07	-0.07	-3.08	-18.15	-23.42	-108.34
2	271.85	2.48	2.60	2.74	1.34	0.21	-4.55	-34.68	-45.22	-214.85
3	-342.54	1.50	1.62	1.62	1.50	1.37	-0.92	-9.85	-2.90	-18.68
4	-686.23	6.93	7.07	6.93	6.80	6.55	5.64	-15.74	-1.89	-32.79
6	365.09	-0.44	0.06	1.58	-3.47	-7.01	-24.09	-135.41	-143.06	-653.05
8	-840.68	11.35	11.49	11.84	13.24	15.01	22.15	65.08	84.08	344.45
9	836.58	11.51	13.04	12.13	9.99	8.22	1.09	-41.64	-60.18	-315.26
10	-419.37	2.72	3.84	2.86	3.73	4.49	8.06	29.42	38.94	168.51
20	-696.20	4.60	4.71	4.85	5.99	7.13	12.30	45.01	56.52	242.05
21	-631.79	3.50	3.63	3.74	4.76	5.90	10.37	39.95	49.90	215.55
22	-299.68	-0.41	-0.29	-0.41	-0.29	-0.16	-0.02	1.69	2.29	11.34
23	-963.57	14.71	14.71	14.84	15.72	16.74	20.93	36.31	57.11	209.95
24	1049.16	20.41	20.65	21.43	18.13	15.73	5.52	-56.13	-81.76	-444.17
25	-1055.57	20.45	20.70	21.46	23.23	25.63	35.86	97.96	124.06	495.55
26	1184.33	28.63	29.00	30.26	25.85	22.81	10.23	-66.32	-97.04	-542.96
27	-1192.06	28.51	28.89	30.28	31.93	34.96	47.56	124.79	156.21	614.50
28	-166.44	0.64	0.75	0.90	-0.38	-1.51	-5.67	-47.93	-42.43	-195.31
29	-509.71	5.30	5.31	5.42	4.16	2.89	-1.72	-54.35	-42.13	-209.76
30	507.40	5.37	5.37	5.49	6.63	7.77	12.39	66.24	52.95	225.01
31	-1102.85	17.06	17.57	19.47	21.24	24.90	39.85	144.37	168.64	710.48
32	1095.55	17.47	17.85	19.74	14.18	10.64	-4.29	-108.10	-132.15	-664.77
33	-1286.84	20.81	21.82	25.86	27.26	32.69	54.61	216.93	244.33	879.80
34	1276.88	20.53	21.54	25.71	16.10	10.79	-11.11	-171.83	-200.17	-986.10
36	-592.59	0.09	0.48	1.74	3.51	6.41	18.71	117.43	123.99	567.18
37	591.47	0.29	0.67	1.94	-2.36	-5.40	-17.57	-115.35	-123.02	-562.80
38	-1263.70	25.64	25.76	26.15	27.54	29.31	36.83	73.27	100.97	372.36
39	-1609.62	41.47	41.60	41.98	43.37	45.01	52.08	78.13	112.69	371.14
40	1591.37	41.07	41.19	41.45	39.55	37.91	30.87	6.32	-39.31	-268.89

*These results also apply to two-star method (stars not necessarily in the Earth-Moon-vehicle plane).

would lead to the most accurate range determination. In the most accurate determination the maximum deviation from the empirical curve is about 5 kilometers, which adds little (in a statistical sense) to errors with magnitudes of those shown in figure 14. It can be seen from table VI, however, that any star within 10 to 20 arc-minutes of the nominal Earth-Moon-vehicle plane would suffice for range measurement. For the star 10 arc-minutes out of this nominal plane, the maximum spread about the empirical curve would be about 7 kilometers, except for trajectory 34 which would be 10 kilometers. For the star 20 arc-minutes out of the plane, the maximum spread would be about 10 kilometers, except for trajectory 34 which would be 15 kilometers. The errors become much more pronounced for stars more than 20 arc-minutes out of the plane and cannot be accounted for empirically.

Summary of Range-Determination Accuracy

The important facts concerning manual range determination at first midcourse are:

1. If the one-star method is employed, the perturbation procedure must be used because only the deviation (from the nominal) in the angle can be measured.

2. Even though it is inherently more inaccurate than the one-star method, the two-star method will probably be required for most lunar missions since preflight analysis would show no navigation stars close enough to the nominal plane to facilitate use of the one-star method.

3. In the two-star method the total angle can be measured, and thus range can be calculated directly from equation (13).

SUMMARY OF CALCULATIONS REQUIRED IN GUIDANCE PROCEDURE

The preflight and onboard calculations required in the present guidance procedure, along with the pertinent equations, are briefly summarized in the following outline. No attempt is made herein to systematize the procedure for the easiest, fastest, and most accurate calculation method. Furthermore, the outline does not include the equations or steps required for alining the thrust vector for the guidance maneuver; they are simple to derive (for example, see ref. 12).

The preflight calculations are made for the nominal trajectory and apply to the predetermined nominal time of the measurements T_{pf}. For the preflight calculations it is assumed that the nominal values of the position and velocity coordinates with respect to both the Earth and the Moon, as well as the Earth-Moon distance and the direction cosines of the required stars, are known and that the required transition matrices have been calculated.

Required preflight calculations:

1. Angle A . . . . . $\cos A = \dfrac{r_{ve}^2 + r_{vm}^2 - r_{em}^2}{2 r_{ve} r_{vm}}$

2. Angle B (or C) . . . . . $\sin B = \dfrac{r_{vm}}{r_{em}} \sin A$

Note: The nominal values of A and of B (or C) are required only if the perturbation method of measuring range is used.

3. Star-to-body angles (θ_1; θ_2; θ_3) . . . . . $\cos \theta = \dfrac{lx + my + nz}{r}$

4. Derivatives of A, θ_1, θ_2, and θ_3 with respect to time for updating the measurements . . . . . Equations (B1) and (B3) in reference 9

5. Slopes from plots similar to figure 7 $\left(\delta D / D_{T_{pf}};\ \delta E / E_{T_{pf}};\ \delta F / F_{T_{pf}}\right)$

6. Guidance matrices $\left([e];\ [g];\ [h]\right)$ . . . . . Equations (7) and (8)

Required onboard calculations:

1. Convert all measurements to a common time T_{pf} . . . . . Equation (21) in reference 9

2. Range r_{ve} . . . . . Equation (13), (14), (15), (18), or (19)

3. Values ΔA, ΔB, ΔC, or $\Delta\theta$, if the perturbation method to calculate range r_{ve} is used . . . . . For example, $\Delta A = A_a - A_n$

4. Quantities D, E, and F for T_{pf} . . . . . Equation (1)

5. Multiply quantities D, E, and F by K_1, K_2, and K_3, respectively

6. Midcourse-velocity corrections $\overline{\Delta V}$ and $\overline{\Delta V_f}$ $\left(\overline{\Delta V_f}\right.$ can be calculated at any time during the mission prior to aim-point time$\left.\right)$ . . . . . Equations (9) and (10)

GUIDANCE ACCURACY CHARACTERISTICS

In this section the more important errors associated with the guidance procedure are defined and analyzed. It is assumed that there are no errors due to human limitations in calculating numbers with many significant figures. Although the guidance procedure described herein has been termed "Manual," all necessary onboard calculations do not have to be done by longhand or slide rule. Longhand calculation would require too much time, and there is no conceivable guidance procedure in which sufficient accuracy could be produced by calculations made entirely by slide rule. Slide-rule accuracy is sufficient for range (or position) determination; but, for the matrix multiplications

required in the guidance computations, at least six-place accuracy is necessary (for a guidance procedure with measurement errors of magnitudes shown in fig. 14). Hence, it is assumed that some means of performing simple desk-type calculations would be available to the navigator.

Test Conditions

In order to determine the general accuracy of the guidance method, specific conditions were selected to be representative of most lunar missions.

First midcourse maneuver.- The time of the first midcourse maneuver T_1 was selected to be 10 hours. This time is close to that for optimum fuel requirements, although this proximity is not necessary for making the subsequent error analysis. The time of the position fix T_{pf} was selected to be 9.5 hours, and thus one-half hour was allowed for performing the guidance calculations (eq. (9)) and for orienting the thrust vector. For practical purposes this time interval seems reasonable; however, the ensuing results could also apply to a longer (or shorter) time interval. A trial calculation of a first-midcourse-maneuver velocity correction was performed in approximately 15 minutes; no checking procedures were included. For this calculation it was assumed that the various measurements required for the position fix had been made shortly before T_{pf} and had all been corrected and updated to T_{pf}. (A simple method for updating these measurements is given in ref. 9.) The calculation for the second-midcourse-maneuver velocity correction (eq. (10)) could be made any time during flight prior to the final (aim-point) time T_f.

Aim points.- In the error analysis two different aim points are investigated: one at perilune (T_f = 70 hours, 37 minutes) and one at a point near the lunar sphere of influence (T_f = 56 hours). The variation of the errors between these two points is also included. For the aim point at perilune, the first midcourse maneuver is used to correct the actual (perturbed) trajectory to the nominal perilune (position only). The second midcourse maneuver (made at perilune) is required to correct the inherent velocity error due to the first midcourse maneuver. For the aim point near the lunar sphere of influence, the actual trajectory is corrected to the point on the nominal trajectory 56 hours from nominal injection time, where the second midcourse maneuver is applied.

The elements of the transition matrices depart from linearity as the central body (Moon) is approached. (See refs. 6 and 13, for example.) Hence, for comparison purposes, the two aim points were investigated, with the one at 56 hours chosen far enough away from the Moon to be relatively unaffected by it. There are other reasons for use of different aim points. For instance, for a particular type of mission, it may be simpler and/or more accurate to apply a terminal guidance procedure (to a trajectory that is supposedly on the nominal course) after having made the second-midcourse-maneuver

correction prior to reaching the Moon (or planet), whereas, for another type of mission, the second-midcourse-maneuver correction might be easily included in the terminal guidance maneuver or in the deboost maneuver.

Other conditions for which to aim, such as a given lunar approach asymptote, could be incorporated in the present method. This procedure would involve a set of terminal coordinates which would linearize the transition matrices for a wide range of perturbations.

Transition Matrices

Examples.- The transition matrices required for the guidance calculations are shown in table VII. These matrices apply to the nominal trajectory (see table II) and were generated by the program in reference 7. The 3×3 submatrices in the first, second, and last matrices ((a), (b), and (e) parts of table VII) are used in the guidance equations. The fourth matrix ((d) part of table VII) is the transformation matrix required for mapping the covariance matrix of injection errors (T = 0) to T_{pf} = 9.5 hours (required in error-ellipsoid calculations previously discussed). The third matrix ((c) part of table VII) was not used in the present analysis, but is included for possible use if an error analysis between the two times shown is desired.

Linear approximation effects.- In order to obtain a general idea of the error caused by linearization of the transition matrices, "perfect" guidance (i.e., guidance with no measurement or execution errors) was applied to the 40 perturbed trajectories in table III. (The fuel requirements for these trajectories are summarized in a subsequent figure.) The guidance was performed for the two different aim points and the results are given in the last four columns of the table. These results apply to the nominal trajectory of table II which comes to within 1665 kilometers of the Moon's surface (r_p = 3403 kilometers). As expected, the discrepancies at the aim points are larger for the trajectories that are farther from the nominal trajectory. The curves in figure 17 illustrate the progressive increase in the aim-point errors as the trajectory is perturbed farther from the nominal. These curves are shown for the position and velocity components for which perturbations have the largest effect on the trajectory (for example, compare the first 12 trajectories in table III).

As noted from table III, the errors at the perilune aim point are larger than those at the 56-hour aim point, with the larger percentage increase being in the velocity error. The position error increases up to three times whereas the velocity error increases as much as 100 times. The great increase in the errors at perilune is caused largely by the aforementioned effect of the Moon on the assumption of linearity. All position and velocity errors shown in table III, however, are generally small in comparison with those caused by errors in the measurements required for the guidance calculations. (For

TABLE VII.- STATE-TRANSITION MATRICES

[Exponent given at end of each number]

(a) Matrix for transitioning from 10 to 56 hr

0.18397068 00	0.16367418 00	0.90780576 -01	0.14164047 +06	0.25834212 +04	0.13015172 +04
0.20618665 00	0.24776638 +01	0.12994105 +01	0.27734888 +04	0.20458872 +06	0.36354531 +05
0.11394173 00	0.12931567 +01	0.87041364 00	0.14036259 +04	0.36264995 +05	0.15882821 +06
0.60015734 -05	0.19635148 -05	0.10805260 -05	0.75236952 00	0.86392488 -01	0.42457492 -01
0.17664494 -05	0.14366116 -04	0.11632002 -04	0.68260383 -01	0.15076761 +01	0.47507985 00
0.95564674 -06	0.11469357 -04	-0.13010716 -06	0.32313430 -01	0.47209395 00	0.89892318 00

(b) Matrix for transitioning from 10 hr to perilune (70 hr, 37 min)

-0.16804177 00	0.11607129 +01	0.63233023 00	0.37760592 +06	0.53896308 +05	0.37585866 +05
0.26125418 00	0.22270348 +01	0.13125725 +01	-0.48636477 +05	0.19298204 +06	0.56686290 +05
0.12585353 00	0.12528484 +01	0.58871565 00	-0.85384851 +04	0.57612417 +05	0.10891148 +06
-0.76817188 -04	-0.47622401 -03	-0.27299891 -03	0.35488797 +02	-0.40694930 +02	-0.16977675 +02
0.53477561 -04	-0.66364833 -04	-0.45173942 -04	-0.79632870 +02	-0.35366604 +01	0.89227447 +01
0.12195098 -04	-0.13885297 -03	-0.41910182 -04	-0.31335628 +02	0.76927085 +01	-0.29492002 +02

(c) Matrix for transitioning from 56 hr to perilune (70 hr, 37 min)

0.21204965 +01	0.16041629 00	0.13682995 00	0.10168238 +06	0.24281123 +03	0.31475286 +04
-0.28738580 00	0.65319876 00	0.80186812 +01	-0.16681536 +05	0.37706714 +05	0.37513230 +04
-0.54127618 -01	0.97726759 -01	0.48629285 00	-0.40828978 +04	0.44341775 +04	0.29211317 +05
0.20071121 -03	-0.13350981 -03	-0.42088363 -04	0.10793003 +02	-0.80042390 +01	-0.26208864 +01
-0.44804018 -03	-0.30181057 -04	0.47614757 -04	-0.21763512 +02	0.14839254 +01	0.36260822 +01
-0.17590183 -03	0.59466203 -04	-0.16495501 -03	-0.84971374 +01	0.41743676 +01	-0.76179589 +01

(d) Matrix for transitioning from 0 to 9.5 hr

0.41948920 +02	-0.61193071 +02	-0.30832064 +02	0.88249186 +05	0.28259802 +04	0.61275881 +04
0.16772236 +02	-0.54822736 +02	-0.20628127 +02	0.67458479 +05	0.20433145 +05	0.12345455 +05
0.12472478 +02	-0.24840537 +02	-0.29174238 +02	0.41960052 +05	0.88120858 +04	0.11975222 +05
0.10350756 -02	-0.17212393 -02	-0.88055056 -03	0.24779977 +01	0.22689039 00	0.25883674 00
0.94137598 -03	-0.24844021 -02	-0.11336515 -02	0.31798932 +01	0.76216386 00	0.57231656 00
0.59758215 -03	-0.12763631 -02	-0.10274083 -02	0.18953488 +01	0.41093051 00	0.37390006 00

(e) Matrix for transitioning from 10 to 9.5 hr $\left(\text{i.e., } [\phi]^{-1}_{9.5 \text{ to } 10 \text{ hr}} = \begin{bmatrix} [\phi_4]^T & -[\phi_2]^T \\ -[\phi_3]^T & [\phi_1]^T \end{bmatrix} \right)$

0.99962930 00	0.14864207 -03	0.83659335 -04	-0.17997740 +04	-0.91610628 -01	-0.51570603 -01
0.14864130 -03	0.10004870 +01	0.49733545 -03	-0.91610389 -01	-0.18002968 +04	-0.30332312 00
0.83658908 -04	0.49733550 -03	0.99988375 00	-0.51570472 -01	-0.30332313 00	-0.17999289 +04
0.41830011 -06	-0.16975658 -06	-0.95562211 -07	0.99961767 00	0.15689809 -03	0.88340428 -04
-0.16975439 -06	-0.55001961 -06	-0.56190313 -06	0.15689728 -03	0.10005027 +01	0.51402240 -03
-0.95560998 -07	-0.56190326 -06	0.13135906 -06	0.88339983 -04	0.51402245 -03	0.99987967 00

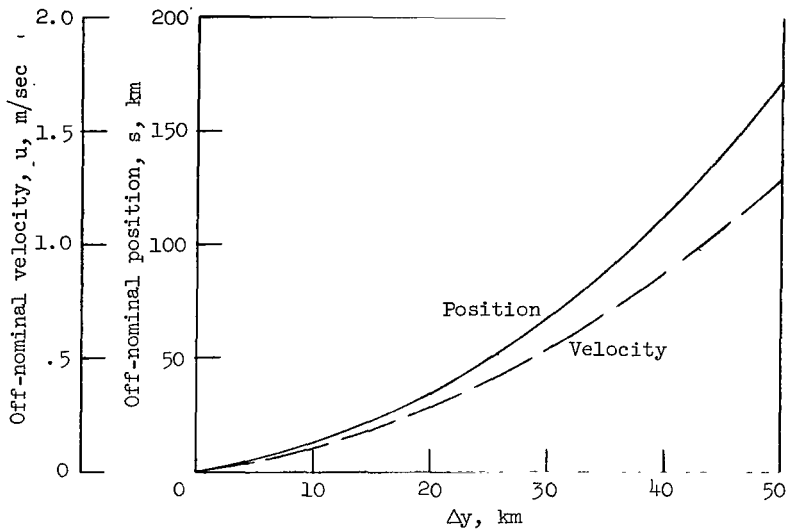

(a) Effect of error in injection position.

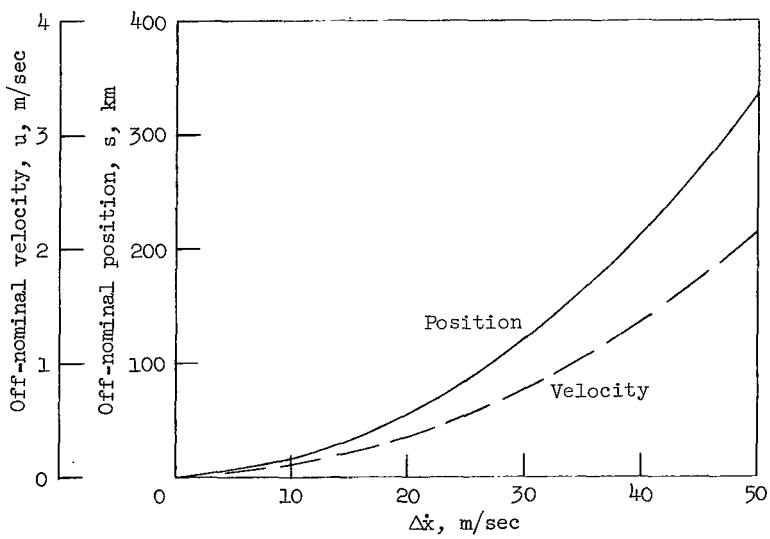

(b) Effect of error in injection velocity.

Figure 17.- Examples of errors at aim point (T_f = 56 hr) caused by linear approximation made in using transition-matrix theory. Results are from guidance maneuver at T_1 = 10 hours.

example, see table I.) Hence, for the range of injection-condition perturbations shown in table III (magnitudes considered to be representative of manned injection systems) and for the nominal trajectory used herein, errors caused by linearization of the transition matrices would have only minor effects on the overall guidance accuracy.

Fuel Requirements

As a matter of interest, the fuel requirements (i.e., midcourse velocity corrections ΔV and ΔV_f) for the present method are shown in figure 18. The data shown apply to "perfect" guidance maneuvers made for some of the trajectories in table III and are for the aim point at $T_f = 56$ hours. For the aim point at nominal perilune, the first-midcourse velocity corrections are about 2 percent lower than those shown for the aim point at $T_f = 56$ hours and the second-midcourse velocity corrections are from 5 to 55 percent lower, with the majority being about 40 percent lower.

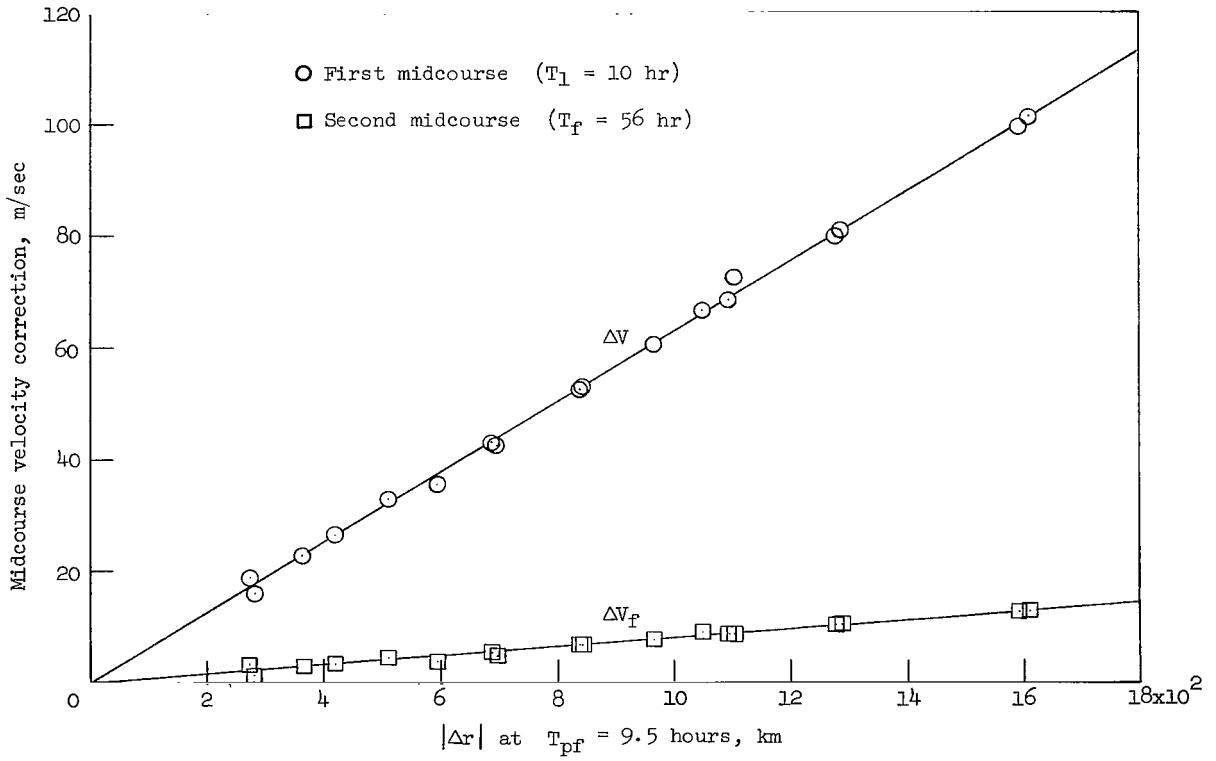

Figure 18.- Midcourse-maneuver fuel requirements for the aim point at $T_f = 56$ hours.

The data in figure 18 show that for the perturbed trajectories used in the present study, the fuel requirements are essentially a direct function of Δr at $T_{pf} = 9.5$ hours. This relationship occurs because, for these trajectories, $\Delta r \approx s$ where s is the

position deviation at T_{pf} = 9.5 hours. For trajectories with larger injection errors, $\Delta r \neq s$; hence, the direct relationship between fuel requirements and Δr would not hold.

Effect of Measurement Error

The results of an analysis to determine the effect of measurement error on guidance accuracy are shown in figures 19 to 28. Trajectory 10 was close to the nominal trajectory and was used to insure that none of the resulting guidance error could be attributed to linear approximation effects (transition matrices).

In the error analysis the effect of scatter in the plots of δD as a function of D (fig. 7) was not included inasmuch as the point for trajectory 10 fell directly on the faired line. The point could be off the line for any given perturbed trajectory; however, the additional guidance error incurred would be relatively small statistically.

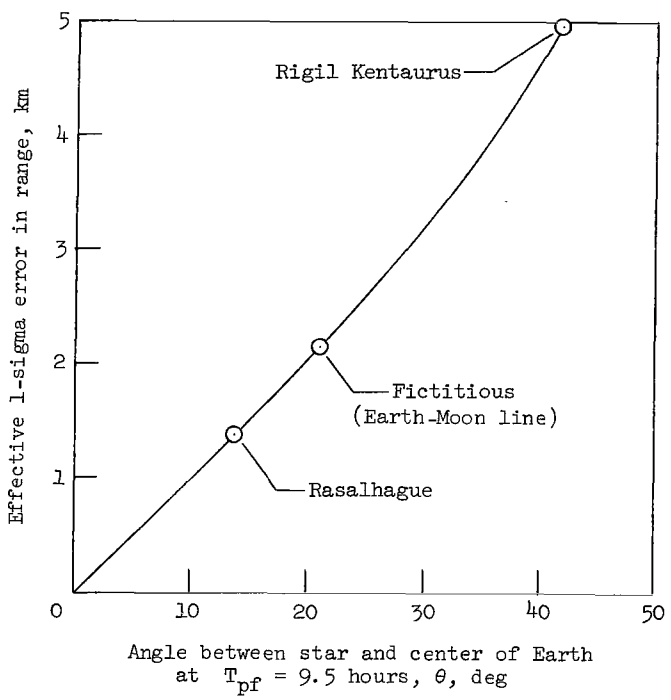

Figure 19.- Effective error in range due to measurement error of 10 arc-seconds in star-to-Earth angle at T_{pf} = 9.5 hours.

The three stars simulated for the angular measurements in the guidance equation (that is, for determining D, E, and F in eq. (1)) are indicated in figure 19. Other combinations of stars could be used for these measurements, as long as each star produces an adequate plot of δD as a function of D (small amount of scatter). If one or two of these stars were also to be used for determining the range, then each must also meet the requirements previously discussed under "Range Determination."

Error at first midcourse.- Data in figures 20 and 21 depict measurement errors at T_{pf} = 9.5 hours and the corresponding errors in the first-midcourse-maneuver velocity at T_1 = 10 hours due to these measurement errors.

The measurements required for the guidance procedure, as shown by equation (1), are range r_a and the three star-to-body angular measurements $\theta_{1,a}$, $\theta_{2,a}$, and $\theta_{3,a}$. Actually, as previously discussed, the range measurement is composed of a combination

of angular measurements, but it will be treated as a different type of measurement for error-analysis purposes. The range-measurement error is the predominant error since most of the position-determination error is in the direction of range (for example, see ref. 9); therefore, the guidance accuracies are presented for the range-measurement error only, as well as for all the measurement errors. The results pertaining only to range-measurement error are shown because they give a good first-order approximation of the overall guidance accuracy characteristics.

In figure 20, the first-midcourse-maneuver velocity errors are represented by open symbols for errors in range measurement only (at T_{pf} = 9.5 hours) and by solid symbols for errors in all measurements. The open-symbol data were obtained by merely solving the guidance equation (eq. (9)) with the use of discrete values of range error. As indicated in the figure, the solid-symbol data were obtained from a Monte Carlo procedure. In the Monte Carlo operation, 100 samples of measurement errors were used to simulate 100 position-determination errors at T_{pf} = 9.5 hours. Each sample consisted of an error in each of the four measurements r, θ_1, θ_2, and θ_3. Each error was assumed to be uncorrelated and from a normal (random) distribution of errors. The covariance matrices obtained for the first-midcourse-maneuver velocity errors are shown in table VIII. Both of the actual matrices (see parts (a) and (c) of table VIII) were determined by performing the calculation

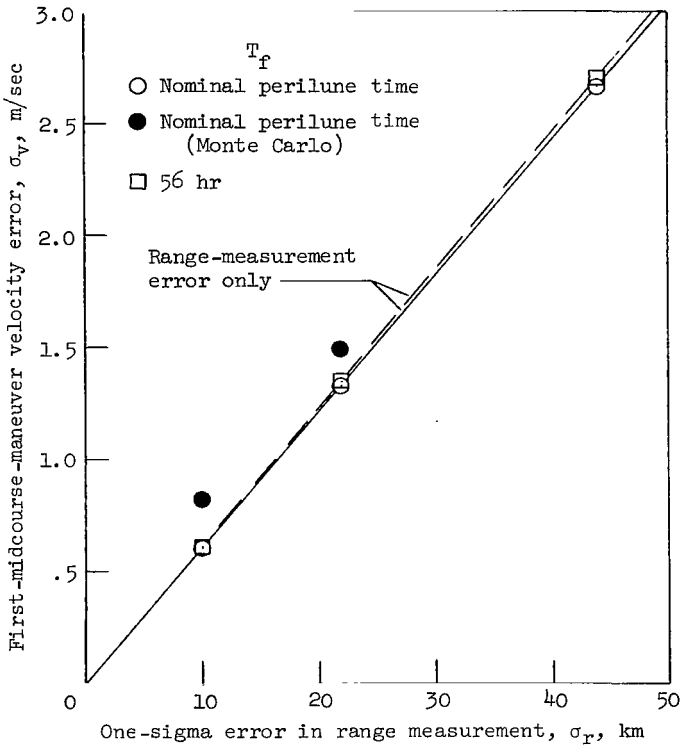

Figure 20.- First-midcourse-maneuver velocity error at T_1 = 10 hours due to measurement errors at T_{pf} = 9.5 hours. Open symbols are for range-measurement error only, whereas Monte Carlo results also include angular-measurement errors σ_{θ_1}, σ_{θ_2}, and σ_{θ_3} of 10 arc-seconds each.

$$\begin{Bmatrix} \Delta\dot{x} \\ \Delta\dot{y} \\ \Delta\dot{z} \end{Bmatrix} \begin{bmatrix} \Delta\dot{x} & \Delta\dot{y} & \Delta\dot{z} \end{bmatrix}$$

for each Monte Carlo sample, summing the respective elements for the 100 samples, and then dividing each summation by 100 to get the average value.

TABLE VIII.- COVARIANCE MATRICES OF FIRST-MIDCOURSE-MANEUVER VELOCITY ERRORS DUE TO MEASUREMENT ERRORS

[Exponent given at end of each number]

(a) Actual matrix; σ_r = 10 km, σ_{θ_1} = 10 arc-sec, σ_{θ_2} = 10 arc-sec, σ_{θ_3} = 10 arc-sec

	x	y	z	$\dot{x}$	$\dot{y}$	$\dot{z}$
x	0	0	0	0	0	0
y	0	0	0	0	0	0
z	0	0	0	0	0	0
$\dot{x}$	0	0	0	0.159076 -06	-0.610913 -07	-0.121657 -06
$\dot{y}$	0	0	0	-0.610913 -07	0.309944 -06	0.170459 -06
$\dot{z}$	0	0	0	-0.121657 -06	0.170459 -06	0.206078 -06

(b) Approximated matrix; σ_r = 10 km, σ_{θ_1} = 10 arc-sec, σ_{θ_2} = 10 arc-sec, σ_{θ_3} = 10 arc-sec

	x	y	z	$\dot{x}$	$\dot{y}$	$\dot{z}$
x	0	0	0	0	0	0
y	0	0	0	0	0	0
z	0	0	0	0	0	0
$\dot{x}$	0	0	0	0.22503 -06	0	0
$\dot{y}$	0	0	0	0	0.22503 -06	0
$\dot{z}$	0	0	0	0	0	0.22503 -06

(c) Actual matrix; σ_r = 22 km, σ_{θ_1} = 10 arc-sec, σ_{θ_2} = 10 arc-sec, σ_{θ_3} = 10 arc-sec

	x	y	z	$\dot{x}$	$\dot{y}$	$\dot{z}$
x	0	0	0	0	0	0
y	0	0	0	0	0	0
z	0	0	0	0	0	0
$\dot{x}$	0	0	0	0.221381 -06	-0.158528 -06	-0.206143 -06
$\dot{y}$	0	0	0	-0.158528 -06	0.142303 -05	0.768859 -06
$\dot{z}$	0	0	0	-0.206143 -06	0.768859 -06	0.572972 -06

(d) Approximated matrix; σ_r = 22 km, σ_{θ_1} = 10 arc-sec, σ_{θ_2} = 10 arc-sec, σ_{θ_3} = 10 arc-sec

	x	y	z	$\dot{x}$	$\dot{y}$	$\dot{z}$
x	0	0	0	0	0	0
y	0	0	0	0	0	0
z	0	0	0	0	0	0
$\dot{x}$	0	0	0	0.739128 -06	0	0
$\dot{y}$	0	0	0	0	0.739128 -06	0
$\dot{z}$	0	0	0	0	0	0.739128 -06

The relative effect of errors in the range measurement and in the three star-to-body angular measurements is shown in figure 21. The circular symbols were determined from figure 20. For example, for σ_r = 10 kilometers, the total error in determining the off-nominal position components D, E, and F (eq. (1)) is $\left(10^2 + 10^2 + 10^2\right)^{1/2}$ kilometers. The square symbol in figure 21 was determined from figure 19; that is, the position-determination error was obtained by taking the square root of the sum of the squares of the three values shown in figure 19. The values shown in figure 19 are actually errors in D, E, and F and were determined from equation (1). It should be noted that this error can be reduced by using stars for which θ is close to 0^o (or 180^o). Also, the increment in midcourse-maneuver velocity error due to error in the three angular measurements (at σ_r = 10 kilometers and σ_r = 22 kilometers) in figure 20 is about identical to the value shown in figure 21 for angular-measurement errors only.

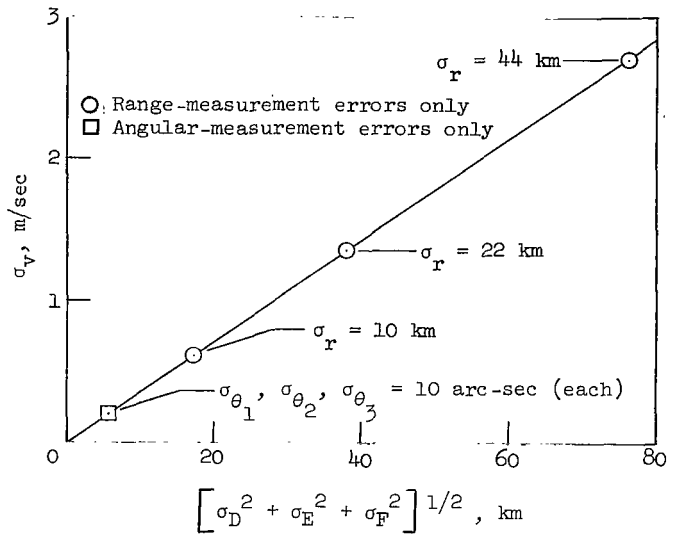

Figure 21.- First-midcourse-maneuver velocity error at T_1 = 10 hours due to total error in determining off-nominal position components D, E, and F at T_{pf} = 9.5 hours.

The important result shown in figures 20 and 21 is the fact that range-measurement error is the predominant error. Hence, every practical consideration should be used to reduce this error. Methods to accomplish this reduction are discussed subsequently.

Error at aim point.- The trajectory position and velocity aim-point errors due to measurement error are shown in figures 22 to 26. Some of these statistical results are shown on normal-probability plots in figures 27 to 28. The position errors (figs. 22 and 24) and perilune-distance errors (fig. 28) are shown for both correlated and uncorrelated errors.

As in figure 20, the results in figures 22 to 25 are shown for range-measurement error only as well as for errors in all measurements. As previously noted, error in the range measurement is the predominant error and analysis of this error, separately, provides a first-order approximation of the overall accuracy at the aim point. The results for this condition were easily determined by incorporating the corresponding first-midcourse-maneuver velocity errors (discrete) of figure 20 into the perturbed trajectory and propagating it to the aim point. The relative effects of position error and velocity error at T_f = 56 hours (caused by measurement error) on the position and velocity error at the Moon are shown in table IX. The position error at T_f = 56 hours accounts for 2/3 of the error at the Moon, probably because of the change in the flight-path angle (with respect to the Moon) at the lunar sphere of influence produced by this position change. The curves in figures 22 to 25 are faired to zero, the error due to linearization being disregarded. As shown by table III, this error would be relatively small and would depend on the particular perturbed trajectory used in the error analysis.

TABLE IX.- COMPARISON OF THE EFFECTS OF POSITION AND VELOCITY ERRORS AT T_f = 56 HOURS ON ACCURACY AT PERILUNE

[Results shown for perturbed trajectory with error of -10 km in range measurement at T_{pf}]

Condition at T_f = 56 hr	At nominal perilune time (T_f = 70 hr, 37 min) –			
	Range from Moon center, km	Position deviation from nominal, s, km	Selenocentric velocity, m/sec	Velocity deviation from nominal, u, m/sec
Position and velocity errors*	3534.6011	142.785	1953.8167	27.2331
Velocity error only (position error assumed to be zero)	3442.8394	41.469	1972.6556	8.4478
Position error only (velocity error assumed to be zero)	3494.9175	101.511	1961.4204	19.2872
Nominal (no errors)	3403.6367		1980.5083	

*s = 140.375 km; u = 1.0617 m/sec.

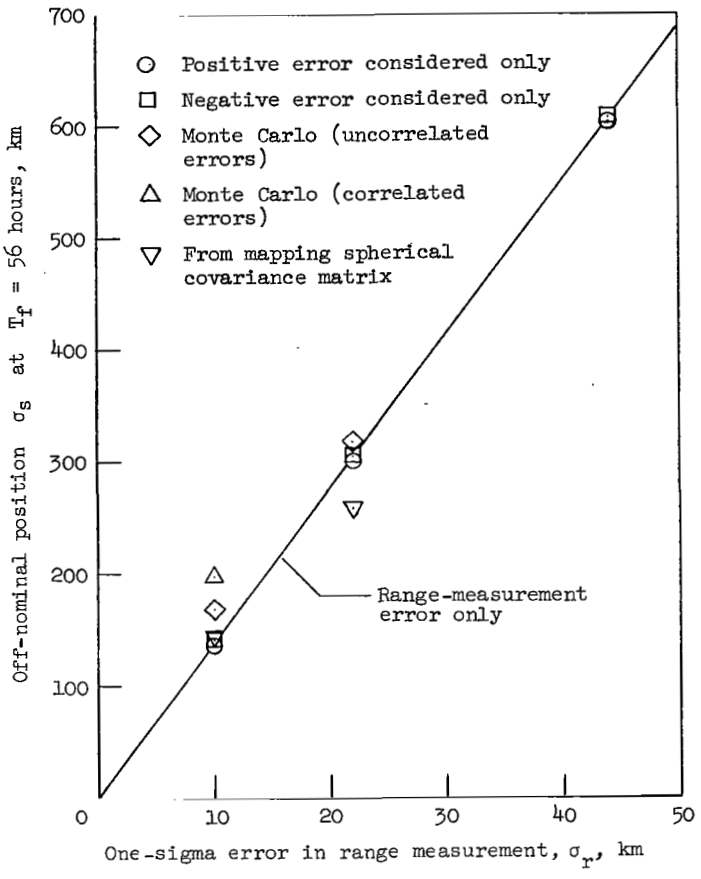

Figure 22.- Effect of range-measurement error on position accuracy at T_f = 56 hours. Monte Carlo results also include angular-measurement errors σ_{θ_1}, σ_{θ_2}, and σ_{θ_3} of 10 arc-seconds each.

The accuracy characteristics are shown in figures 22 to 25 for the two aim points previously discussed and in figure 26 for any point that might be selected within the lunar sphere of influence. The Monte Carlo results in figures 22 to 25, as well as the results in figure 26, were obtained by mapping the covariance matrices of first-midcourse-maneuver velocity errors (parts (a) and (c) of table VIII) to the aim points. The mapping was accomplished with the use of the program in reference 7. In several instances, the 100 trajectories resulting from the Monte Carlo samples were individually propagated to the aim point and the resulting 1-sigma error calculated. The results obtained in this manner matched those obtained from mapping the covariance matrices, the indication being that the sample size of 100 Monte Carlo selections was large enough for a true statistical representation of the errors. The results were also obtained by mapping

spherical covariance matrices of first-midcourse-maneuver velocity errors (parts (b) and (d) of table VIII). These matrices were arbitrarily obtained by taking each diagonal element equal to 1/3 the total σ_v^2 (from fig. 20 or from the sum of the diagonal elements of the actual covariance matrices in table VIII) and setting the off-diagonal elements equal to zero. Figures 22 to 25 show that use of this simple procedure may be adequate when range-measurement error is as small as about 10 kilometers but not when it is larger. If the spherical covariance matrix could be used, the 100 Monte Carlo selections would not be needed for determining the covariance matrix; the data of figure 21 would be sufficient.

A Monte Carlo error analysis was also made for the method which employs separate measurements at T_{pf} and T_1. This method differs from the present one in that the knowledge of position deviation at T_1 is not based on the measurement of the position deviation at T_{pf}; hence, the position errors at these two times are not correlated. The results of the analysis are shown in table I along with some results obtained with

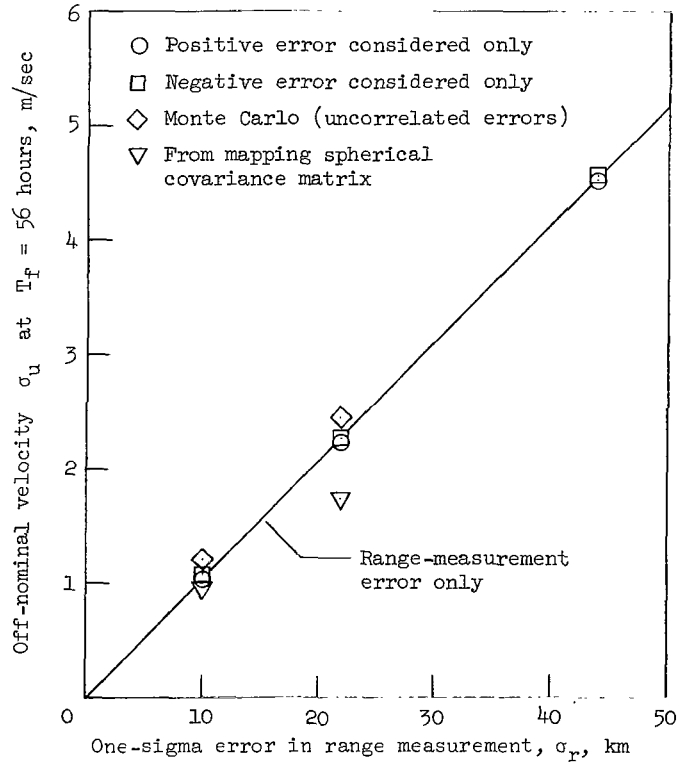

Figure 23.- Effect of range-measurement error on velocity accuracy at T_f = 56 hours. Monte Carlo results also include angular-measurement errors σ_{θ_1}, σ_{θ_2}, and σ_{θ_3} of 10 arc-seconds each.

the present method. The data shown correspond to 1-sigma measurement errors of 10 kilometers in the range and 10 arc-seconds in the star-to-body angles. Based on the comparison in table I, the present method is about 15 times as accurate as the two-star measurement method.

It may be noted from figure 24 that the results at perilune are the same whether the aim point is at 56 hours or at the nominal perilune time (70 hours, 37 minutes). This fact is true for both the Monte Carlo results and the results of using errors only in the range measurement in figure 24, for all the velocity results in figure 25, and for the perilune-distance-error results in figure 28. Hence, the selection of the aim point has no effect on the final accuracy at the Moon. Also shown in figures 22 and 24 for the position error is the fact that the effect of error in the three star-to-body measurements is reduced as σ_r increases.

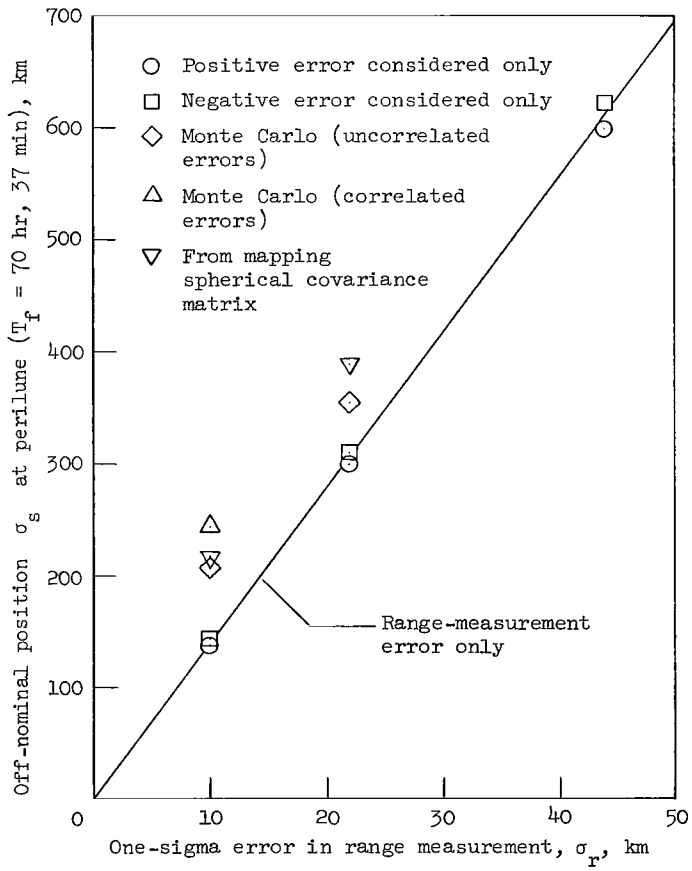

Figure 24.- Effect of range-measurement error on position accuracy at perilune. Monte Carlo results also include angular-measurement errors σ_{θ_1}, σ_{θ_2}, and σ_{θ_3} of 10 arc-seconds each. Results apply to T_f = 56 hours and T_f = nominal perilune time.

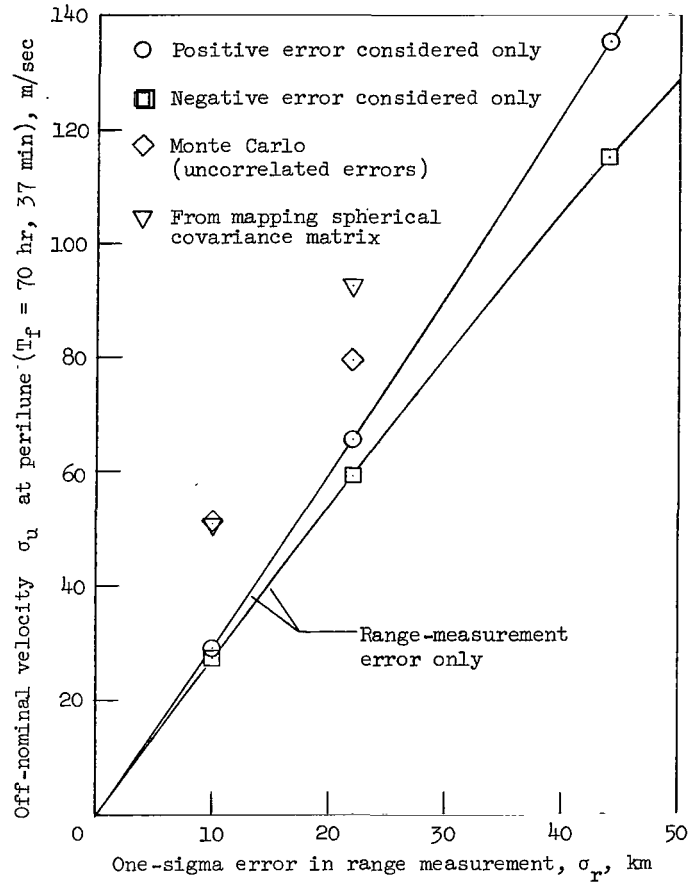

Figure 25.- Effect of range-measurement error on velocity accuracy at perilune. Monte Carlo results also include angular-measurement errors σ_{θ_1}, σ_{θ_2}, and σ_{θ_3} of 10 arc-seconds each. Results apply to T_f = 56 hours and T_f = nominal perilune time.

In comparing the accuracies at the two aim points it is seen that there is little difference in the position values, whereas the velocity error at perilune is much larger than that at T_f = 56 hours. The large errors at perilune, however, are not too critical since they could be easily corrected for in a terminal-guidance procedure. In figure 26, the bends in the curves for times near perilune are caused by the focusing effect of the Moon.

The position-error results from the Monte Carlo analysis for T_f = 56 hours are presented on a normal-probability plot in figure 27. Similarly, perilune-distance-error results are plotted in figure 28; these results apply to either of the aim points. Normal-probability graph paper can be used as a simple qualitative test for a normal distribution; the scale is adjusted so as to produce a straight-line probability plot for normally

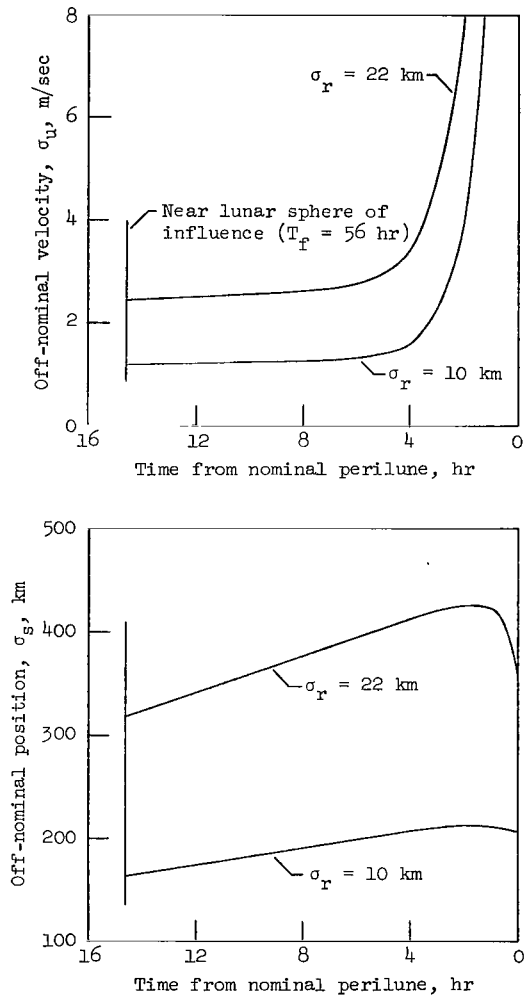

Figure 26.- Aim-point errors showing focusing effect of Moon on trajectory error resulting from midcourse-guidance uncorrelated measurement error. Data also include angular-measurement errors σ_{θ_1}, σ_{θ_2}, and σ_{θ_3} of 10 arc-seconds each.

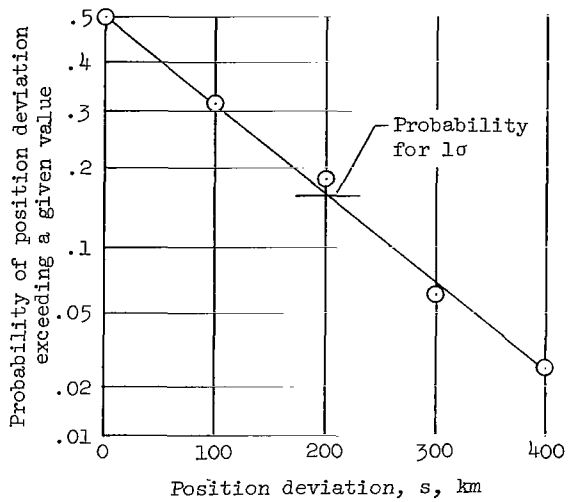

Figure 27.- Probability distribution of the position deviation at T_f = 56 hours for 100 Monte Carlo samples of correlated position-measurement errors at first midcourse. σ_r = 10 km; σ_{θ_1} = 10 arc-sec; σ_{θ_2} = 10 arc-sec; σ_{θ_3} = 10 arc-sec.

distributed data. Examination of the plots in figures 27 and 28 shows that the aim-point errors can be considered normally distributed; therefore, they can be analyzed by standard statistical procedures. For example, approximately 68 percent of the errors will be less than 1σ and the maximum error expected would be about 3σ.

The probability values in figure 27 were obtained by assuming an equal distribution of "negative" position deviations at the aim point. The position-deviation value indicated for 1σ in this figure compares with that shown for the corresponding case in figure 22. It is of interest to note from figure 28 that the 1-sigma values of the perilune-distance error are considerably different from the values of position deviation shown for corresponding cases in figure 24. This difference indicates that the position errors at the Moon are not necessarily in a radial (from the Moon) direction.

Effect of correlated errors.- As seen by equation (1), if one of the stars used for θ_1, θ_2, or θ_3 is also used for determining the value of r_a, then there is 100 percent correlation between the errors in r_a and $\theta_{1,a}$, $\theta_{2,a}$, or $\theta_{3,a}$; if different stars are used, there is no correlation. Depending upon where the star is located, the correlation can have either a helpful or detrimental effect on the accuracy of **D**, **E**, or **F**. The effect will be detrimental if the location of the star is such that the two factors in $r_a \cos \theta_a$ both increase (or decrease) for a given error in the measurement of θ_a. For example, if $\theta_{1,a}$ is in error by +10 arc-seconds, then $\cos \theta_{1,a}$ is decreased; and if, for example, $\theta_{1,a}$ is used in equation (19) to determine range, the value for r_a will also be decreased for certain locations of the star.

In the error analysis (see figs. 22 to 28), the results are shown for uncorrelated and correlated errors. For the correlated errors, the star was located so that the effect of the correlation was detrimental; that is, the position deviation at the aim points increased by 18 percent (figs. 22 and 24) and the perilune-distance error, by about 15 percent (fig. 28). Effects of correlated errors that are equal and opposite to those shown in these figures could be obtained for other stars.

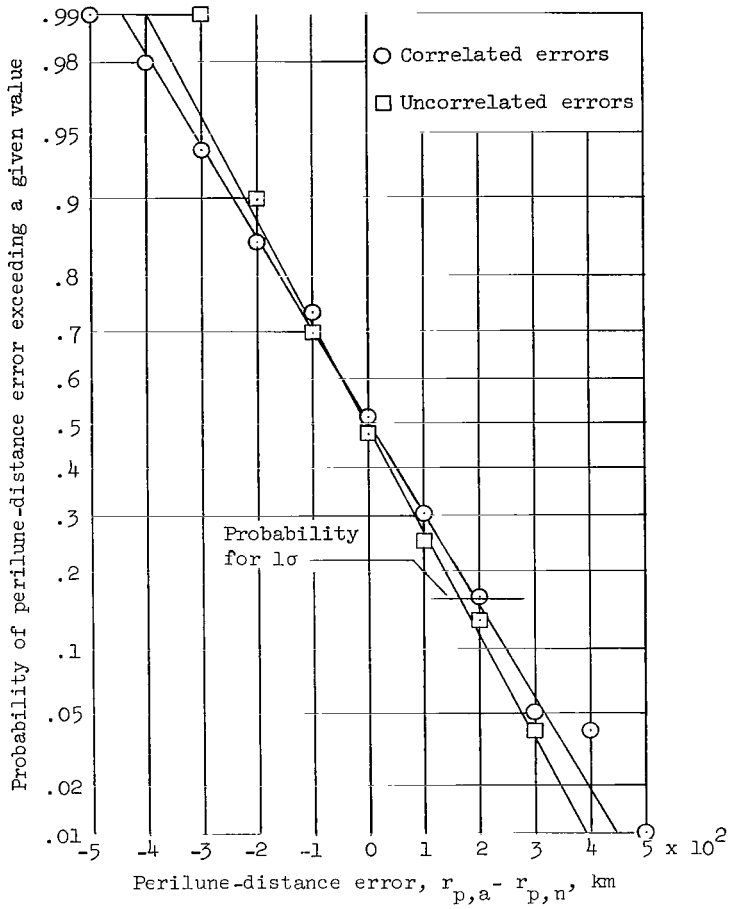

Figure 28.- Probability distribution of perilune-distance error for 100 Monte Carlo samples of position-measurement errors at first midcourse. Results apply to T_f = 56 hours and T_f = nominal perilune time. σ_r = 10 km; σ_{θ_1} = 10 arc-sec; σ_{θ_2} = 10 arc-sec; σ_{θ_3} = 10 arc-sec.

Effect of range-measurement error.- The range-measurement error that can be expected for 1-sigma errors of 10 arc-seconds in the angular measurements is about 40 kilometers and 80 kilometers for methods using one and two star measurements, respectively. (See fig. 14.) As shown in figures 22 to 25, range-measurement error is the predominant factor in determining the guidance accuracy and errors of this order would produce excessive errors at the aim point. Any means to reduce the range-measurement error would be of great benefit. One possibility would be to incorporate into the measurement schedule a series of range measurements. More specifically, each angular measurement required for range determination would be measured a number of times (updated to a common time) and averaged so that the resulting accuracy in

range determination would be increased by the statistical law

$$\sigma_{averaged} = \frac{\sigma_{unaveraged}}{\sqrt{N}}$$

where N is the number of measurements made for each angle.

There is a limit as to how far the reduction in range-measurement error should be taken. This limit is set by the inherent error due to scatter in the plots of δ_D as a function of D (fig. 7), which is equivalent to a measurement error. From the equation

$$D = r_a \cos \theta_a - r_n \cos \theta_n = r_a \cos \theta_a - \text{constant}$$

it is seen that

$$dD = \cos \theta_a \, dr - r_a \sin \theta_a \, d\theta$$

For θ_a near 0^o (or 180^o) and for representative errors in r and θ of 10 kilometers and 10 arc-seconds, respectively, it can be shown that the error in r_a is approximately equal to the error in D. It is seen in figure 7 that plots with minimum scatter have a scatter of at least ±1 kilometer in δD and that this scatter represents an error of about ±10 kilometers in D or in r_a. It is not possible to reduce the minimum scatter shown in figure 7 by use of other stars; therefore, any attempt to reduce the error in r_a much below 10 kilometers by adding more measurements would be useless.

Effect of Nominal Perilune Altitude

The results in this report pertain to trajectories with a perilune altitude of 1665 kilometers – that is, trajectories designed to miss the surface of the Moon by a relatively large distance of 1665 kilometers. There may be some question as to what extent the guidance accuracy would be affected for trajectories aimed closer to the Moon. Any changes in the accuracy would be caused by (1) effect of linear approximation in transition-matrix theory and (2) Moon's focusing effect on error propagation. In order to resolve this question, the accuracy characteristics were investigated for a nominal trajectory similar to the one used throughout this report, but with a perilune altitude of 155 kilometers.

The effect of linear approximation on aim-point error was examined for trajectories with perturbations corresponding to those for the seven trajectories from table III listed in table X. The results shown in table X for the two nominal perilune altitudes indicate that this effect does not increase appreciably for trajectories closer to the Moon. The effect on the velocity error, however, is seen to increase in most of the trajectories by a factor of 2 or 3.

TABLE X.- EFFECT ON ACCURACY OF LINEAR APPROXIMATION USED IN TRANSITION-MATRIX THEORY FOR TWO NOMINAL PERILUNE ALTITUDES

Trajectory with same perturbation as trajectory no.	Off-nominal conditions at nominal perilune time for perfect measurements and perfect guidance maneuver at first midcourse when –			
	Nominal perilune altitude = 1665 km		Nominal perilune altitude = 155 km	
	s, km	u, m/sec	s, km	u, m/sec
4	45.028	10.676	36.211	18.818
8	40.700	9.589	57.819	31.126
10	13.804	3.005	41.109	22.279
26	29.669	7.922	27.782	18.684
29	39.704	9.070	44.648	23.414
33	82.143	20.390	105.453	60.190
36	36.697	9.009	37.779	21.314

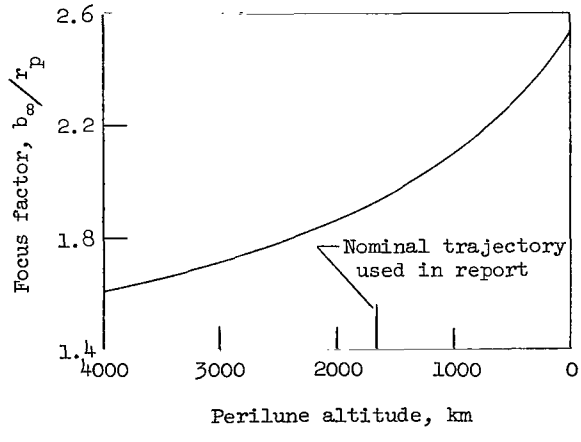

Figure 29.- Effect of perilune altitude on focus factor of Moon.

The Moon's focus factor (see appendix C) is shown in figure 29 as a function of nominal perilune altitude. This factor causes the so-called Moon's focusing effect on the position and velocity errors very near the Moon, as illustrated in figure 26. The focusing effect on the errors for the near-miss nominal trajectory was investigated by mapping the actual covariance matrices of first-midcourse-maneuver velocity error (parts (a) and (c) of table VIII) to the nominal perilune time. The aim-point errors for this trajectory are shown in table XI along with those for the nominal trajectory having the larger perilune altitude. The difference in the errors for the two altitudes is due, for the most part, to the focusing effect. As shown, this effect on the position errors is about the same for both altitudes; on the other hand, the effect on the velocity errors is much greater for the lower perilune altitude.

TABLE XI.- PERILUNE AIM-POINT ERRORS FOR TWO NOMINAL TRAJECTORIES

Measurement error*	Off-nominal conditions at T_f = nominal perilune time when –			
	Nominal perilune altitude = 1665 km		Nominal perilune altitude = 155 km	
	s, km	u, m/sec	s, km	u, m/sec
σ_r = 10 km	206.0	51.0	212.5	127.5
σ_r = 22 km	354.0	79.5	344.0	190.5

*Angular-measurement errors σ_{θ_1}, σ_{θ_2}, and σ_{θ_3} of 10 arc-seconds each are also included.

Maneuvering Errors

The effect of guidance-maneuvering errors on the accuracy at the aim point was briefly examined. (See figs. 30 to 32.) No statistical analysis was performed; rather, the individual effects of the three most important errors associated with the first midcourse maneuver (other than alining the reference system) were determined.

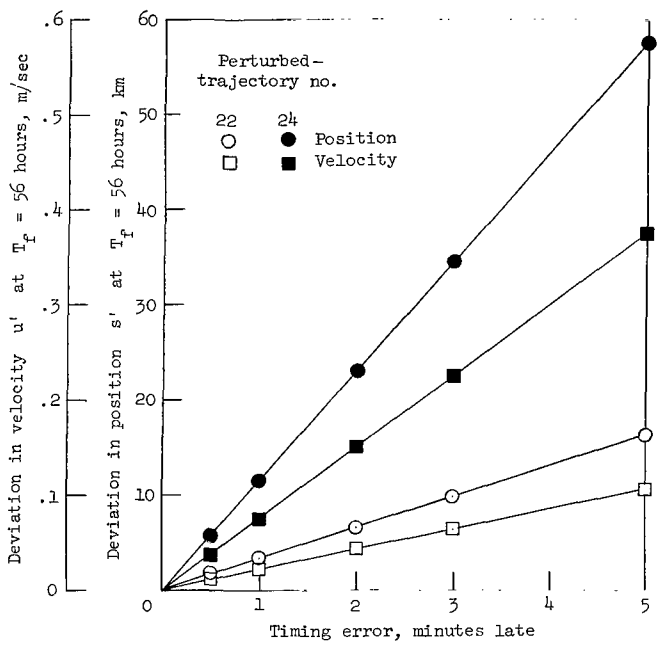

Figure 30.- Effect of first-midcourse-maneuver timing errors on position and velocity accuracy at T_f = 56 hours.

Timing errors.- The effects of first-midcourse-maneuver timing errors on the position and velocity errors at the aim point (T_f = 56 hours) are shown in figure 30 for two perturbed trajectories. As shown in table III, trajectory 24 is perturbed to a much higher degree than trajectory 22. The position and velocity deviations in figure 30, as well as in figures 31 and 32, are given in terms of the perfect guidance aim-point conditions of the actual (perturbed) trajectory rather than the aim-point conditions for the nominal trajectory in

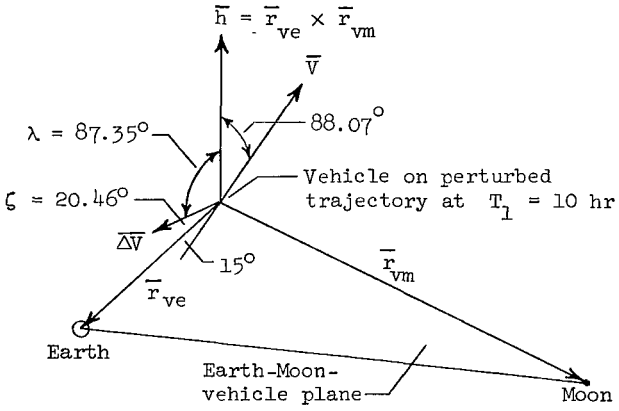

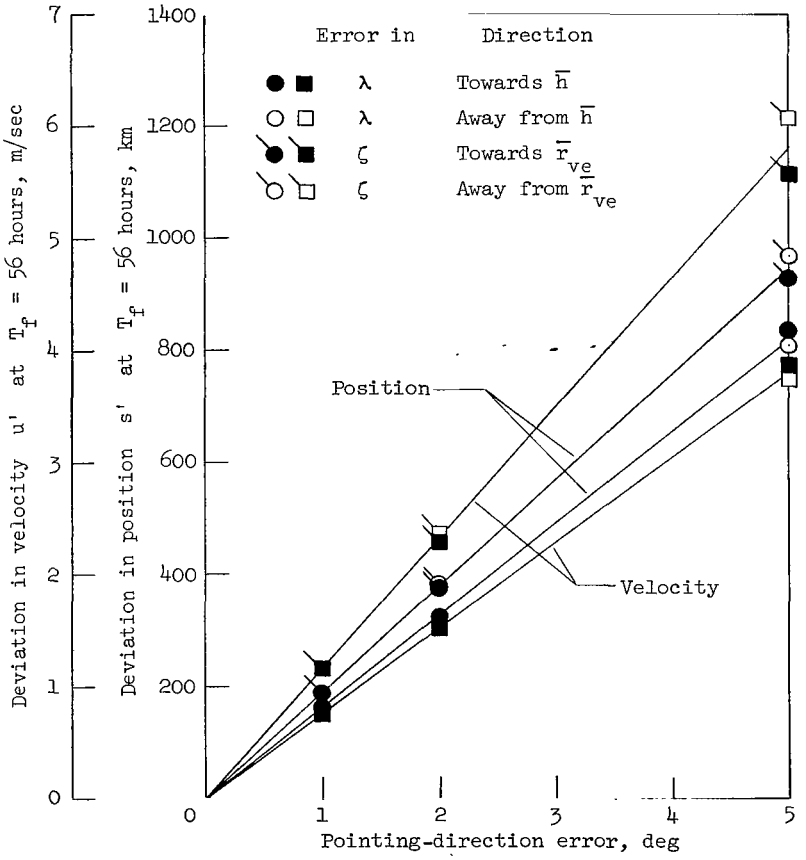

Figure 31.- Effect of first-midcourse-maneuver pointing-direction errors on position and velocity accuracy at T_f = 56 hours for trajectory 24.

order to eliminate the linear approximation effects. It is apparent by comparing the data of figure 30 with those of figures 22 and 23 that, regardless of the amount the actual trajectory is off the nominal trajectory, a timing error, even on the order of several minutes, has a negligible effect in the overall guidance accuracy.

Pointing errors.- The effect of pointing-direction errors is shown in figure 31. The data were calculated for only one perturbed trajectory (trajectory 24 in table III) but are representative of trajectories which require a vector $\overline{\Delta V}$ in the general direction of the trajectory. For perturbed trajectories requiring a vector $\overline{\Delta V}$ more nearly perpendicular to the trajectory, the effects of pointing errors would be smaller than those shown. The results are given for pointing errors that are either in-plane or out-of-plane and indicate that pointing errors up to about 0.5^{o} could be tolerated – that is, would have no large effect on the overall aim-point accuracy (based on the errors shown in figs. 22 and 23 for σ_r = 10 kilometers).

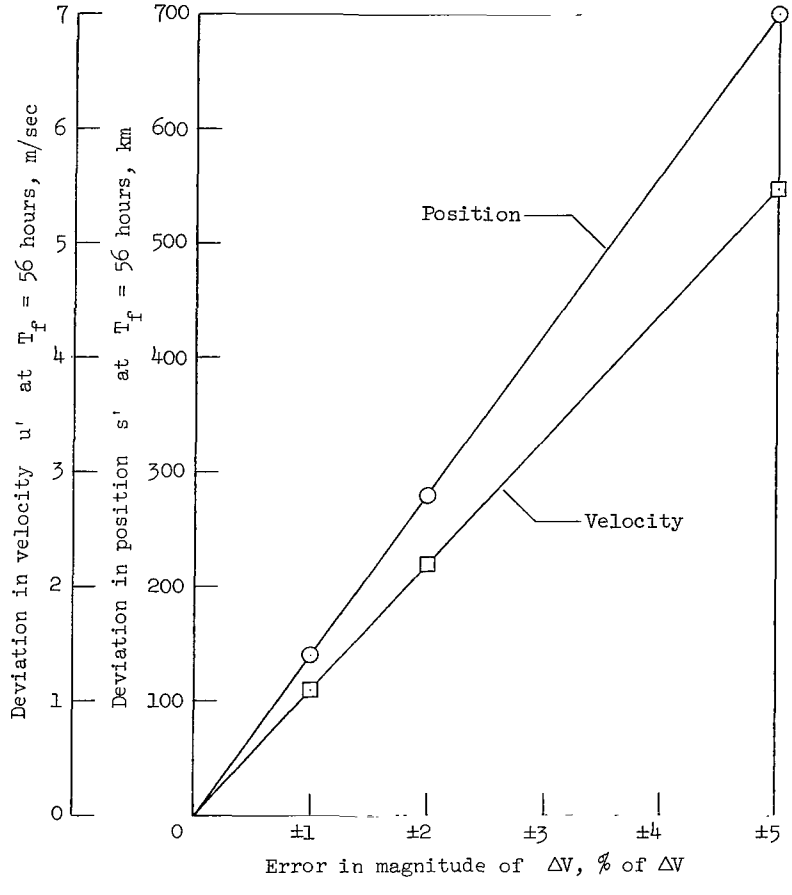

Figure 32.- Effect of errors in magnitude of first-midcourse-maneuver velocity correction on position and velocity accuracy at T_f = 56 hours for trajectory 24. Required first-midcourse-maneuver velocity correction ΔV is 66.63652 m/sec.

Magnitude errors.- The effect of first-midcourse-maneuver velocity-magnitude (thrust-cutoff) errors is shown in figure 32. The results are for trajectory 24 of table III which is perturbed relatively far from the nominal trajectory. Naturally, for trajectories perturbed to a lesser degree, the effect of the magnitude error would be less. Also, the results shown are representative of perturbed trajectories which require a velocity correction in the general direction of the trajectory. Calculations pertaining to the various perturbed trajectories of table III showed that the direction of the required velocity correction was almost always in the direction of the trajectory. For the trajectory represented in figure 32 and for a comparison similar to that made in figure 31, it is evident that errors in the first-midcourse-maneuver velocity magnitude up to about 1 percent could be tolerated in the present manual guidance procedure.

CONCLUSIONS

A method for determination of midcourse-velocity corrections for a space vehicle has been presented. The method has been applied to a lunar trajectory; however, it would also apply to an interplanetary trajectory. The method makes use of knowledge (preflight calculations) of a nominal or reference trajectory and a linear perturbation procedure (transition matrices) to determine the velocity corrections. The linearity characteristics of the method are such that sufficient accuracy can be obtained even though large differences may exist between the actual and nominal trajectories. In addition to an instrument to measure angles, the only items required by the navigator are a small amount of precalculated information on the nominal trajectory, several simple equations which can be solved within a time of 15 minutes by employing a desk-type calculator, and some manual procedure to aline the thrust vector.

It has been shown that the present method essentially involves a two-step calculation procedure: (1) calculation of the range to the Earth by use of one or two star-to-body measurements along with the angle measurement between the Earth and Moon, and (2) calculation of the midcourse-velocity vector by use of the range determination and three star-to-Earth measurements. From the error analyses made on range determination and on the aim-point conditions, the important results concerning manual guidance are:

1. Error in the range measurement is the predominant factor in the overall guidance accuracy. The aim-point accuracy is essentially proportional to this error, regardless of any other measurement error or maneuver error.

2. For a 1-sigma error of 10 arc-seconds in angular measurements, the error in determining range for one set of required measurements is about 40 and 80 kilometers, respectively, for the one-star and two-star methods. Errors of this magnitude lead to

relatively large aim-point errors; however, the accuracy can be increased greatly through use of several range measurements.

3. Because of the inherently large range-measurement error and its effect on the aim-point accuracy, more work on improving range-measurement accuracy is needed.

4. The aim-point position error does not change greatly as the Moon is approached, whereas the aim-point velocity error increases rapidly near the Moon. This increased error, however, can be easily corrected for in a terminal guidance procedure.

5. The final accuracy at the Moon (nominal perilune time) is independent of the aim point selected in the guidance procedure.

6. The effect of correlated errors caused by making measurements to certain stars can be advantageously used to increase the guidance accuracy.

7. The aim-point errors have been shown to be normally distributed; hence, standard statistical procedures can be applied in analysis of these errors.

Langley Research Center,
National Aeronautics and Space Administration,
Langley Station, Hampton, Va., June 6, 1967,
125-17-05-09-23.

APPENDIX A

A METHOD OF SELECTING INJECTION ERRORS

The errors in both the position vector and the velocity vector at injection are basically of two types: (1) direction errors caused by misorientation of the vector and (2) magnitude errors. For example, in considering the velocity errors (see fig. 33), the components of the injection velocity are

$$\left.\begin{aligned} \dot{x} &= V \cos \theta' \cos \phi' \\ \dot{y} &= V \cos \theta' \sin \phi' \\ \dot{z} &= V \sin \theta' \end{aligned}\right\} \tag{A1}$$

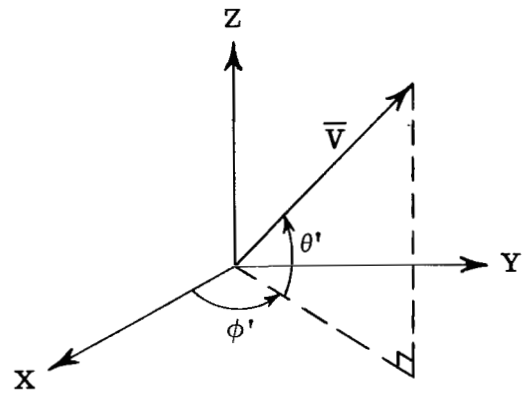

Figure 33.- Orientation of injection-velocity vector.

After taking the variation in equations (A1), the velocity error is

$$\left.\begin{aligned} \delta\dot{x} &= \frac{\dot{x}}{V}\,\delta V - \dot{z} \cos \phi' \,\delta\theta' - \dot{y}\,\delta\phi' \\ \delta\dot{y} &= \frac{\dot{y}}{V}\,\delta V - \dot{z} \sin \phi' \,\delta\theta' + \dot{x}\,\delta\phi' \\ \delta\dot{z} &= \frac{\dot{z}}{V}\,\delta V + V \cos \theta' \,\delta\theta' \end{aligned}\right\} \tag{A2}$$

Similar equations would be obtained for error in the injection-position vector. In solving equations (A2), if δV, $\delta\theta'$, and $\delta\phi'$ are assumed to be independent random errors, the variances of the errors in the velocity components are

$$\left.\begin{aligned}
\sigma_{\dot{x}}^2 &= \left(\frac{\dot{x}}{V}\sigma_V\right)^2 + \left(\dot{z}\cos\phi'\sigma_{\theta'}\right)^2 + \left(\dot{y}\sigma_{\phi'}\right)^2 \\
\sigma_{\dot{y}}^2 &= \left(\frac{\dot{y}}{V}\sigma_V\right)^2 + \left(\dot{z}\sin\phi'\sigma_{\theta'}\right)^2 + \left(\dot{x}\sigma_{\phi'}\right)^2 \\
\sigma_{\dot{z}}^2 &= \left(\frac{\dot{z}}{V}\sigma_V\right)^2 + \left(V\cos\theta'\sigma_{\theta'}\right)^2
\end{aligned}\right\} \qquad \text{(A3)}$$

The values used for σ_V, $\sigma_{\theta'}$, and $\sigma_{\phi'}$ in the present analysis were obtained as follows. A value of 10 m/sec was arbitrarily chosen for σ_V. Then, in order to determine values for $\sigma_{\theta'}$ and $\sigma_{\phi'}$, this value of 10 m/sec was applied separately to each of the three nominal velocity components and the largest difference in each angle (θ' and ϕ') from the nominal value was selected (see table XII).

TABLE XII.- DATA USED IN DETERMINING $\sigma_{\theta'}$ AND $\sigma_{\phi'}$ FOR EQUATIONS (A3)

Condition	$\dot{x}$, km/sec	$\dot{y}$, km/sec	$\dot{z}$, km/sec	V, $(\dot{x}^2+\dot{y}^2+\dot{z}^2)^{1/2}$, km/sec	$\sin\theta'$, $\lvert\dot{z}/V\rvert$	θ', deg	$\sin\phi'$, $\lvert\dot{y}/V\cos\theta'\rvert$	ϕ', deg
Nominal	-10.519851	-2.6309587	-2.0283715	11.031930	0.1838637	10.594890	0.2426221	14.041349
Error applied to $\dot{x}$	-10.509851	-2.6309587	-2.0283715	11.022395	.1840228	10.604164	.2428393	14.054178
Error applied to $\dot{y}$	-10.519851	-2.6209587	-2.0283715	11.029550	.1839034	10.597199	.2417531	13.990029
Error applied to $\dot{z}$	-10.519851	-2.6309587	-2.0183715	11.030096	.1829877	10.543831	.2426221	14.041349

As shown in table XII, the maximum differences in θ' and ϕ' from their nominal values are, in both instances, approximately 0.051°. By using this value (in radians) for $\sigma_{\theta'}$ and $\sigma_{\phi'}$ in equations (A3), the values,

$$\sigma_{\dot{x}}^2 = 0.00009948\ (\text{km/sec})^2$$

$$\sigma_{\dot{y}}^2 = 0.00009355\ (\text{km/sec})^2$$

$$\sigma_{\dot{z}}^2 = 0.00009653\ (\text{km/sec})^2$$

as listed in table IV, are obtained.

APPENDIX B

TWO-STAR METHOD OF RANGE DETERMINATION

As described in the section "Range Determination," a measurement is required of the angle B or the angle C (depending on the method used) or of the deviation of this angle from the nominal value. Once this angle is obtained, procedures for determining range are relatively simple. The angle B (or the angle C) can be obtained from onboard measurements of two star-to-body angles.

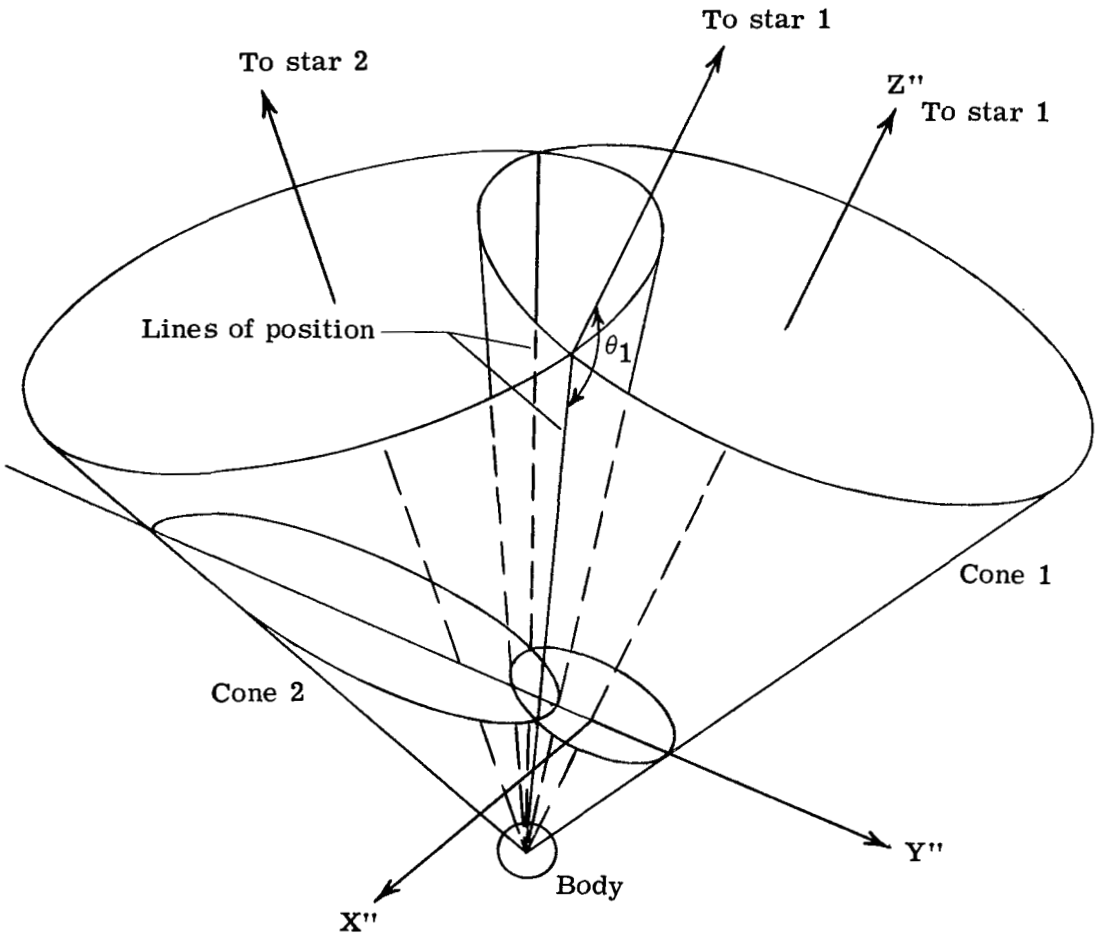

Figure 34.- Cones of position formed by star-to-body measurements.

APPENDIX B

Figure 34 represents the two cones of position formed by the two star-to-body measurements. The vehicle will lie on one of the two lines of position (intersection). The geometry shown in figure 34 (that is, stars in a direction from the vehicle opposite to that of the Earth (or Moon)) represents star-to-body angles between 90^{o} and 180^{o}. For angles less than 90^{o} the stars would be in the same general direction from the vehicle as the Earth (or Moon). The angle B (or C), as shown in figure 12, can be determined from the calculation of the direction of the pertinent line of position, along with information on the direction of the line between the Earth and the Moon. Although the calculations are lengthy, they can be performed before the mission and presented in graphical form.

The derivation of the direction of the line of position follows and is given in two parts. First, the coordinates of the line are determined for a right-hand rectangular coordinate system in which the Z''-axis is along the line of sight to one of the stars. Next, these coordinates are transformed to the conventional inertial coordinate system used throughout the paper.

In figure 34 the right-hand rectangular coordinate system is centered in a plane perpendicular to the axis of cone 1 and at a unit distance from the body center; the Z''-axis is along the axis of this cone and the Y''-axis intersects the axis of cone 2. The intersection of the X''Y''-plane with the two cones forms an ellipse and a circle, as shown in figure 35.

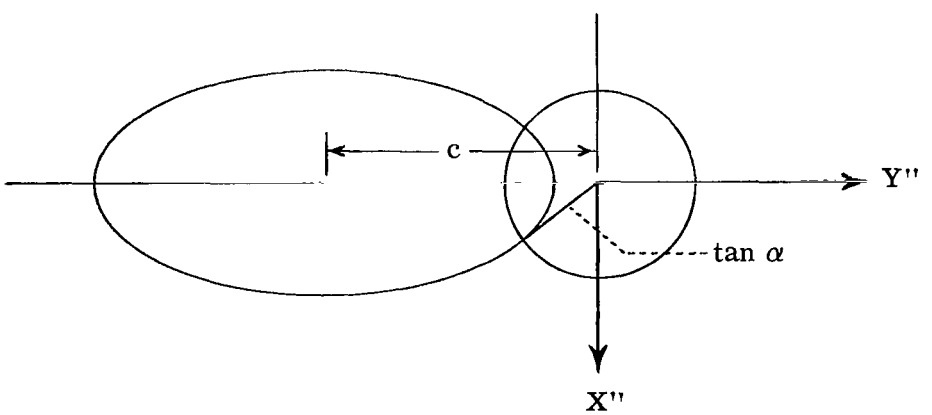

Figure 35.- Ellipse and circle formed by intersection of two cones and X''Y''-plane.

A limitation to this approach is the requirement that

$$(\beta + \gamma) < 90^{o}$$

(See fig. 36.) Thus, in selecting stars to be used in this method of range determination, the two axes of the cones should be reasonably close together; that is, $\beta < (90^{o} - \gamma)$. This condition, in general, is easily met, as the same stars are ordinarily used for the position-component measurements in the guidance equations; as shown by table V, the best stars for these measurements provide lines of sight which are all fairly close together.

The equation for the circle is

$$x''^2 + y''^2 = \tan^2\alpha \tag{B1}$$

and the equation for the ellipse is

$$\frac{x''^2}{a^2} + \frac{(y'' + c)^2}{b^2} = 1 \tag{B2}$$

Solving these equations simultaneously yields the intersection of the two curves, given by

$$y'' = \frac{-a^2c \pm \left(a^4b^2 - a^2b^2\tan^2\alpha + c^2a^2b^2 - a^2b^4 + b^4\tan^2\alpha\right)^{1/2}}{a^2 - b^2} \tag{B3}$$

$$x'' = \pm\left(\tan^2\alpha - y''^2\right)^{1/2} \tag{B4}$$

As noted, the equations yield four possible combinations of values for x'' and y''. The correct sign of y'' is easily determined, however, by testing equation (B4); the wrong sign gives no solution. The correct sign of x'' must be obtained from predetermined knowledge of the direction of the line of position for the nominal trajectory. The line of position for the actual trajectory will lie close to this nominal line. As previously stipulated,

$$z'' = 1 \tag{B5}$$

The terms a^2, b^2, and c can be solved by the procedure explained in the discussion that follows.

First, the coordinates in the equation for cone 2 (see fig. 36) are given in terms of the X'', Y'', and Z'' system by

APPENDIX B

$$\begin{Bmatrix} x''' \\ y''' \\ z''' \end{Bmatrix} = \begin{bmatrix} 1 & 0 & 0 \\ 0 & \cos\beta & \sin\beta \\ 0 & -\sin\beta & \cos\beta \end{bmatrix} \begin{Bmatrix} x'' \\ y'' \\ z'' \end{Bmatrix}$$

or

$$x''' = x''$$

$$y''' = y'' \cos\beta + z'' \sin\beta$$

$$z''' = -y'' \sin\beta + z'' \cos\beta$$

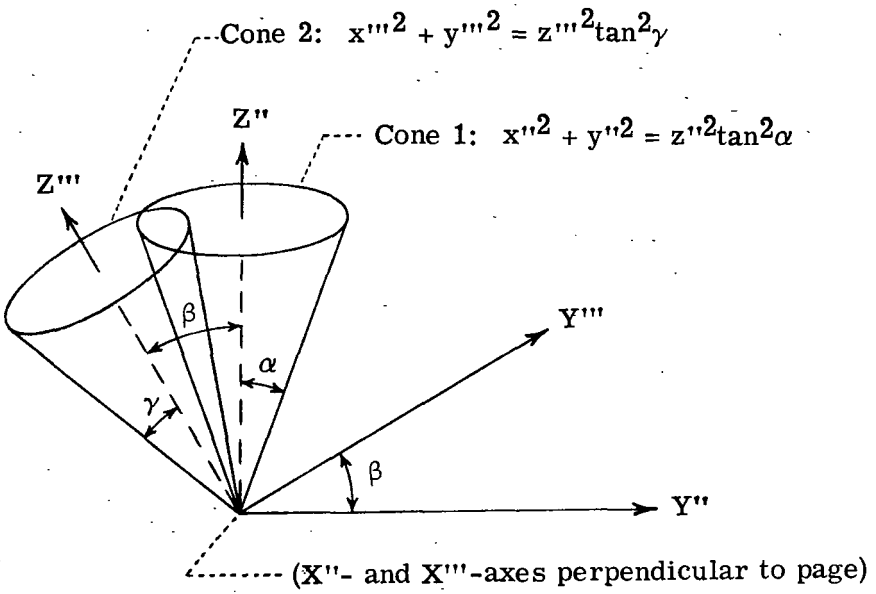

Figure 36.- Two cones in two rectangular right-hand coordinate systems.

In the X'', Y'', and Z'' system, then, the cone equations are given as

Cone 1: $x''^2 + y''^2 = z''^2\tan^2\alpha$

Cone 2: $x''^2 + (y'' \cos\beta + z'' \sin\beta)^2 = (-y'' \sin\beta + z'' \cos\beta)^2\tan^2\gamma$

After expanding the equation for cone 2 and collecting terms,

$$x''^2 + y''^2(\cos^2\beta - \sin^2\beta \tan^2\gamma) + 2y''z'' \sin\beta \cos\beta(1 + \tan^2\gamma) = z''^2(\cos^2\beta \tan^2\gamma - \sin^2\beta)$$

APPENDIX B

A plane perpendicular to the Z''-axis at a unit distance from the origin is given by the equation

$$z'' = 1$$

The intersection of this plane with cone 1 is given by

$$x''^2 + y''^2 = \tan^2\alpha$$

and the intersection with cone 2 is given by

$$x''^2 + y''^2(\cos^2\beta - \sin^2\beta \tan^2\gamma) + 2y'' \sin\beta \cos\beta(1 + \tan^2\gamma) = \cos^2\beta \tan^2\gamma - \sin^2\beta$$

Adding the term $\dfrac{\sin^2\beta \cos^2\beta(1 + \tan^2\gamma)^2}{\cos^2\beta - \sin^2\beta \tan^2\gamma}$ to both sides of the equation for the intersection of the plane with cone 2 gives

$$x''^2 + (\cos^2\beta - \sin^2\beta \tan^2\gamma)\left[y''^2 + \frac{2y''\sin\beta \cos\beta(1 + \tan^2\gamma)}{\cos^2\beta - \sin^2\beta \tan^2\gamma} + \frac{\sin^2\beta \cos^2\beta(1 + \tan^2\gamma)^2}{\left(\cos^2\beta - \sin^2\beta \tan^2\gamma\right)^2}\right] = \cos^2\beta \tan^2\gamma - \sin^2\beta + \frac{\sin^2\beta \cos^2\beta(1 + \tan^2\gamma)^2}{\cos^2\beta - \sin^2\beta \tan^2\gamma}$$

or, after some algebraic manipulation,

$$x''^2 + (\cos^2\beta - \sin^2\beta \tan^2\gamma)\left[y'' + \frac{\sin\beta \cos\beta(1 + \tan^2\gamma)}{\cos^2\beta - \sin^2\beta \tan^2\gamma}\right]^2 = \frac{\tan^2\gamma}{\cos^2\beta - \sin^2\beta \tan^2\gamma}$$

or

$$\frac{\cos^2\beta - \sin^2\beta \tan^2\gamma}{\tan^2\gamma} x''^2 + \frac{(\cos^2\beta - \sin^2\beta \tan^2\gamma)^2}{\tan^2\gamma}\left[y'' + \frac{\sin\beta \cos\beta(1 + \tan^2\gamma)}{\cos^2\beta - \sin^2\beta \tan^2\gamma}\right]^2 = 1$$

which is in the form of equation (B2). Therefore,

$$a^2 = \frac{\tan^2\gamma}{\cos^2\beta - \sin^2\beta \tan^2\gamma}$$

$$b^2 = \frac{a^2}{\cos^2\beta - \sin^2\beta \tan^2\gamma}$$

$$c = \frac{\sin\beta \cos\beta(1 + \tan^2\gamma)}{\cos^2\beta - \sin^2\beta \tan^2\gamma}$$

Next, the coordinates given by equations (B3), (B4), and (B5) must be transformed to the X, Y, Z axis system. If $\bar{i}$, $\bar{j}$, and $\bar{k}$ are unit vectors along the X-, Y-, and Z-axes, respectively, then

$$\bar{z}'' = l_1\bar{i} + m_1\bar{j} + n_1\bar{k}$$

where l_1, m_1, and n_1 are known direction cosines of star 1 with respect to these axes.

Since by definition (fig. 37) X'' is perpendicular to the plane passing through the lines of sight to the two stars, $\bar{x}''$ is given by the cross product of the position vectors of the two stars as

$$\bar{x}'' = \left(m_1n_2 - n_1m_2\right)\bar{i} + \left(n_1l_2 - l_1n_2\right)\bar{j} + \left(l_1m_2 - m_1l_2\right)\bar{k}$$

where l_2, m_2, and n_2 are known direction cosines of star 2 with respect to the X-, Y-, and Z-axes.

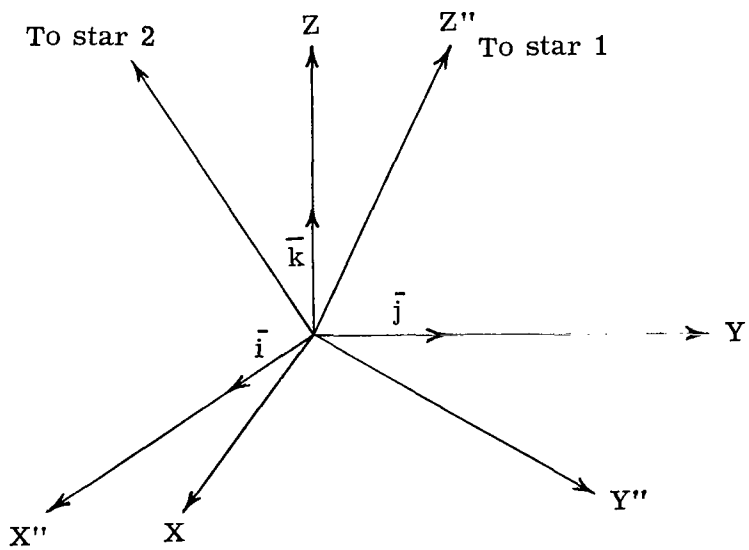

Figure 37.- Illustration of two rectangular right-hand coordinate systems.

APPENDIX B

With the vectors $\bar{z}''$ and $\bar{x}''$ defined, the vector $\bar{y}''$ is then given by

$$\bar{y}'' = \bar{z}'' \times \bar{x}''$$

or

$$\begin{aligned}\bar{y}'' = &\left(l_1m_1m_2 - l_2m_1^2 - l_2n_1^2 + l_1n_1n_2\right)\bar{i} \\ &+ \left(n_1n_2m_1 - n_1^2m_2 - l_1^2m_2 + l_1l_2m_1\right)\bar{j} \\ &+ \left(l_1l_2n_1 - l_1^2n_2 - n_2m_1^2 + n_1m_1m_2\right)\bar{k}\end{aligned}$$

The direction cosines of the vectors $\bar{x}''$, $\bar{y}''$, and $\bar{z}''$ form the transformation matrix $[P]$ such that

$$\begin{Bmatrix} x \\ y \\ z \end{Bmatrix} = [P]^{-1} \begin{Bmatrix} x'' \\ y'' \\ z'' \end{Bmatrix}$$

where the elements of $[P]$ are defined by

$$p_{11} = \frac{m_1n_2 - n_1m_2}{\left[\left(m_1n_2 - n_1m_2\right)^2 + \left(n_1l_2 - l_1n_2\right)^2 + \left(l_1m_2 - m_1l_2\right)^2\right]^{1/2}} = \frac{m_1n_2 - n_1m_2}{|\bar{x}''|}$$

$$p_{12} = \frac{n_1l_2 - l_1n_2}{|\bar{x}''|}$$

$$p_{13} = \frac{l_1m_2 - m_1l_2}{|\bar{x}''|}$$

$$p_{21} = \frac{\left(l_1m_1m_2 - l_2m_1^2 - l_2n_1^2 + l_1n_1n_2\right)}{\left[\left(l_1m_1m_2 - l_2m_1^2 - l_2n_1^2 + l_1n_1n_2\right)^2 + \left(n_1n_2m_1 - n_1^2m_2 - l_1^2m_2 + l_1l_2m_1\right)^2 + \left(l_1l_2n_1 - l_1^2n_2 - n_2m_1^2 + n_1m_1m_2\right)^2\right]^{1/2}}$$

$$= \frac{l_1m_1m_2 - l_2m_1^2 - l_2n_1^2 + l_1n_1n_2}{|\bar{y}''|}$$

$$p_{22} = \frac{n_1 n_2 m_1 - n_1^2 m_2 - l_1^2 m_2 + l_1 l_2 m_1}{|\bar{y}''|}$$

$$p_{23} = \frac{l_1 l_2 n_1 - l_1^2 n_2 - n_2 m_1^2 + n_1 m_1 m_2}{|\bar{y}''|}$$

$$p_{31} = l_1$$

$$p_{32} = m_1$$

$$p_{33} = n_1$$

The angle B (or C), then, is determined by the dot product of the position vectors of the vehicle and Moon (or Earth) center, as referenced from the Earth (or Moon). For example,

$$\cos B = \frac{x_{ev}x_{em} + y_{ev}y_{em} + z_{ev}z_{em}}{r_{ev}r_{em}}$$

where x_{em}, y_{em}, z_{em}, and r_{em} are known ephemeris values.

APPENDIX C

FOCUS FACTOR OF MOON

The focusing effect of the Moon is shown in figure 38.

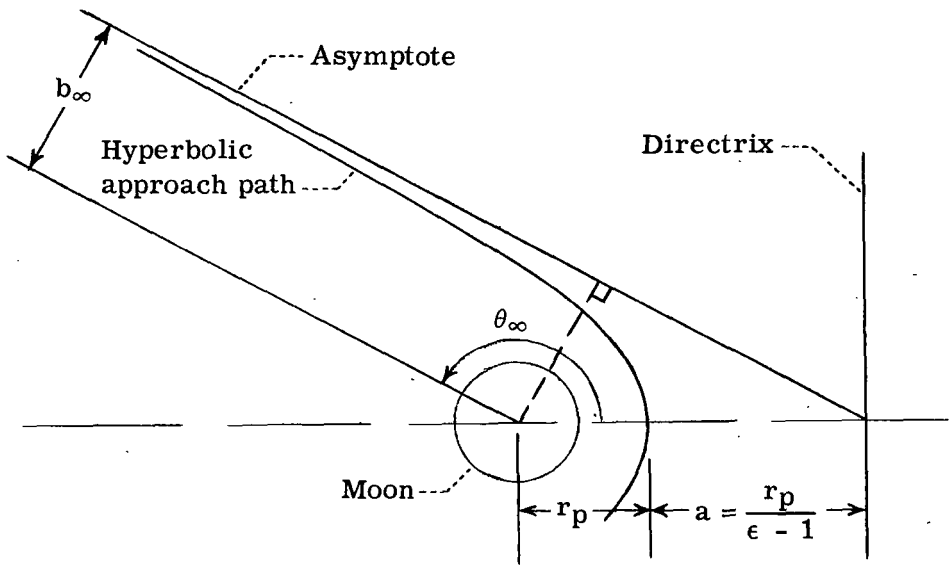

Figure 38.- Sketch showing focusing effect of the Moon.

In this figure, a is the semimajor axis and ϵ is the eccentricity of the orbit. The distance b_∞ is the effective aim-point radius – that is, the radius within which a desired perilune distance or radius r_p can be reached. It is seen that

$$b_\infty = r_p\left(1 + \frac{1}{\epsilon - 1}\right)\cos\left(\theta_\infty - \frac{\pi}{2}\right) = \frac{\epsilon}{\epsilon - 1} r_p \sin \theta_\infty \qquad \text{(C1)}$$

Now, as shown by the well-known equation

$$r = \frac{l}{1 + \epsilon \cos \theta}$$

where l is the semilatus rectum, r tends to infinity as $1 + \epsilon \cos \theta$ approaches 0, or as θ approaches the value

$$\theta_\infty = \cos^{-1}\left(-\frac{1}{\epsilon}\right) \tag{C2}$$

Therefore, from equations (C1) and (C2),

$$b_\infty = \frac{\epsilon}{\epsilon - 1}\frac{\sqrt{\epsilon^2 - 1}}{\epsilon} r_p = \frac{\sqrt{\epsilon^2 - 1}}{\epsilon - 1} r_p = f_f r_p$$

where f_f is the focus factor.

The eccentricity can be determined from

$$\epsilon = \frac{r_p V_p^2}{\mu} - 1$$

where μ is the product of the universal gravitational constant and mass of the Moon. The perilune velocity can be determined from

$$V_p = \left(\frac{2\mu}{r_p} + V_s^2 - \frac{2\mu}{r_s}\right)^{1/2}$$

where V_s is the vehicle velocity (with respect to the Moon) at the sphere of influence and r_s is the distance or radius of the sphere of influence (approximately 57 500 km).

In calculating the results shown in figure 29, data given in reference 14 were used to determine the value of V_s for the nominal trajectory used in this report. All results shown in the figure apply to trajectories having the same energy (that is, V_s is constant).

REFERENCES

1. Battin, Richard H.: A Statistical Optimizing Navigation Procedure for Space Flight. R-341 (Contracts NAS-9-103 and NAS-9-153), Instrumentation Lab., M.I.T., Sept. 1961.

2. Smith, Gerald L.; Schmidt, Stanley F.; and McGee, Leonard A.: Application of Statistical Filter Theory to the Optimal Estimation of Position and Velocity on Board a Circumlunar Vehicle. NASA TR R-135, 1962.

3. Blair, W.: Manual Space Navigation Computer Program. NASA CR-250, 1965.

4. Nordtvedt, Kenneth: A Theory of Manual Space Navigation. NASA CR-841, 1967.

5. Van Cott, Harold P.: An Optical System for Manned Vehicle Terminal Guidance. Human Factors, vol. 5, no. 3, June 1963, pp. 329-333.

6. McLean, John D.; Schmidt, Stanley F.; and McGee, Leonard A.: Optimal Filtering and Linear Prediction Applied to a Midcourse Navigation System for the Circumlunar Mission. NASA TN D-1208, 1962.

7. Anon.: Programmer's Manual for Interplanetary Error Propagation Program. WDL-TR2184 (Contract NAS 5-3342), Philco Corp., Nov. 15, 1963.

8. Mayo, Alton P.; Hamer, Harold A.; and Hannah, Margery E.: Equations for Determining Vehicle Position in Earth-Moon Space From Simultaneous Onboard Optical Measurements. NASA TN D-1604, 1963.

9. Hamer, Harold A.: Manual Procedure for Determining Position In Space From Onboard Optical Measurements. NASA TN D-1852, 1964.

10. Gapcynski, John P.; and Woolston, Donald S.: Characteristics of Three Precision Circumlunar Trajectories for the Year 1968. NASA TN D-1028, 1962.

11. Hannah, Margery E.; and Mayo, Alton P.: A Study of Factors Affecting the Accuracy of Position Fix for Lunar Trajectories. NASA TN D-2178, 1964.

12. Liebelt, Paul B.: Manual Extraterrestrial Guidance and Navigational System. AIAA J., vol. 1, no. 9, Sept. 1963, pp. 2142-2144.

13. Jones, Ruben L.; and Mayo, Alton P.: A Study of Some Transition Matrix Assumptions in Circumlunar Navigation Theory. NASA TN D-1812, 1963.

14. Hamer, Harold A.; and Hodge, Ward F.: Trajectory Entry Conditions at the Lunar Sphere of Influence for Application to Detailed Studies of Near-Moon Trajectory and Impact Conditions. NASA TN D-1820, 1963.

NASA-Langley, 1967 —— 21 L-5310

"The aeronautical and space activities of the United States shall be conducted so as to contribute . . . to the expansion of human knowledge of phenomena in the atmosphere and space. The Administration shall provide for the widest practicable and appropriate dissemination of information concerning its activities and the results thereof."

—NATIONAL AERONAUTICS AND SPACE ACT OF 1958

NASA SCIENTIFIC AND TECHNICAL PUBLICATIONS

TECHNICAL REPORTS: Scientific and technical information considered important, complete, and a lasting contribution to existing knowledge.

TECHNICAL NOTES: Information less broad in scope but nevertheless of importance as a contribution to existing knowledge.

TECHNICAL MEMORANDUMS: Information receiving limited distribution because of preliminary data, security classification, or other reasons.

CONTRACTOR REPORTS: Scientific and technical information generated under a NASA contract or grant and considered an important contribution to existing knowledge.

TECHNICAL TRANSLATIONS: Information published in a foreign language considered to merit NASA distribution in English.

SPECIAL PUBLICATIONS: Information derived from or of value to NASA activities. Publications include conference proceedings, monographs, data compilations, handbooks, sourcebooks, and special bibliographies.

TECHNOLOGY UTILIZATION PUBLICATIONS: Information on technology used by NASA that may be of particular interest in commercial and other non-aerospace applications. Publications include Tech Briefs, Technology Utilization Reports and Notes, and Technology Surveys.

Details on the availability of these publications may be obtained from:

SCIENTIFIC AND TECHNICAL INFORMATION DIVISION

NATIONAL AERONAUTICS AND SPACE ADMINISTRATION

Washington, D.C. 20546